Title
Enhancing Non-Viral Gene Delivery in Porous Hyaluronic Acid Hydrogels

Author
Truong, Norman

Publication Date
2018

Peer reviewed|Thesis/dissertation

UNIVERSITY OF CALIFORNIA

Los Angeles

Enhancing Non-Viral Gene Delivery in Porous Hyaluronic Acid Hydrogels

A dissertation submitted in partial satisfaction of the

requirements for the degree Doctor of Philosophy

in Chemical Engineering

by

Norman Franklin Truong

2018

ABSTRACT OF THE DISSERTATION

Enhancing Non-Viral Gene Delivery in Porous Hyaluronic Acid Hydrogels

by

Norman Franklin Truong

Doctor of Philosophy in Chemical Engineering

University of California, Los Angeles, 2018

Professor Tatiana Segura, Co-Chair

Professor Harold G. Monbouquette, Co-Chair

The efficient and sustained delivery of therapeutic genes *in vitro* and *in vivo* has a wide range of applications in studying biology and in developing therapies for treating disease or repairing tissue. Porous hydrogels have been widely used as three-dimensional scaffolds for both cell culture and tissue repair due to their ability to mimic the structural and biochemical properties of native tissue. In addition, therapeutics such as DNA-loaded nanoparticles called polyplexes can be delivered from these scaffolds to infiltrating cells; however, the main challenge plaguing such efforts has been insufficient transgene expression from the delivery of the transgene. It is hypothesized that this is due to significant aggregation of inherently charged polyplexes upon encapsulation in the hydrogel. To mitigate this issue, our laboratory has previously developed a method called caged nanoparticle encapsulation to load polyplexes in porous hyaluronic acid hydrogels at high concentrations; however, low transgene expression has been observed both *in*

vitro and *in vivo*, prompting the search for alternative methods to enhance non-viral gene delivery from hydrogels.

In considering this problem, we first developed two methods of loading polyplexes within porous hydrogel scaffolds and examined mechanisms of polyplex uptake. In the first method, we addressed the hypothesis that the high surface charge of polyplexes triggers aggregation by developing a PEGylated variant of the DNA-complexing polymer polyethyleneimine (PEI) to decrease the surface charge of polyplexes. While this technique did result in decreased polyplex aggregation upon encapsulation in the hydrogel, it also exhibited decreased internalization and transfection efficiency due to the decreased surface charge. In the second method, polyplexes were loaded into hydrogels by coating onto the hydrogel pore surfaces instead of encapsulation to improve DNA availability to infiltrating cells. This presentation resulted in long-term sustained transgene expression *in vitro* over a period of 30 days, which we concluded was due to the occurrence of re-transfection events.

Lastly, we studied how material properties of a new promising class of injectable porous scaffolds known as microporous annealed particle (MAP) scaffolds can affect transgene expression. We found that building block size, stiffness, cell adhesion peptide concentration and presentation, and induced integrin specificity affect transgene expression upon polyplex transfection of cells cultured within MAP scaffolds, and that transfection of cells cultured in MAP scaffolds occur via different mechanisms that that of cells cultured two-dimensionally on tissue culture plastic. These findings provide further insight on how MAP scaffold design can be optimized for enhancing gene delivery.

The dissertation of Norman Franklin Truong is approved.

Yvonne Y. Chen

Stephanie Kristin Seidlits

Harold G. Monbouquette, Committee Co-Chair

Tatiana Segura, Committee Co-Chair

University of California, Los Angeles

2018

To my family

婆婆

Mom and Dad

Wesley

TABLE OF CONTENTS

LIST OF FIGURES AND TABLES

ACKNOWLEDGEMENTS

I am indebted to those whose efforts have made this dissertation possible. First, thank you, Tatiana; you have been an amazing advisor over the past five and a half years. Thank you for providing me with the space and support to pursue my ideas and interests. I have become a better scientist and person through your mentorship and through learning from your almost inhuman ability to balance work and family.

I would also like to thank all my lab mates for their friendship and support, and of course for all the laughs and antics along the way. Cynthia, you were my first mentor in the lab, and I learned so much from you; thank you for being so kind and patient. Don, Allyson, Lina, Sasha Cai, and Lucas, thank you for sharing with our lab community your expertise and advice from a postdoc perspective, both about research and about life. Talar, Jon, Suwei, and Shiva, I appreciate your help and advice as the older grad students in our lab; I am glad we have been able to stay in touch throughout my time at UCLA. Sandy, Giovanny, Shayne, Victor, Elias, Rob, Kat, Yining, Lindsay, Peter, and Drew, you have been great lab mates and have made our lab a fun and enjoyable place to work. Sandy, I already miss our carpool chats. I would like to give a special thank you to Nikki; I am so grateful that we were able to go on this PhD journey together. I also cannot forget the undergraduate and high school students whom I have had the pleasure of mentoring, especially Adrian, Ben, Olivia, Nairi, and Mabel; I hope you learned as much from me as I did from working with you. I deeply appreciate your hard work, patience, and above all, your trust in me as your mentor.

I would also like to extend my gratitude to the other mentors who have guided my research and career development along the way: Dr. Yvonne Chen, Dr. Stephanie Seidlits, Dr. James Liao, and Dr. Harold Monbouquette, for your questions, suggestions, and comments which have taught

me to think more critically about my work and to always keep the overall context and significance of my work in mind; Dr. Luisa Iruela-Arispe and Dr. Julia Mack, for your guidance and generosity during my rotation as an NIH training fellow; and Dr. Karthik Rajagopal and Dr. Amin Famili, for your mentorship and career advice during my internship at Genentech.

I am grateful for funding support from the National Institutes of Health (R01HL110592) and the NIH Biotechnology Training Grant (T32GM067555), without which this work would not have been possible.

Jeff, you have supported me in more ways than you can imagine; thank you for everything.

Thank you to my friends, especially Leo, Claire, Andrew, Carly, and Janise, for your kindness and support.

And finally, a heartfelt thank you to my mother, father, 婆婆, and brother for their unfaltering love and encouragement.

Chapter II is a version of "Lam, J., Truong, N. F. & Segura, T. Design of cell-matrix interactions in hyaluronic acid hydrogel scaffolds. *Acta Biomater.* **10,** 1571–1580 (2014). doi:10.1016/j.actbio.2013.07.025."

Chapter III is a version of "Youngblood, R.L., Truong, N.F., Segura, T. & Shea, L.D. It's all in the delivery: Designing hydrogels for cell and non-viral gene therapies. In revision."

Chapter IV is a version of "Siegman, S., Truong, N. F. & Segura, T. Encapsulation of PEGylated low-molecular-weight PEI polyplexes in hyaluronic acid hydrogels reduces aggregation. *Acta Biomater.* **28,** 45–54 (2015). doi:10.1016/j.actbio.2015.09.020."

Chapter V is a version of "Truong, N. F. & Segura, T. Sustained Transgene Expression via Hydrogel-Mediated Gene Transfer Results from Multiple Transfection Events. *ACS Biomater. Sci. Eng.* (2018). doi:10.1021/acsbiomaterials.7b00957. In press."

Chapter VI is a version of "Truong, N.F., Tahmizyan, N., Lesher-Perez, S.C., Chen, M., Darling, N.J., Xi, W. & Segura, T. Physical and cell adhesion properties of microporous annealed particle (MAP) hydrogels control fibroblast spreading, proliferation, and gene transfer. Submitted."

VITA

Education
B.S. in Bioengineering and B.A. in Asian Studies, *magna cum laude*
Rice University, Houston, TX | 2012

Honors and Awards
Biomaterials Area Graduate Student Award | American Institute of Chemical Engineers | 2016
Student Travel Achievement Recognition Award | Society for Biomaterials | 2015
NIH Biotechnology Training Grant | UCLA | 2013-2015
NSF Graduate Research Fellowship, Honorable Mention | 2013
Tau Beta Pi Engineering Honor Society | 2011-
Rice Engineering Alumni Leadership Scholarship | 2011, 2012
L.J. Walsh Engineering Scholarship | Rice University | 2010
Trustees Distinguished Scholarship | Rice University | 2008-2012
Century Scholars Research Program and Scholarship | Rice University | 2008 – 2010
National Merit Scholar | 2008

Research Experience

09/2012 - 03/2018	Graduate student researcher | Principal investigator Tatiana Segura Department of Chemical and Biomolecular Engineering, UCLA
09/2014 – 03/2015	Drug delivery R&D intern | Manager Karthik Rajagopal Genentech, South San Francisco, CA
03/2014 – 06/2014	Graduate student researcher | Principal investigator Luisa Iruela-Arispe Department of Molecular, Cell, and Developmental Biology, UCLA
01/2010 – 05/2012	Undergraduate research assistant | Principal investigator Amina Qutub Department of Bioengineering, Rice University
05/2011 – 08/2011	Undergraduate research intern | Principal investigator Pin Wang Department of Chemical Engineering, USC

Publications

1. **Truong NF** and Segura T. Sustained transgene expression via hydrogel-mediated gene transfer results from multiple transfection events. ACS Biomat Sci & Eng. 2018. In press.
2. Bryson PD, Han X, **Truong NF**, Wang P. Breast cancer vaccines delivered by dendritic cell-targeted lentivectors induce potent antitumor immune responses and protect mice from mammary tumor growth. Vaccine 35:5842-49, 2017.
3. Cam C, Zhu S, **Truong NF**, Scumpia PO, Segura T. Systematic evaluation of natural scaffolds in cutaneous wound healing. J Mater Chem B 3:7986-92, 2015.
4. Siegman SN*, **Truong NF***, Segura T. Encapsulation of PEGylated low-molecular-weight PEI polyplexes in hyaluronic acid hydrogels reduces polyplex aggregation. Acta Biomater 28:45-54, 2015.
5. Lam J*, **Truong NF***, Segura T. Design of cell-matrix interactions in hyaluronic acid hydrogel scaffolds. Acta Biomater 10(4):1571-80, 2014.
6. **Truong NF**, Nathan JC, Ochoa GA, Prevost MA, Yoon DH, Yun S, Oden ZM, Razavi M. Abdominal fat suspension device for maintaining normal cardiorespiratory function in

patients undergoing conscious sedation during surgery: A feasibility study. The Texas Heart Institute Journal 41(4):368-72, 2014.

*Co-first authorship

Presentations

1. Truong NF, Segura T. Sustained transgene expression via substrate-mediated gene transfer results from extended transfection events. 2016 American Institute of Chemical Engineers Annual Meeting, San Francisco, CA. 15 Nov 2016. Oral presentation.
2. Truong NF, Segura T. Surface-associated DNA presentation for sustained gene delivery with porous hyaluronic acid hydrogels. 2015 Society for Biomaterials Conference, Charlotte, NC. 16 April 2015. Oral presentation.
3. Truong NF, Cheng J, Segura T. Surface-associated DNA presentation for controlled gene delivery with porous hydrogels. 2013 Vasculata, North American Vascular Biology Organization, San Diego, CA. 30 July 2013. Poster presentation.
4. Truong NF, Ochoa GA, Prevost MA, Yoon DH, Yun S, Oden ZM, Razavi M. A novel abdominal suspension device to maintain normal cardiorespiratory function in obese patients during surgery. 2012 Resuscitation Science Symposium, American Heart Association Conference, Los Angeles, CA. 4 Nov 2012. Poster presentation.
5. Truong NF, Nathan JC, Qutub AA. Oxygen- and ROS-sensitive fluorescent micro- and nanoparticles: synthesis and characterization. 2011 Rice University Undergraduate Research Symposium, Houston, TX. 15 Apr 2011. Poster presentation.
6. Ching G, Ryan D, Zaunbrecher R, Long B, Truong NF, Qutub AA. Defining metrics for the identification of morphological phenotypes during stimulation of endothelial cells. 2012 Rice University Undergraduate Research Symposium, 13 Apr 2012. Poster presentation.

Teaching Assistantships

Fall 2016	CBE 115/215 Biochemical Reaction Engineering
Winter 2016	CBE 104D Biotechnology Laboratory
Spring 2013	CBE 101C Mass Transfer

I Overview of dissertation and specific aims

1.1 Motivation and objectives

The efficient delivery of therapeutic genes has a wide range of applications in studying biology and in developing therapies for tissue repair. *In vitro* applications may include studying the transdifferentiation and cellular transition of various types of cell lines, processes with durations on the order of weeks[1–3]. Because such processes are guided by the sustained expression of factors over an extended period of time, strategies to achieve sustained transgene expression for longer-term availability of the therapeutic signal are appealing. *In vivo,* local non-viral gene delivery can serve as a therapy for regenerative medicine applications by delivering a gene encoding for a therapeutic protein to tissues to promote a specific repair process. In addition, many of these target processes require specific levels of overexpression of a gene of interest as a function of time in order to maintain proper progress of the process. While this type of sustained expression may be achieved with stably integrated viral delivery methods, many of these delivery strategies also carry inherent additional risks associated with immunogenicity and insertional mutagenesis[4]. Therefore, methods that use non-integrating non-viral vectors for long-term expression would be

a safer and more appropriate approach for achieving transient expression for tissue repair applications.

Naked DNA delivery has been shown to achieve transgene expression and guide regeneration *in vivo*[5,6], but often results in poor delivery efficiency because the plasmid's negative charge and large hydrodynamic radius trigger plasmid degradation, ineffective internalization and trafficking by the cell and induces immune responses due to the bacterial elements of the plasmids[7]. Instead, a number of different polymers used to complex with DNA to form nanoscale structures have been developed to enhance DNA uptake. One promising class of polymers that can be used as gene carriers are cationic polymers such as polyethyleneimine (PEI) which complex with DNA to form nanoparticles called polyplexes. While the delivery of naked DNA to the cell nucleus is largely viewed as inefficient, charged polyplexes can readily be associated with the plasma membrane, endocytosed by cells, after which the delivered DNA can ultimately be trafficked to the nucleus to result in enhanced levels of transfection.

Sustained transgene expression can be achieved with a sustained polyplex-based gene delivery strategy that allows for long-term availability of DNA to cells from their substrate. Hydrogels, highly hydrated crosslinked polymer networks, show great promise as substrates for cell culture over more conventional two-dimensional stiff plastic substrates due to the ability to tune their mechanical properties to match conditions favorable for the cell lines of interest[8]. They can therefore serve as a more accurate *in vitro* model to study biological processes or to test new therapies. Hydrogels can also support and enhance the regeneration of tissues when delivered *in vivo*; this role is especially relevant in regenerative medicine applications such as in wound healing, stroke recovery, or cartilage and bone regeneration, especially when these scaffolds are also used to locally deliver therapeutic genes to infiltrating cells. One polymer that shows potential for

scaffold-based therapies is hyaluronic acid (HA). HA is an anionic, non-sulfated glycosaminoglycan and a natural component of the extracellular matrix that exhibits high biocompatibility and low immunogenicity[9]. Its ability to be used as a "blank slate" makes it an appealing candidate for creating hydrogel scaffold implants that can be functionalized with various bioactive signals, including DNA, to direct a specific cellular or tissue response. Furthermore, porosity, can be introduced into HA hydrogels through techniques such as sphere templating[10] and salt-leaching[11] to facilitate cell infiltration into and proliferation throughout the hydrogel.

Various bioactive signals can be loaded into hydrogels to be made available to infiltrating cells to instruct cell behavior as a function of their proliferation[8]. In particular, the hydrogel scaffold can serve as depots for polyplexes of DNA encoding for therapeutic genes which are encapsulated within the hydrogel to be released into the local cellular microenvironment, enabling sustained expression. However, such efforts have in the past resulted in insufficient transgene expression, which we hypothesize is due to significant aggregation of the charged polyplexes upon encapsulation in the hydrogel at high concentrations. To alleviate the extent of such aggregation, our group has previously developed a method of polyplex preparation and incorporation into hydrogels known as caged nanoparticle encapsulation[12]; however, insufficient transgene expression levels were observed, likely due to the decreased ability of polyplexes from this preparation to be released from the scaffold. These results prompted the search for alternative methods to enhance non-viral gene delivery from hydrogels.

The broad objective of the research presented in this dissertation was to develop methods to enhance the efficacy of local non-viral gene delivery from HA hydrogel scaffolds and to study the role of scaffold properties in modulating transfection. As described in Figure 1.1, we investigate three strategies to enhance and study polyplex-mediated gene delivery in porous HA

scaffolds. There are two methods of loading DNA polyplexes in porous scaffolds: encapsulation within the gel phase and adsorption, or surface-coating, of polyplexes along the pore surfaces. While encapsulation allows for gene delivery to be dependent on the rate of cell-mediated degradation of the hydrogel, it introduces the issue of polyplex aggregation, which decreases transfection efficiency. Alternatively, the surface coating of hydrogel pores with polyplexes allows for easier availability of polyplexes to infiltrating cells. Aside from these two methods focusing on polyplex-matrix interactions, the transgene expression profile enabled by gene delivery can also be enhanced or modulated by the design of the plasmid vector used to deliver the transgene. Lastly, we focus on cell-scaffold interactions to enhance transfection efficiency in a new class of porous biomaterials known as microporous annealed particle (MAP) hydrogels.

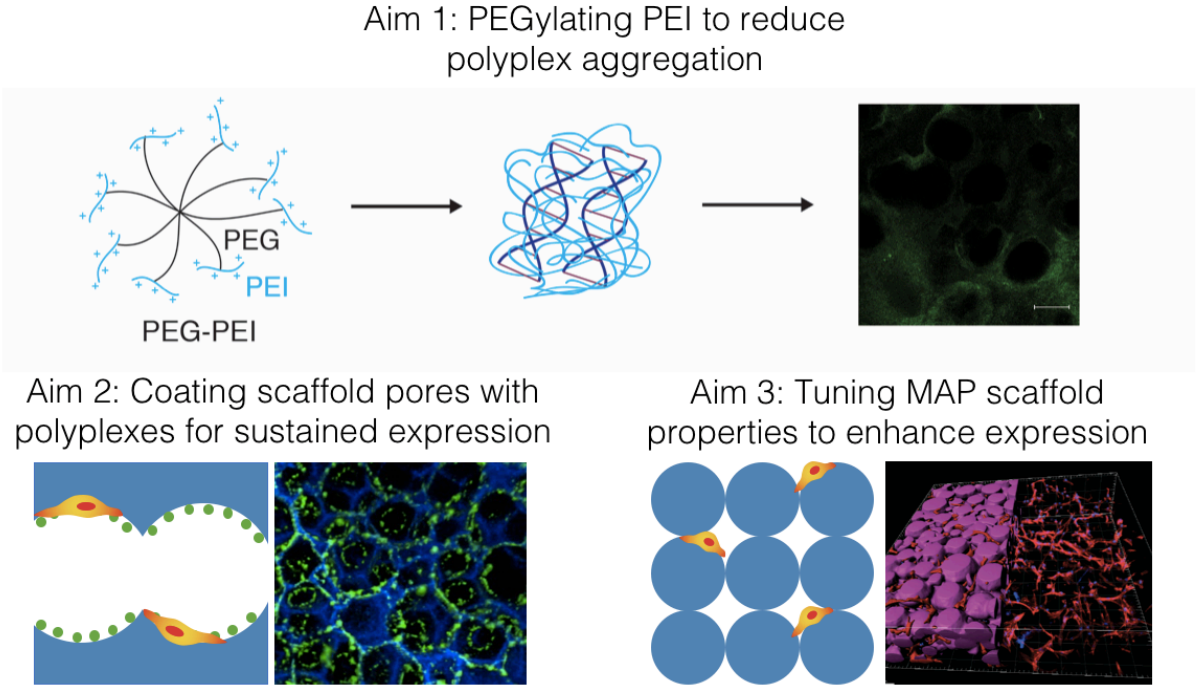

Figure 1.1: Dissertation aims.

1.2 Dissertation outline and specific aims

After this introduction, chapters II and III provide relevant background for the original research in this dissertation. Chapter II reviews published studies in the development of HA scaffolds to elaborate on HA scaffold design to direct cell-matrix interactions through the incorporation of biochemical cues, mechanical cues, spatial cues, and different crosslinking chemistries. Chapter III describes design parameters specifically for functionalizing hydrogels for non-viral gene delivery for tissue repair. Through a review of the literature, we elaborate on the status of advancements in scaffold-mediated gene delivery.

Chapters IV, V, and VI summarize the three research strategies for this dissertation:

Specific Aim 1 (Chapter IV)

One method for presenting DNA polyplexes in porous HA scaffolds is the encapsulation of polyplexes within the gel phase of the scaffold; however, the charged nature of both the polyplexes and the HA induces significant aggregation of polyplexes, decreasing transfection efficiency. We hypothesized that PEGylating the cationic polymer used to prepare polyplexes can decrease the overall polyplex surface charge and subsequently reduce aggregation upon encapsulation in HA hydrogels.

Specific Aim 2 (Chapter V)

Here, we developed a surface coating method as an alternative approach to encapsulation as a method to load DNA polyplexes in HA hydrogels in order to bypass the problem of low transfection efficiency due to aggregation. We hypothesized that surface coating would result in sustained transgene expression and that this sustained expression was due to the occurrence of multiple transfection events.

Specific Aim 3 (Chapter VI)

Our group has developed a new class of hydrogel biomaterials known as microporous annealed particle (MAP) scaffolds, a simultaneously porous and injectable scaffold material which enables the homogeneous distribution of cells *in vitro* seeding and has resulted in enhanced wound repair in mouse models *in vivo*[13–15]. The objectives of this aim were to understand how MAP scaffold material properties can modulate transfection and how transfection mechanisms in culture in MAP scaffolds differ from culture on tissue culture plastic.

II Design of cell-matrix interactions in hyaluronic acid hydrogel scaffolds

2.1 Introduction

Hyaluronic acid (HA), a naturally occurring glycosaminoglycan (GAG) and one of the primary components of the extracellular matrix (ECM), is increasingly being utilized in biomedical applications due to both its ability to serve as a blank slate and its biological activity. In particular, it is commonly used to form hydrogel scaffolds for tissue engineering[16], which may in turn be employed for localized drug and DNA delivery purposes[17,18]. This chapter aims to give a brief overview of the biological functions of HA, knowledge needed to fully realize the potential that HA has for tissue engineering applications, before describing recent and novel ways in which HA scaffolds have been engineered to deliver various classes of signals to influence and ultimately command greater control over cell-matrix interactions and cell behavior (Figure 2.1).

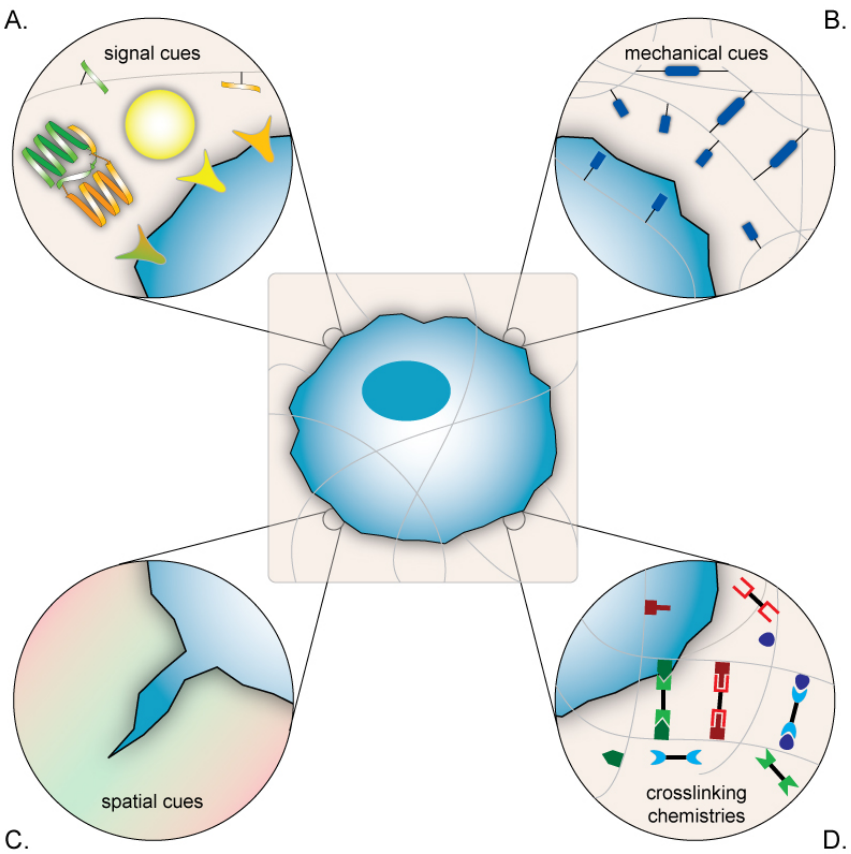

Figure 2.1: Hyaluronic acid scaffolds can be engineered in several ways to control encapsulated cell behavior.
(A) Bioactive signals can be incorporated into the scaffold in suspension or covalently bound to the polymer. (B) Tuning the mechanical properties by utilizing degradable crosslinkers and/or degree of crosslinking can regulate cell mechanosensing. (C) Spatial cues such as patterned bioactive signals, porosity control, and topographical patterns can direct cell migration. (D) New "click chemistries" have been employed to provide new ways to covalently crosslink the hydrogel network.[9]

Hyaluronic acid is a linear polysaccharide that consists of two alternating units, B-1, 4-D-glucuronic acid and B-1, 3-N-acetyl-D-glucosamine (Figure 2.2). This unmodified polymer has a molecular mass between 10^3 and 10^4 kDa, which can reach a length of 25 μm when fully extended. Its negative charge attracts positive ions and results in an osmotic balance that brings in water. This allows HA to exist as a highly hydrated molecule and paves the way for a myriad of uses in the body.

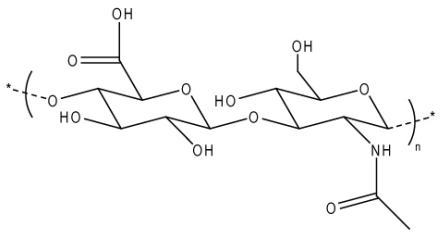

Figure 2.2: Structure of hyaluronic acid.
Chemical modifications are commonly performed at (a) and (b).

After synthesis in the inner face of the plasma membrane of fibroblasts, HA is translocated to the pericellular space and the interstitial matrix[19]. This characteristic makes HA distinct from other GAGs, which are typically synthesized in the Golgi and contain a protein core. Three transmembrane glycosyltransferase isoenzymes, HAS1-3, regulate the synthesis process. Hormones and growth factors, among other bioactive molecules, can also help regulate the production of HA.

2.2 Biological function

One property of hyaluronic acid that can potentially be exploited is that its biological function depends on its molecular weight. While it typically exists as a high molecular weight polymer over 10^6 daltons, it can be cleaved by the enzyme hyaluronidase (HAse) to obtain molecules of much lower molecular weights[20]. In fact, high and low molecular weight HA exhibit opposing effects on cell behavior. In addition to inhibiting cell proliferation, high molecular weight HA is also anti-angiogenic[21]. In fetal development of rat follicles, HA acts as a high molecular weight barrier that blocks endothelial cell migration and subsequent angiogenesis. However, cleaving the polymer into shorter fragments with hyaluronidase enables endothelial cells to migrate and initiate angiogenesis[22]. These high molecular weight polymers are also anti-inflammatory and immunosuppressive[23,24]. This feature may be particularly important as the

amniotic fluid of fetuses have high concentrations of high molecular weight HA. In contrast, low molecular weight HA (< $3.5x10^4$ Da) has been implicated as pro-inflammatory and pro-angiogenic[25]. In particular, oligomers of the 6-20 kDa range activate antigen-presenting cells, such as dendritic cells, while slightly larger HA ($2x10^4$-$4.5x10^5$ Da) stimulates inflammatory cytokines[26]. In addition, fragments consisting of 4 to 25 disaccharide units are able to promote blood flow to injury sites and subsequent angiogenesis[21,25,27].

On the molecular level, HA primarily interacts with the cell-surface receptor cluster determinant 44 (CD44) and receptor for hyaluronate-mediated motility (RHAMM). CD44 plays a key role in tissue organization by mediating ECM remodeling, cell-cell interactions, and cell-matrix interactions[28,29]. A normal wound healing model in CD44-knockout mice exhibited decreased cell migration, motility, and ECM turnover[30]. Interactions between HA and RHAMM can result in a variety of downstream signaling pathways that affect protein kinases like focal adhesion kinases, MAP kinases, phosphatidylinositol kinases, and tyrosine kinases as well as other molecules like RAS[29,31,32]. Furthermore, *in vivo* experiments blocking HA-RHAMM interactions inhibited fibroblast growth factor-induced neovascularization[33].

An issue worthy of consideration in HA hydrogel design is the pathological context of hyaluronic acid. For example, increased levels of HA in the extracellular environment have been correlated to several types of cancer malignancies[34]. In particular, 3-8-fold higher levels of HA were found in prostate cancer tissues, and elevated levels of Hyal-1, a hyaluronidase, were also observed in prostate cancer tissues when compared to normal tissues[35]. Excess HA synthesis by hyaluronan synthases in conjunction with elevated expression of HAse has also been shown to drive the development of a metastatic phenotype in prostate tumor cells and accelerate the metastatic progression of prostate cancer[36]. A reason for this correlation is that the degradation of

HA by HAse results in HA oligomers, which enhance the cleavage of CD44[37]. Therefore, the increased presence of HA oligomers in various tumor tissues can promote tumor cell mobility and invasion. For more information on the involvement of HA and HAses in cancer biology, readers may refer to other reviews focusing on these biological interactions[38].

Understanding the diverse ways in which HA functions in native tissue can give insight into designing more efficient and novel tissue engineering scaffolds. Because these scaffolds can be synthesized from a variety of synthetic and natural scaffolds, we will briefly touch on some of the differences between the main synthetic polymer used by researchers, polyethylene glycol (PEG), and our polymer of interest, HA. PEG is a non-toxic, non-immunogenic polymer that is often referred to as a "stealthy molecule" because it is not recognized by biological molecules like proteins. This polymer can be used as a blank slate by researchers who wish to control all interactions between cells and the hydrogel. Unlike HA, PEG is non-degradable, so degradable crosslinkers must be incorporated to create a non-permanent hydrogel. While HA will degrade into smaller fragments, PEG will remain in its original form until it is cleared by the body. For a more comprehensive look at PEG and other material-based hydrogels, we refer you to the following reviews[39,40].

This chapter reviews new and innovative ways traditional HA hydrogels have been modified to direct encapsulated cell behavior *in vitro* and promote wound healing *in vivo*.

2.3 Incorporating bioactive signals

Hyaluronic acid hydrogels are typically synthesized from high molecular weight HA. However, as mentioned above, high molecular weight HA is a natural barrier for angiogenesis and proliferation. Thus, to allow cellular infiltration and remodeling of the material by cells in vitro,

HA is crosslinked with protease-degradable peptides and modified with cell adhesion ligands. The sequence of the degradable peptide determines the ability by which different cells can infiltrate the material. For example, for mesenchymal stem cells, HA crosslinked with MMP-degradable peptides results in more infiltration than for gels crosslinked with plasmin-degradable peptides. For *in vivo* experiments, it appears that if the HA scaffold has significantly large pores, incorporation of protease degradable bonds and addition of adhesion ligands are not necessary for the cells to infiltrate the scaffold and remodel the material[41]. Because HA behaves as a barrier to cell adhesion and migration in vitro, it can be used as a blank slate to investigate the roles of different ligands on cell behavior and differentiation.

Cell-matrix interactions of HA hydrogel scaffolds with embedded or infiltrating cells can be engineered to promote survival, proliferation, and/or differentiation. Traditionally, cell-matrix interactions in hydrogels for tissue regeneration are engineered with motifs found in the natural ECM of the relevant tissue. For example, the ubiquitous RGD sequence found in several cell adhesion proteins and tissues in the body as well as other adhesion peptides have been routinely introduced to promote cell adhesion to the material through integrin receptors. Further, since these peptides are unable to fully or specifically engage cell surface receptors, unlike their more structurally complex parents, approaches to engineer protein fragments or incorporate full-length proteins are also commonly employed. In addition, antibodies, small molecules, and nucleic acids, all of which are not typically present in the natural ECM, have been introduced to recruit a desired cell type or promote differentiation. Full-length proteins that do exist in the ECM, such as growth factors, are also commonly loaded into hydrogels. Common challenges in incorporating growth factors include doing so without damaging secondary structures and controlling the release kinetics.

This section focuses on recent advances in the field that continue to push the innovation of bioactive signal incorporation in HA hydrogels (Figure 2.3).

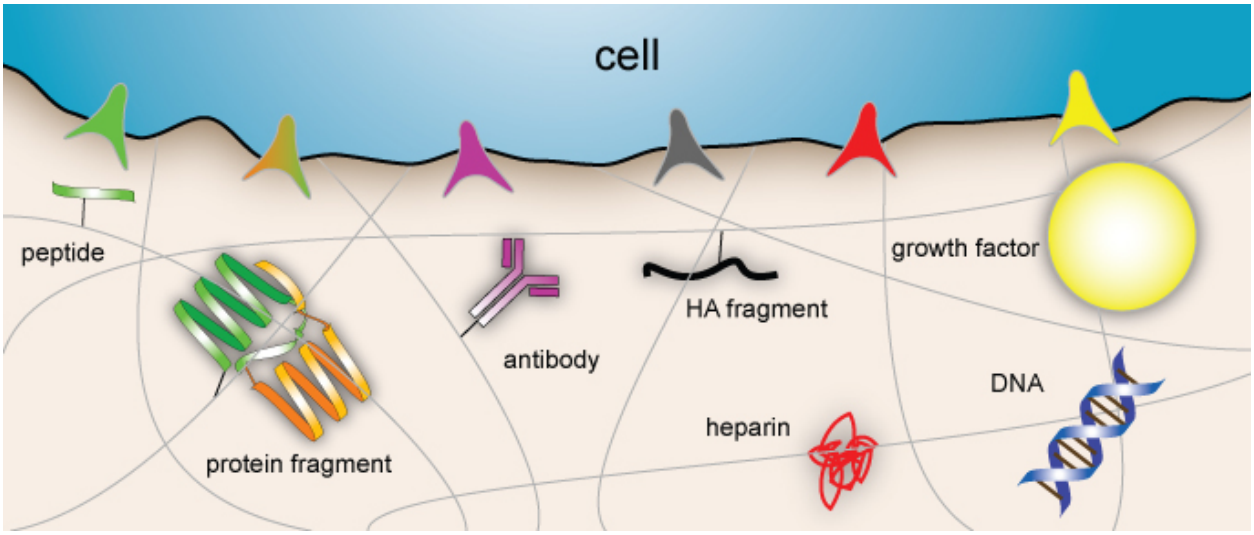

Figure 2.3: Bioactive signals are commonly incorporated into HA hydrogels to direct cell behavior. Some signals, like peptide fragments and antibodies, can be covalently linked to the HA backbone whereas other signals, like heparin and DNA, are loaded into the hydrogel without any permanent bond.

2.3.1 Incorporation of cell adhesion motifs

Integrin binding anchors cells to the ECM and initiates signaling events that control cell behavior[42–45] and remodel the matrix[46,47]. Two-dimensional studies in hydrogel scaffolds have shown that RGD presentation at the nanoscale level influences cell spreading and motility[48–51], stem cell differentiation[52], and nanoparticle internalization[53]. Up until recently, however, for cells seeded within hydrogel scaffolds, only RGD total content (μM-mM range) had been shown to modulate cell motility, spreading, and proliferation[16,54,55]. Our lab designed a HA hydrogel to alter the presentation of the RGD peptide and then studied the effect of peptide incorporation in stem cell integrin expression and gene transfer[16,56]. By pre-reacting a specific portion of the total hyaluronic acid with the RGD adhesion peptide, we were able to modulate the distribution of the peptide inside the hydrogel. Results from five degrees of clustering of three total peptide

concentrations (10, 100, 1000 μM) suggest an optimal degree of clustering for the spreading of encapsulated murine mesenchymal stem cells (mMSC) (Figure 2.4A-C). Furthermore, integrin expression can be modulated through this peptide-clustering parameter. In a separate study, we investigated the effect that RGD presentation had on gene delivery in our HA hydrogel system and found that an intermediate clustering promoted the transfection of encapsulated cells[18]. In both of these studies we found that the degree of clustering affected cellular behavior and that for a particular RGD concentration an optimal clustering amount can be obtained that is in between a completely homogeneous distribution and high clustering. The globular protein sonic hedgehog (SHH) was tethered to linear HA to compare the effect of tethered and soluble protein presentation to cells. The tethered form of SHH was significantly more potent than the soluble form while multivalent constructs enhanced this effect even more[57]. These studies show the importance of bioactive signal distribution on encapsulated cell behavior and how this parameter can be exploited to drive cell behavior.

Aiming to bridge the gap between shorter peptide fragments and native proteins, groups have worked on engineering fibronectin fragments[58]. We have incorporated these fragments into our HA system and have seen a great effect on cell spreading. Compared to incorporating RGD peptide fragments, a much smaller number of the fibronectin fragments was needed to induce mMSC spreading[9]. Evidence of downstream signaling overlap between growth factors and integrins prompted a group to engineer a fibronectin fragment-functionalized hyaluronic acid hydrogel that released bone morphogenic protein-2 (BMP-2)[59]. This functionalization, when compared to blank HA hydrogels and standard cell-culture plates, improved *in vitro* mMSC attachment and spreading. In an *in vivo* ectopic bone formation mouse model, the combination of BMP-2 release with the fibronectin-functionalized hydrogel resulted in twice as much bone

formation with better collagen fiber organization than a non-functionalized, BMP-2-loaded hydrogel. However, it would be been interesting to directly compare the effects of the fibronectin fragment with shorter peptide fragments in their *in vivo* bone formation model. The incorporation of protein fragments has been more thoroughly investigated *in vitro* to modulate epithelial to mesenchymal transition (EMT) or using other biomaterial scaffolds such as fibrin or fibrin mimics[60–63]. Although these approaches have not been applied to hyaluronic acid scaffolds, the chemistry is completely compatible with this system and could be easily translated.

2.3.2 Incorporation of hyaluronic acid fragments

As described earlier, the molecular weight of hyaluronic acid affects its biological activity, primarily by affecting its angiogenic potential with short fragments promoting angiogenesis[25,27]. Delivering 100 micrograms of low molecular weight HA (1-4 kDa) promoted revascularization of skin grafts. Two additional approaches to directly exploit and control this bioactive signal have focused on the crosslinking of different HA molecular weights into scaffolds such as upon degradation different HA fragments sizes are released or the direct tethering of HA fragments with different molecular weights onto the scaffold again such that upon release of the tether different fragment sizes are released. Both approaches demonstrated that the presence of HA oligomers (rather than high molecular weight HA) promoted endothelial cell attachment and proliferation *in vitro* or enhanced vascularization in vivo at weight percentages of ~10%[64,65].

2.3.3 Incorporation of non-ECM motifs

An alternative approach inspired by cardiovascular stents used antibodies for targeted cell attachment. CD34 antibodies were functionalized onto hyaluronic acid hydrogels to specifically capture endothelial cells[66]. Attachment of endothelial cells was significantly greater than non-CD34 expressing macrophages during cell seeding experiments. Furthermore, a dose-dependent

response of endothelial cell attachment to antibody-immobilization concentration was observed. This innovative antibody approach can be used to engineer more specialized cell recruitment scaffolds.

2.3.4 Incorporation of growth factors and controlled release

Delivering full-length proteins such as growth factors in scaffolds is desirable because systemic delivery does not allow for targeted treatments and may result in unwanted side effects. Traditional approaches include direct loading of the scaffold; however, these proteins can also be incorporated into scaffolds by utilizing intermediary molecules like heparin. This glycosaminoglycan has the ability to bind growth factors and gives researchers a method to indirectly incorporate heparin-binding proteins into their system. Furthermore, this GAG/growth factor interaction can be exploited for controlled release.

A variety of growth factors have been loaded into hyaluronic acid-based hydrogel systems. For example, basic fibroblast growth factor (FGF-2) and bone morphogenic protein-2 were delivered over the course of 28-35 days[67,68]. After ensuring the bioactivity of the released FGF-2, scaffolds were loaded with 250 ng of FGF-2 and implanted subcutaneously in mice. Hydrogels released ~70% of the FGF-2 and promoted more neovascularization than control scaffolds as well as bolus FGF-2 injections. Additionally, a commercially available hyaluronic acid/heparin sulfate was loaded with 1.5 ng of insulin growth factor and injected into the stroke cavity of mice. Amazingly, a sustained release of IGF-1 occurred over 4 weeks after implantation[69].

Using a nanoparticle approach, heparin-decorated HA nanoparticles were synthesized to carry and release 200 ng of BMP-2[70]. Heparin was immobilized on HA hydrogel nanogels and the BMP-2 release kinetics were modulated by nanoparticle composition. Near zero-order release kinetics were reached through a series of optimization experiments with ~46% of the BMP-2

released over 13 days. Furthermore, the heparin decoration increased BMP-2 loading capacity two-fold and produced the efficient differentiation of MSC's into chondrocytes *in vitro*.

2.3.5 Incorporation of gene-encoding nucleic acids

Gene delivery has been widely researched as a tool for gene therapy in tissue regeneration and cancer therapy. While both non-viral and viral vehicles have been used to deliver genes in the form of nucleic acids, non-viral systems such as hydrogel scaffolds loaded with DNA have a lower risk of causing an immune response and insertion mutagenesis. Although delivering naked DNA has been attempted, transfection efficiency was shown to be very low and much of the DNA diffused away from the local scaffold implant site. Hence, DNA is most commonly delivered in scaffolds when electrostatically complexed with polyethyleneimine (PEI) in the form of nanosize polyplexes, which also allow for higher loading of DNA into the scaffold. Our group had previously developed a technique called caged nanoparticle encapsulation (CnE), which uses the saccharides agarose and sucrose to protect the polyplexes from aggregation when incorporating them into hydrogels, allowing us to load up to 5 μg of DNA polyplexes per microliter of HA hydrogel without significant aggregation while still achieving gene transfer *in vitro* and *in vivo*[71]. Gene transfer efficiency in HA hydrogels was found to be a function of the DNA-to-PEI ratio during polyplex synthesis[18]. In addition, gene transfer efficiency was found to significantly correlate with nanoporous HA hydrogel stiffness, with the highest gene expression observed in the softest hydrogels. This is due to greater cell infiltration and migration through the softer hydrogels. Our group has also been able to encapsulate DNA/PEI polyplexes via CnE into nonporous HA scaffolds *ex ovo*. Using a chorionic chick embryo (CAM) assay, enhanced angiogenesis was observed with hydrogels loaded with pVEGF-containing polyplexes, demonstrating the efficacy and maintenance of activity of the CnE polyplexes[12]. In addition, DNA polyplex-loaded

microporous HA hydrogels containing cells seeded in the pores resulted in sustained gene transfer and expression over ten days[72]. *In vivo* implantation in a wound healing model in mice also showed transfection and subsequent gene expression in cells that had infiltrated the gel (unpublished data).

2.4 Introducing spatial signals

Topographical cues introduced into the environment have been observed to also significantly affect cell behavior (Figure 2.1C). Cells seeded along grooves and ridges tended to elongate and align along these topographical features, behaviors that were not observed on smooth surfaces, a phenomenon known as "contact guidance"[73]. However, the extent of multicellular organization can also be a function of spatial cues, and this has been shown in HA hydrogel cell culture[74]. HUVECs were seeded in microgrooves of varying diameters on HA-dextran hydrogels. After 24 h of culture, HUVECs that were cultured in channels of 30 μm and 50 μm in width self-organized into 3-D vessels, while those cultured in channels of greater widths only organized into 2-D monolayers covering the bottom of the channels. The investigators speculated that contact guidance on the spatial scale of no more than a few cells allowed cells to communicate and form interactive structures. In addition, co-culturing of HUVECs with fibroblasts resulted in elongated morphologies of the fibroblasts along the endothelial cords[74].

Varying porosity as a spatial signal to be introduced in HA hydrogels has also been studied. Our group subcutaneously implanted hydrogels without micron-size pores and hydrogels with 100-μm pores in mice and observed substantial infiltration of the porous HA hydrogel by cells even after one week, while there was minimal infiltration of the nonporous hydrogel. It is speculated that designing porous hydrogels will allow for greater cell infiltration over time when compared to hydrogels without pores of the scale of cell diameter[72].

Spatial control has been employed to not just affect morphology and multicellular organization, but also to control the direction of cell proliferation in culture. A strategy currently being investigated as a means of HA hydrogel design with stringent spatial control is to use light to photo-initiate pattern formation in a hydrogel, which is thought to mimic the heterogeneity of physical and chemical properties found throughout native tissues. By conjugating the caged and inactivated RGDS adhesion peptide sequence to the surface of a HA hydrogel, cell-adhesive regions were created by exposing those regions to near-UV light, thereby uncaging and activating the RGDS peptides present in those regions. This chemically patterned hydrogel supported patterned and robust 2D cell culture on the activated regions. Furthermore, this system could be manipulated temporally by introducing more cell-adhesive regions during cell culture, allowing for control over cell proliferation direction over time[75].

2.5 Introducing mechanical signals

Mechanical properties of a cell's substrate have profound effects on the progression of various cellular processes, and tissue scaffolds have been designed to direct cell mechanosensing and mechanoresponse[76]. Therefore, studying this type of cell-material interaction is a major point of consideration in hyaluronic acid hydrogel design. The mechanical properties of HA hydrogels can be varied by either adjusting the concentration of HA in the gel precursor solution or by controlling the degree of crosslinking in the gel, either by modulating the concentration of crosslinker or the extent of crosslinker reaction, depending on the type of chemistry used in crosslinking (Figure 2.1B). Generally, increasing the gel precursor solution's HA concentration increases the storage modulus of the hydrogel, with stiffnesses ranging from hundreds of Pa to thousands of Pa.

Several groups have studied general cell behavior, such as cell attachment, spreading, and proliferation, as a function of gel stiffness in HA hydrogels. The stiffness of nonporous HA hydrogels can be controlled by modulating both HA concentration and crosslinking density. By decoupling the two parameters and seeding mesenchymal stem cells (MSCs) in the gel, migration and proliferation both increased with decreasing HA concentration from 5% to 3%, resulting in a storage modulus decrease from 1920 Pa to 177.1 Pa, and decreasing crosslinking density from a crosslinking ratio (r) of 0.5 to 0.25, resulting in a storage modulus decrease from 387.4 Pa to 177.1 Pa[16]. The porosity of the gel is also another parameter worth considering in conjunction with varying stiffness, as cells cultured in nonporous gels exhibit different cell behavior than those cultured in porous gels. In another study, the stiffness of methacrylated HA macroporous hydrogels (250 μm) is tuned by using UV-initiated free radical polymerization at different UV exposure times for varying extents of crosslinking[77]. However, after seeding and culturing with MSCs, less cell spreading and proliferation were observed in 1.5 kPa gels versus stiffer gels (up to 7.4 kPa) by analyzing cell morphology and DNA content. This highlights a crucial difference between nonporous and macroporous gels; proliferation occurs in nonporous gels via the degradation of the gel by the cells, while cells cultured in macroporous gels proliferate and migrate along the surface of the pores, relying on two-dimensional surface interactions as mechanical signals. To further support this point, in 2D glioma culture, significantly more cell spreading, proliferation, and motility were observed on stiffer gels with storage moduli of up to 5 kPa than on 150-Pa gels; however, there was almost no gel infiltration and cell proliferation when glioma spheroids were cultured within 5-kPa 3D nonporous hydrogels, while gel infiltration was observed in 150-Pa gels[78]. However, it was interesting to note in this study that initial glioma cell attachment was not affected by gel stiffness. Furthermore, this study highlights the potential applications that HA

hydrogels have as a tunable biomimetic platform for studying cancer biology. In summary, HA hydrogels with relatively lower storage moduli are generally required to achieve spreading of a 3D culture, and if stiffer gels are used, micron-size pores must be introduced.

Various studies have also investigated the effects of HA hydrogel stiffness on stem cell differentiation, inspired by research showing that the mechanics of the cellular microenvironment are an influencing factor in the direction and extent of differentiation of stem cells *in vivo.* Hence, hydrogels of different stiffnesses have been used that mimic stem cells' native environment in order to direct a stem cell's development toward a specific phenotype[79]. This has been applied to HA hydrogel applications; ventral mesencephalic neural progenitor cells (NPCs) differentiated furthest towards a neuronal phenotype in a 3D culture in HA hydrogels with a stiffness most closely resembling that of the neonatal brain, while the same NPCs differentiated into the astroglial phenotype when cultured for three weeks on HA hydrogels with a stiffness that resembles the adult brain[80]. Temporal control of the environment's mechanics is a second approach that is of interest. Cardiomyocyte differentiation in hydrogels may progress in a more *in vivo*-like fashion if the mechanical properties of the hydrogel environment were designed to progressively stiffen over time at a rate closely mimicking that of the maturation of the cells' native tissue environment[81]. This temporal control was due to a time-dependent Michael-type addition reaction modulated by HA molecular weight. It would be interesting to see a significant enhancement in differentiation in this system as compared to a constant-stiffness HA hydrogel. Another approach to detect extent of differentiation as a function of gel stiffness is by monitoring the secretion levels of angiogenic and cytokine proteins. Human mesenchymal stem cells were cultured over two weeks on HA hydrogels of a range of storage moduli from 1.5 kPa to 7.4 kPa (measured by dynamic mechanical analysis) and differences in the secretion levels between cases were noted. It was found that MMP-

9 was initially more highly expressed in stiffer gels, while IL-8 secretion was overall stronger in softer gels. These results suggest that stiffness is a parameter that must be considered when designing hydrogels for the purpose of controlling stem cell differentiation[77].

Aside from controlling individual cell development and behavior, it has also been shown that multicellular organization can be influenced by modulating the mechanical signals from the hydrogel environment. Endothelial colony-forming cells (ECFCs) were seeded in HA hydrogels of two different viscoelasticities (Young's modulus) to investigate the effect of gel mechanics on 3D vascular tubulogenesis[82]. They observed significant increases in mean tube length, mean tube area, and percent of area covered by capillary-like structures with decreasing hydrogel viscoelasticity.

2.6 New HA scaffold syntheses

Numerous HA modifications and crosslinking schemes have been developed and used to form HA hydrogel scaffolds. Some of these methods are highlighted in other comprehensive review articles[11,83]. We would like to report here recent and intriguing scaffold formation chemistries (Figure 2.1D).

Several novel strategies to synthesize HA hydrogels have employed click chemistry as the crosslinking mechanism, since such reactions generally demonstrate high specificity and are unreactive with other functional groups that may be present in the reaction environment. One such synthesis that was developed relies on a Diels-Alder click reaction between a furan-modified HA molecule and a bis(maleimide) PEG crosslinker. Because the functional groups here are not self-reactive, the overnight reaction proceeds in a cleaner fashion and the end crosslinked product is much more predictable[84]. Another study utilized click chemistry between HA and chondroitin

sulfate modified with 11-azido-3,6,9-tri-oxaundecan-1-amine and propiolic acid-modified gelatin, catalyzed by Cu(I)[85]. A third study investigated using oxime chemistry to create injectable hydrogels. HA that was previously oxidized with $NaIO_4$ to form aldehyde groups was then reacted with the crosslinker four-armed aminooxy-PEG (AO-PEG) to form oxime bonds[86,87]. As the reaction is acid-catalyzed, *in vitro* gelation is tunable, and *in vivo* gelation was achieved within 20 minutes after injection.

With the objective of developing a more clinically translatable product, a novel HA-blood hydrogel was synthesized for stem cell transplantation. Lysed whole blood was used as a crosslinker for reaction with N-hydroxysuccinimide (NHS)-modified HA[88]. The NHS groups react with primary amines found in whole blood to form hydrogels that would be able to be used to encapsulate stem cells. Blood was utilized as a crosslinker because of its ease of acquisition in the clinical environment and also because of the presence of fibronectin, vitronectin, and various growth factors in blood. The HA-blood hydrogel stiffness was tunable depending on the amount of blood used, and both cultured cell viability and proliferation after one week was higher than in HA-PEG hydrogels.

While most HA hydrogel-forming chemistries today rely on reactions between reactive functional groups, one study developed a novel strategy relying on strong and selective supramolecular interactions using natural receptor-ligand pairs to mimic traditional crosslinking[89]. Specifically, the investigators formed hydrogels by the binding of cucurbituril-conjugated HA to diaminohexane-conjugated HA, bypassing the relative instability and possible toxicity of the usage of some functional groups.

2.7 Conclusion and future directions

Hyaluronic acid hydrogels have been widely engineered and researched for their biocompatibility as well as the ability to incorporate a wide variety of cues to modify cell-material interactions and ultimately to influence and to allow for greater control over the behavior of cells. Recent studies have shown that incorporating various chemical, mechanical, and spatial cues can lead to a tuned individual cell as well as multicellular response, and in some cases, a cell-specific response. New and interesting HA hydrogel syntheses show potential in higher and cleaner reaction specificity. In addition, being able to control other HA gel-specific cellular functions not previously mentioned above, such as cell-mediated hydrogel degradation, is useful in designing a system with a multi-pronged approach and application[90]. As research in HA hydrogels continues to move forward, more intelligent and cleaner systems with a clearer, more cell-directed purpose will be developed.

III Non-viral gene delivery from hydrogel scaffolds for tissue repair

3.1 Introduction

Tissue regeneration following disease or injury may require exogenous inputs to augment natural healing programs and suppress inhibitory processes. Given the essential role that the extracellular matrix (ECM) has in maintaining the physiological stability of the microenvironment and guiding tissue-specific function, biomaterial scaffolds have been employed in promoting tissue regeneration. Hydrogels, a class of biomaterial scaffolds, are highly hydrated crosslinked polymer networks that have been constructed from a wide range of both naturally and synthetically derived polymers[39,91–93]. Several key characteristics of hydrogels make them particularly well suited for tissue regeneration applications, namely their biocompatibility[94–96]; their permeability to oxygen, nutrient growth factors, and metabolic waste[97,98]; their tunable mechanical properties[99–101]; and their tissue-like viscoelastic characteristics[102,103].

While hydrogel designs largely depend on the location of implantation (e.g. tissue type to be repaired), several design parameters can be manipulated to mimic the native ECM and

consequently function to promote new tissue formation. On the most fundamental level, hydrogels should define a three-dimensional (3D) space for tissue formation, as the 3D architecture can support the infiltration and assembly of host cells into structures and induce gene expression programs associated with normal growth or development. Cell seeding and infiltration of the hydrogel scaffold can be facilitated by micron-scale porosity and/or cell-mediated degradation cues introduced into the hydrogel design. Furthermore, ECM derived adhesion peptides, ECM protein fragments or native ECM proteins can promote cell adhesion leading to a number of specific cell processes such as vascularization, bone regeneration, or the creation of a tissue-specific niche. Trophic factors may also be necessary within the environment to drive cellular responses leading to tissue formation. Localized and sustained release of trophic factors from biomaterials has been a research focus for nearly 20 years[104,105], yet substantial challenges remain regarding formulations that retain activity without developing immune responses[106]. Alternatively, the delivery of gene therapy vectors encoding for trophic factors or other tissue inductive factors may avoid some of the challenges associated with protein delivery while providing the opportunity for sustained and localized availability of the factor. Finally, tissue engineering and regenerative medicine appears to be crossing a tipping point with investments in industry and an increasing number of products and clinical trials. For translational purposes, the approach should consider manufacturing issues such as availability, reproducibility, processing strategies and generally the issues that will be needed for FDA regulatory approval and commercial viability. Here, we discuss the challenges and progress in the incorporation of non-viral vectors within hydrogels to induce the expression through bioactive cues that promote tissue repair. We focus on non-viral approaches due to the greater flexibility in vector design and refer interested readers to excellent reviews on viral vector delivery from biomaterials[107,108].

The delivery of proteins has been employed to augment pro-repair mechanisms; however, to date, protein delivery for tissue regeneration applications has seen limited success despite several clinical trials, where most success has been observed with decellularized matrices. Therefore, alternative approaches to induce gene expression programs associated with normal growth or development are needed. One such approach is to target gene expression directly through the delivery of genes. In this approach, genes encoding for key transcription, tropic, or growth factors would be delivered from the scaffold to transfect transplanted or host cells, which would in turn express the delivered protein. This strategy has the potential to provide more control over the duration of expression, the activity of the delivery protein, and the delivery of multiple signals from the same hydrogel. Furthermore, the use of non-viral approaches avoids safety concerns surrounding the use of viral vectors, including immunogenicity associated with repeated injections and insertional mutagenesis[109]. However, it has been difficult to translate non-viral vectors to the clinical stage, mainly due to the primary challenge of achieving sufficient transgene expression to elicit a significant therapeutic response.

Local gene delivery through implantable or injectable hydrogels has been investigated in two different manners---either as a depot which houses plasmid DNA for sustained release into surrounding tissue[110] or as a DNA-loaded biomimetic scaffold that encourages cellular infiltration into the scaffold. In this second approach, cells infiltrate and degrade the scaffold, leading to transfection and local expression of the therapeutic gene. In general, the same scaffold design principles used for cell delivery can apply for gene delivery. In addition, the development of DNA-loaded hydrogels must take into account the plasmid components, hydrogel properties that affect DNA loading and release, and the interactions between cells and the scaffold which affect gene transfer, with the ultimate goal of promoting effective transgene expression and a therapeutic

benefit.

3.2 Plasmid design

Not surprisingly, the design of the plasmid has significant impact on the level and duration of the resulting transgene expression and the therapeutic response of the expressed protein. Aside from designing the recombinant protein to be expressed, other elements of the expression cassette, such as the promoter and mRNA stabilization elements, are critical for effective, controlled, and long-lasting expression.

The selection of the transgene to be delivered is highly dependent on the target regenerative process. From the first report of hydrogel scaffold-mediated non-viral gene delivery *in vivo* in 1996 to date, it can be noted that most reported regenerative medicine strategies have delivered genes encoding for native-form secreted growth factors that are functional in the extracellular microenvironment, primarily targeting bone and vessel regeneration strategies (Table 2). While some of these studies have resulted in significant therapeutic responses, there is still much room for improvement in terms of transgene selection as well as of transgene optimization via engineering to enhance its potency. In fact, out of these studies, only one has delivered a gene encoding for a protein other than a growth factor[111]. Given the ease of diffusion of growth factors away from the target site, more investigation should be placed in delivering genes encoding for proteins which are active intracellularly in order to enhance the potency of what is delivered. Furthermore, this study also delivered a hypoxia-insensitive variant of transcription factor hypoxia-inducible factor 1-alpha as opposed to its native form, demonstrating the potential to enhance the potency of therapeutic genes through engineering[111].

Gene delivered	Year	Scaffold material	Delivery strategy	Target	Ref.
Bone morphogenetic protein (BMP)-4 and parathyroid hormone	1996	Collagen	naked	Bone regeneration	[112]
Parathyroid hormone	1999	Collagen	naked	Bone regeneration	[5]
Hypoxia-inducible factor-1α (HIF-1α)	2006	fibrin	DNA/PLL	Vessel formation	[111]
Vascular endothelial growth factor (VEGF)	2009	Collagen	DNA/TMC	Vessel formation	[113]
VEGF	2010	Collagen-chitosan	DNA/TMC	Vessel formation	[114]
Fibroblast growth factor-2, BMP-2	2012	Gelatin, collagen	PEI-linoleic acid	Bone regeneration	[115]
Platelet-derived growth factor (PDGF)	2014	Collagen	DNA/PEI	Bone regeneration	[116]
VEGF	2014	HA	DNA/PEI	Vessel formation (wound healing)	[117]
VEGF	2015	HA	DNA/PEI	Vessel formation (wound healing)	[118]

Table 3.1: Inductive hydrogel scaffold-mediated delivery of therapeutic genes *in vivo*.

In addition to the target gene itself, other elements in the expression cassette such as promoters and post-regulatory elements can also control the transgene expression profile and therapeutic response. The magnitude of transgene expression from various constitutive and inducible promoters can vary widely both in comparison to one another and in different cell lines, suggesting that much attention should be placed in promoter selection[119]. Attention to these differences is needed in *in vivo* scaffold-mediated gene delivery applications as well, as demonstrated by a study which compared elongation factor 1-alpha, ubiquitin C, and cytomegalovirus (CMV) promoters in driving transgene expression from a scaffold *in vivo*[120]. In

particular, while the CMV promoter is a commonly used constitutive promoter in mammalian gene expression, it is known to exhibit methylation, resulting in transcriptional silencing in mammalian systems[121]. Furthermore, the development of hypoxia-inducible promoters to control gene expression in ischemic environments is particularly relevant to tissue regeneration applications[122]. Cell- or tissue-specific promoters may also be considered, especially with respect to the types of cells infiltrating the scaffold or being transplanted with the scaffold. Lastly, post-regulatory elements such as WPRE can also be added to the expression cassette to enhance mRNA stabilization to result in enhanced and longer expression[123].

Another source of transcriptional silencing in transgene expression in mammalian systems due to DNA methylation is the presence of elements of bacterial origin, namely CpG motifs in commonly used plasmid vectors. The use of minicircle vectors, which are circular DNA molecules free of any sequences of prokaryotic origin and typically only consist of the expression cassette, instead of conventional plasmids may enhance expression magnitude and duration *in vivo* in scaffold-mediated delivery[124]. These constructs eschew the risk of immunogenic responses to material of bacterial origin, therefore resulting in reduced inflammation and the avoidance of transgene silencing through methylation of bacterial motifs[125,126]. Scaffold-based and systemic administrations of minicircle DNA have resulted in enhanced and prolonged transgene expression *in vivo*[127,128].

3.3 Gene carrier considerations and loading of DNA therapeutics into hydrogel scaffolds

Many DNA delivery systems have been developed for systemic administration, including delivery of naked DNA or packaging the DNA using a gene carrier into a nanostructure. Such carriers may include cationic polymers which interact with the negatively charged DNA to form

nanoparticles called polyplexes, lipids to form liposomes or lipoplexes, or niosomes to form nioplexes, all of which generally significantly enhance the uptake of DNA compared to using naked DNA, resulting in greater transgene expression. For a more thorough survey of advances in developing non-viral gene carriers, we direct readers to this review[129]. However, delivering DNA as a therapeutic from hydrogel scaffolds for regenerative medicine applications concerns the local, not systemic, delivery of this therapeutic, and the design of such strategies present their own challenges and constraints. One key parameter in facilitating cell access to encapsulated DNA in the hydrogel is the cell-mediated degradation of the hydrogel by both infiltrating and transplanted cells to release and allow access to the loaded DNA. In fact, transgene expression in cells cultured in a hydrogel scaffold has been shown to be dependent on the rate of hydrogel degradation[130]. Challenges of loading DNA into hydrogel scaffolds are largely dependent on the delivery vehicle and physical nature of the final delivery formulation. Below we describe unique challenges posed by the loading of naked and condensed plasmids into hydrogel scaffolds.

3.3.1 Naked plasmid

The incorporation of naked plasmid is relatively straightforward, as the plasmid can be directly encapsulated within the hydrogel matrix during synthesis or *in situ* injection. Some of the earliest scaffolds developed for gene delivery, termed "gene-activated matrices", combined plasmid DNA solution at high concentrations (about 1 mg DNA per scaffold) with neutralized collagen before freezing and lyophilization to form a DNA-loaded collagen scaffold[5]. The plasmid is relatively robust and these naked encapsulation approaches have resulted in a positive therapeutic effect *in vivo*. Although large quantities of naked DNA are required to observe gene transfer *in vivo*, gene transfer is observed yielding high levels of transgene expression. However,

there are several limitations that have limited the translation potential of naked DNA-loaded scaffolds. First, bacterial unmethylated CpG motifs present in naked plasmids are recognized by Toll-like receptor-9, resulting in a strong immunogenic response[131,132]. Given that large quantities of DNA are needed to achieve high transgene expression, this immune response is problematic. Furthermore, naked plasmids are easily degraded by serum nucleases, limiting the long-term efficacy of the delivered plasmid[133]. Lastly, naked plasmids do not result in visible transfection *in vitro*, leaving all testing to be done *in vivo*.

3.3.2 Condensed plasmid using cationic polymer- and lipid-based gene carriers

In an effort to overcome the limitations associated with naked DNA, plasmids are commonly condensed with gene carriers into nanoparticles that result in enhanced transgene expression due to facilitated transport, protects the DNA from serum nucleases[133], and can transfect cells both in vitro and in vivo. However, the materials used to condense DNA are typically highly positively charged, resulting in nanosized aggregates that are prone to aggregation, especially at the concentrations required for incorporation into a hydrogel material. DNA can be complexed with cationic polymers to form polyplexes or lipid-based polymers to form lipoplexes or nioplexes. There are two general methods to incorporate condensed DNA into hydrogel scaffolds: surface coating and encapsulation.

Surface coating of condensed DNA relies on electrostatic interactions between the polyplexes and the scaffold material. Such methods often involve incubating a porous scaffold in a solution rich in condensed DNA before washing the scaffold to remove unbound particles[134–136] or hydrating a lyophilized hydrogel in a condensed DNA solution[113,114,116,137].

Encapsulating condensed DNA within hydrogels by mixing the condensed DNA into the gel precursor solution before crosslinking. The Shea lab has encapsulated lipoplexes in PEG and

fibrin hydrogels for *in vitro* cell culture[130,138] and coated PLG scaffolds with lipoplexes for *in vivo* delivery to a spinal cord injury site[139]. More recently, nioplexes, which are similar vesicular particles formed from an aminolipid and a non-ionic surfactant complexed with a nucleic acid, have been encapsulated in methylcellulose and carrageenan hydrogels, demonstrating 80% release of nioplexes over 30 hours[140]. Released nioplexes were able to transfect plated HeLa cells to induce gene silencing upon delivery of anti-sense oligodeoxynucleotides and transgene expression upon delivery of pGFP plasmid. Another recent study used PEI along with graphene oxide nanosheets to form nanoparticles with DNA encoding for VEGF and then encapsulating in a methacrylated gelatin hydrogel improved cardiac outcomes after implanting in a myocardial infarction model[141].

However, encapsulation poses an obstacle due to the tendency of polyplexes, lipoplexes, and nioplexes to aggregate at higher concentrations as they are incorporated into hydrogels; as a result, many studies have only been able to load lower concentrations of condensed DNA[7,71,111,142,143]. PEGylating the cationic polymer to reduce surface zeta potential of polyplexes has been demonstrated as one way to decrease aggregation of polyplexes in hyaluronic acid hydrogels, though at the expense of gene transfer efficiency[136]. The Segura lab has also previously developed an approach for concentrated loading of polyplexes called caged nanoparticle encapsulation (CnE) in which polyplexes are formed at low concentrations but lyophilized in the presence of agarose and sucrose to mitigate these charge-based interactions and to preserve particle integrity during the lyophilization before resuspending in low volumes of buffer[12,71]. This technique has been used to incorporate polyplexes into porous hyaluronic acid hydrogels produced using a sphere templating method and tested in a mouse wound healing model for in vivo gene transfer[117,118]. Similarly, trehalose, another saccharide, can also be used in the lyophilization process to preserve the stability and activity of polyplexes[144].

3.3.3 Dependence of gene transfer on cell-scaffold interactions and cytoskeletal mechanics

Cell interactions with the composition and mechanical properties of the matrix substrate have also been shown to modulate gene transfer, presenting opportunities to design scaffolds that enhance transfection. In addition to determining proliferation, migration, and differentiation behaviors of cells, substrate stiffness plays an important role in modulating gene transfer, with transgene expression increasing as a function of substrate stiffness in 2-D cell culture[145]. However, in 3-D culture of encapsulated cells and polyplexes in hyaluronic acid hydrogels, the inverse result was observed, with transgene expression increasing with decreasing hydrogel stiffness. This difference in outcomes is likely due to the dependence of cell proliferation and migration as well as polyplex release on the degradability of the hydrogel. This finding suggests that the efforts in designing biomaterials for gene delivery purposes should also take stiffness into consideration. In addition, surface charge and chemistry influence transfection efficiency, with cells cultured on charged hydrophilic surfaces with carboxyl groups exhibiting increased transfection and cells on uncharged methyl-coated surfaces showing decreased transfection[146]. Lastly, topography was also found to influence lipoplex-mediated transfection efficiency, with cells cultured on nanopillar-coated surfaces observing highest level of transfection compared to blank and micropillar-coated surfaces[147].

Matrix composition can directly determine the efficiency of gene transfer through pathways related to integrin-mediated cell adhesion. For cells seeded in two dimensions, increasing concentrations of the RGD cell adhesion peptide leads to increases in transgene transfer and expression, while an increase in the physical spacing of the ligand on a substrate resulted in decreased transgene expression[53]. However, in cells cultured in three dimensions in a nonporous hyaluronic acid hydrogel, an intermediate RGD concentration of 100 μM and clustering ratio of

0.4 mmol RGD/mmol HA resulted in the highest levels of transfection[18]. However, these effects on both cell behavior and transfection efficiency are specific to cell type and require optimization for the transplanted cell type or for the expected range of cell types of infiltrating cells. Different ECM components as substrates also have varying effects on gene transfer. For example, in mouse mesenchymal stem cells administered a bolus polyplex transfection, collagen I-coated surfaces inhibit gene transfer, while fibronectin-coated surfaces enhance gene transfer, and different ECM substrates trigger different internalization pathways by which polyplexes are trafficked into the cell[148]. A separate study showed that mouse fibroblasts exhibited increased gene transfer on surfaces coated with fibronectin over collagen in surface-mediated transfection in which polyplexes were coated on the substrate, but the inverse effect was found upon bolus polyplex administration[149]. Cell culture on surfaces coated with the $\alpha_5\beta_1$ integrin-binding domain of fibronectin resulted in significantly enhanced expression due to polyplex-mediated transfection compared to cell culture on surfaces coated with a polymer of similar charge but lacking in cell-binding domains, suggesting that the bioactive integrin-binding function of ECM components are at least partially responsible for such effects[150].

A better understanding of the mechanisms which govern gene transfer may lend insight on how to design more effective scaffold-mediated gene delivery methods. A study has elucidated the mechanisms by which cytoskeletal dyanamics and RhoGTPases control gene transfer and trafficking of polyplexes; introducing bioactive signals to manipulate these pathways may be a method of enhancing gene transfer[151]. For example, in a separate study, the inhibition of polo-like kinase-1 (PLK1) was identified as a means of enhancing gene transfer[152]. Microarray analysis has also been used to reveal genes which are upregulated in transfected cells as compared to non-transfected cells using both polyplexes and lipoplexes; notable targets include genes involved in

integrin-mediated signaling, cytoskeletal mechanics, and membrane trafficking[153–155]. However, it is important to note that different mechanisms govern gene transfer in 2-D culture versus in 3-D hydrogel-supported cell culture, suggesting the importance of more thorough studies in studying how a particular scaffold design influences gene transfer through cell-matrix interactions[156].

IV Encapsulation of PEGylated polyethyleneimine polyplexes reduces aggregation in hyaluronic acid hydrogels

4.1 Introduction

Scaffolds for tissue repair aim to promote the repair of diseased or injured tissues through the use of a biocompatible material that support cellular infiltration and contain bioactive signals that guide invading cells through tissue formation[157,158]. Because cells can sense and respond to mechanical properties of their environment, a general approach to designing a scaffold for tissue engineering is to choose a material that mimics the extracellular matrix and provides structural support that can resist tensile and compressive stresses[159]. In addition to the structural characteristics of the scaffold, the effective delivery of bioactive signals is necessary to induce regeneration. Delivery of growth factors from scaffolds is a commonly utilized approach; however, encapsulation or incorporation of growth factors into scaffolds can often result in protein denaturation or degradation and the delivery method must be optimized for each protein[160]. An alternative approach in guiding cellular response is through DNA delivery. Naked DNA delivery

has been shown to achieve transgene expression and guide regeneration in vivo[5,6], but often results in poor delivery efficiency because the plasmid's negative charge and large hydrodynamic radius triggers plasmid degradation, ineffective internalization and trafficking by the cell and induces immune responses due to the bacterial elements of the plasmids[7]. This motivated the use of encapsulated DNA inside nanoparticles as a means to improve DNA stability, delivery, intracellular trafficking and reduce immune interactions with the host. Cationic polymers are one type of DNA encapsulation approach that is commonly used. Through charge interactions of the positively charged polymer (amines) to the negatively charged DNA (phosphates) an aggregate forms (polyplex) that can protect the DNA from degradation and improve delivery. Poly(ethylene imine) (PEI) is one such cationic polymer that has been shown to successfully transfect cells both *in vitro* and *in vivo* and serves as the gold standard for non-viral gene delivery[161].

We have been interested in incorporating PEI/DNA polyplexes inside hyaluronic acid (HA) hydrogel scaffold to guide soft tissue repair. HA is an anionic, non-sulfated polysaccharide that is widely distributed throughout the ECM of connective tissues[9]. HA is an exciting scaffold candidate for tissue engineering therapies due to its high biocompatibility and low immunogenicity[7,80,162]. HA interacts with CD44, RHAMM, and ICAM-1 surface receptors that contribute to cell proliferation and migration, which are processes that are necessary for tissue regeneration to occur[163,164]. Moreover, HA chains have been known to promote matrix metalloproteinase (MMP) expression[165–167]. MMPs are typically present in high concentration as diseased sites and are upregulated in tissue repair and microenvironment remodeling and can therefore serve as a trigger for bioactive signal delivery[168,169].

Semi-synthetic HA hydrogels, which can be degraded my matrix metalloproteinases (MMPs) and hyaluronidases, have been previously developed for culturing stem cells in

3D[142,170,171]. Although we have previously demonstrated the ability to deliver DNA-PEI polyplexes from HA gels, direct polyplex encapsulation resulted in aggregation when concentrations exceeding 0.3 μg/μL[71]. To mitigate this issue, Lei *et al*. developed a caged nanoparticle encapsulation (CnE) technique that utilized neutral saccharides (sucrose) and polysaccharides (agarose) to protect the polyplexes from inactivation and aggregation during hydrogel formation, respectively[12,71]. This technique was coupled with the introduction of micron-sized pores within gels in an attempt to promote increased cell migration and infiltration to the scaffold. Although gene delivery was achieved both in vitro and in vivo, transgene expression levels remained low[72,117,118]. We hypothesize that CnE and acetone processing during micron-size pore hydrogel formation, which causes an increase in gel stiffness, reduces pore size, resulting in a slower rate of gel degradation and polyplex release.

In order to maintain high DNA loading concentrations in HA gels without using CnE, it is necessary to overcome aggregation issues that occur during gelation and at high DNA polyplex concentrations. Herein, we present an approach to prevent polyplex aggregation within porous HA hydrogels. This approach utilizes polyethylene glycol modification of PEI to mitigate charge-charge interactions between polyplexes and the scaffold (sPEG-PEI) (Figure 4.1A).

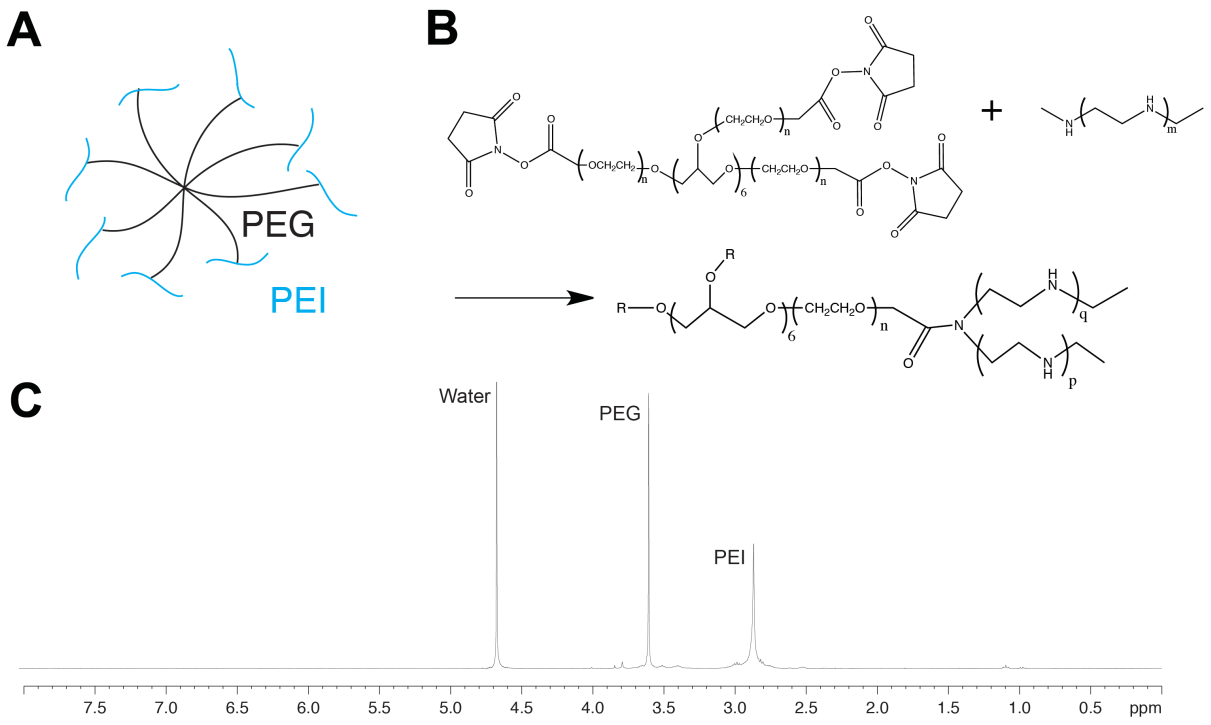

Figure 4.1: sPEG-PEI chemistry.
Schematic of PEI conjugated to 8-arm PEG (sPEG-PEI) (A). Reaction scheme of sPEG-PEI synthesis (B). ^{1}H-NMR spectra of sPEG-PEI (C).

4.2 Materials and Methods

4.2.1 Materials

Peptides Ac-GCRDGPQGIWGQDRCG-NH_2 (HS-MMP-SH) and Ac-GCGYGRGDSPG-NH_2 (RGD) were purchased from Genscript (Piscataway, NJ). Sodium hyaluronan (HA) was a gift from Genzyme Corporation (60 kDa, Cambridge, MA). High molecular weight linear poly(ethylene imine) (LPEI, 25kDa) and low molecular weight linear poly(ethylene imine) (LMW-PEI, 2.5kDa) were purchased from Polysciences (Warrington, PA). 8-arm poly(ethylene gycol) succinimidyl carboxyl methyl ester (PEG-SCM, 10kDa) was purchased from Creative PEGWorks (Winston Salem, NC). Vectors for the mammalian expression of Gaussia luciferase (pGluc) and secreted embryonic alkaline phosphatase (pSEAP) were purchased from New England

Biolabs (Ipswich, MA) and BD Biosciences (San Jose, CA), respectively. Both vectors were expanded using a Giga Prep kit from Qiagen (Valencia, CA) per manufacturer's protocol. All other chemicals were purchased from Fisher Scientific (Pittsburgh, PA) unless otherwise noted.

4.2.2 Synthesis of sPEG-PEI

LMW-PEI was conjugated to the 8-arm PEG-SCM to using amine to carboxylic acid chemistry. LMW-PEI (190.8mg, 0.07632 mmol) was dissolved in MES buffer (100uM, pH 5.5), and once fully dissolved the pH was increased to 7.4. After the PEI had fully dissolved, 50 mg of PEG-SCM (0.00477mmol) was dissolved in separate MES buffer pH 7.4. The PEG-SCM solution was added dropwise to the PEI solution while maintaining a constant pH, and the mixture was allowed to react overnight. The product was purified by dialysis (10,000 MWCO) against water for five days with two water changes per day to remove any unreacted PEI, and the product was analyzed using ^{1}H-NMR (D_2O). ^{1}H-NMR (D_2O) spectroscopy indicated attachment of PEI to every arm of the 8-arm PEG-SCM by assessing the ratio of the PEI peak ($\delta = 2.85$) to the PEG-SCM peak ($\delta = 3.6$).

4.2.3 Polyplex formation and characterization

To form polyplexes, 3 μg of plasmid DNA was diluted in 150 μl of nuclease free water and the desired amount of either LPEI or sPEG-PEI, depending on the required N/P ratio (ratio of the number of nitrogen groups on the polymer to the number of phosphate groups on the DNA backbone), was diluted into a separate 150 μl of nuclease free water. For polyplexes formed at N/P 7, 4 μg sPEG-PEI was used and 2.73 μg LPEI was used. For polyplexes formed at N/P 12, 6.87 μg sPEG-PEI was used and 4.69 μg LPEI was used. The PEI solution (either LPEI or sPEG-PEI) was drop wise added to the DNA while vortexing, and each sample was incubated at room temperature for 15 min. 150mM NaCl or PBS was then added to each polyplex solution and the size and ζ-

potential of the polyplexes were determined by photon correlation spectroscopy (Malvern Zetasizer, Malvern Instruments Ltd., U.K.). The measurements were performed at 25°C.

4.2.4 Agarose gel retardation assay

An agarose hydrogel retardation assay was performed in order to assess the N/P ratio at which the polyplexes are fully condensed. Polymer/pDNA complexes were prepared at N/P ratios 1-7 in nuclease free water per the aforementioned protocol, with naked DNA containing no polymer as the control. The polyplexes were electrophoresed through a 1% (w/v) agarose hydrogel containing a 1/10,000 dilution of SYBR® Safe DNA Stain (Life Technologies, Grand Island, NY) in 1X Tris-acetate-EDTA (TAE) buffer at 80 V for 30 min. The hydrogel was then analyzed on a Hydrogel Doc EZ Imager (Bio Rad, Hercules, CA) to observe the fluorescence of each polyplex relative to naked DNA.

4.2.5 Cell culture

HEK293T cells were a kind gift from Lonnie Shea of the University of Michigan, and HEK293T-MMP2 cells were a kind gift from Jeffrey Smith from the Burnham Institute for Medical Research. Mouse-bone-marrow-derived mesenchymal stem cells (D1, CRL12424) were purchased from ATCC (Manassas, VA). HEK293T, HEK293T-MMP2, and D1 cells and cultured in Dulbecco's modified Eagle medium (DMEM) (Invitrogen, Grand Islands, NY) supplemented with 10% bovine growth serum (BGS, Hyclone, Logan, UT) and 1% penicillin/streptomycin (Invitrogen) at 37°C and 5% CO_2. The cells were passaged using trypsin following standard cell culture protocols every 2-3 days.

4.2.6 Cytotoxicity of sPEG-PEI and LPEI polyplexes

An MTT assay (CellTiter 96^{R} AQ_{ueous} One Solution Cell Proliferation Assay, Promega, Madison, WI) was used to quantify the metabolic activity of cells exposed to sPEG-PEI or LPEI

polyplexes in order to correlate metabolic activity to cell viability. 12,000 D1 cells were cultured in a 96-well plate for 16 hours, then transfected with 20 μL of either sPEG-PEI or LPEI polyplexes at DNA concentrations ranging from 0-0.2 μg/μL and N/P ratios 7 and 12. After a 2 day incubation, the media in each well was aspirated and cells were then incubated with 20 μL of MTT reagent and 100 μL of DMEM for 2 hours at 37°C. Following the 2 hour incubation, 25 μL of 10% sodium dodecyl sulfate was added to each well to stop the reaction, the solutions were transferred to a new plate, and the absorbance was measured at 490 nm using a standard plate reader.

4.2.7 In vitro 2-D bolus transfection

To assess the tranfection efficiency of sPEG-PEI compared to LPEI, pGluc or pSEAP polyplexes of N/P ratios 7 and 12 were created using both polymers. D1 cells were seeded on a 48-well plate at a density of 40,000 cells/well in 500 μL of media, and allowed to incubate for 16 hours. Following this incubation, the media from each well was removed and replaced with fresh media. 50 μL of polyplex solution (0.02 μg DNA/μL in 150 mM NaCl) was added to each well. The cells were allowed to incubate for 2 days, after which the media was collected and frozen at -20C until assayed. To quantify secreted Gaussia luciferase levels in the media, the samples were thawed on ice and assayed using a BioLux Gaussia Luciferase Assay Kit (New England Biolabs, Ipswich, MA) as per the manufacturer's protocol. Briefly, 20 μL of each sample were mixed with 50 μL of substrate solution, pipetted for 2 to 3 seconds to mix, and read for luminescence with a 5 s integration time using a Modulus Fluorometer (Turner BioSystems, South San Francisco, CA). To quantify secreted embryonic alkaline phosphatase levels in the media, the samples were thawed on ice and assayed using a pSEAP Assay Kit (Life Technologies, Grand Island, NY). Briefly, 100 μL of sample was incubated with 200 μL of dilution buffer and incubated at 65°C for 30 min. 100 μL of the diluted sample was then mixed with 100 μL of assay buffer and incubated for 20 min.

100 μL of reaction buffer was then added to each sample, incubated for 20 min, and samples were read for luminescence with a 1 s integration time.

4.2.8 Internalization of DNA over different periods of polyplex exposure

D1 mouse mesenchymal stem cells were seeded in a tissue culture-treated 48-well plate at a seeding density of 20,000 cells per well 16 h prior to transfection. 1.25 μg plasmid DNA was radiolabelled with ^{32}P-dCTP (250μCi, PerkinElmer, Waltham, MA) using a Nick translation kit (Roche, Indianapolis, IN) according to the manufacturer's protocol. The reaction mixture was purified using the DNA Clean and Concentrator kit from Zymo Research (Irvine, CA) and mixed with 498.75 μg non-radiolabelled DNA to make a 0.25% "hot" plasmid DNA solution. Polyplexes were then formed with the radiolabelled DNA and either sPEG-PEI or L-PEI at N/P ratios of 7 and 12. 1 μg of DNA's worth of polyplexes was added to each well and incubated at 37C for 2, 4, 8 h. At each of the timepoints, the cells were washed with PBS + $CaCl_2$, CellScrub buffer (Genlantis, San Diego, CA) to remove any un-internalized polyplexes, and then PBS twice before trypsinizing. The cells were then harvested and added to 2 mL Bio-Safe II scintillation cocktail (Research Products International Corp., Mt. Prospect, IL) and measured using a scintillation counter at the UCLA chemistry facility. The readout was analyzed using a standard curve.

4.2.9 Internalization of DNA and transgene expression under inhibition of endocytosis pathways

D1 cells were seeded in a tissue culture-treated 48-well plate at a seeding density of 20,000 cells per well 16 h prior to treatment. Clathrin-mediated endocytosis was inhibited with 10 μg/mL chlorpromazine (Fisher Scientific), caveolae-mediated endocytosis with 200 μM genistein (Sigma Aldrich, St. Louis, MO), and macropinocytosis with 100 μM amiloride hydrochloride (Sigma Aldrich, St. Louis, MO), for 1 h at 37C. Polyplexes were formed with either radiolabelled DNA as described above to track cell internalization or pGLuc as described above to assess transgene

expression and added to the wells in the presence of inhibitors for a 4-h incubation. The cells exposed to radiolabelled DNA were then washed with PBS + $CaCl_2$, CellScrub buffer, and then PBS twice before trypsinizing, harvesting, and reading with a scintillation counter as described above. For the pGLuc transfections, the media was replaced with fresh media after 4 h. Gaussia luciferase expression was assayed as described above.

4.2.10 Hyaluronic acid modification

Sodium hyaluronan was modified to contain acrylate function groups via a two-step reaction as previously described[25]. HA (2 g, 60 kDa) was reacted with 36.77 g (211.07 mmol) adipic acid dihydrazide (ADH) at pH 4.75 with 4 g 1-ethyl-3-[3-dimethylaminopropyl] carbodiimide hydrochloride (EDC) overnight. The product was purified through dialysis (8000 MWCO) against a NaCl gradient for 1 day. Further dialysis was done in DI water for 4 days. The purified product HA-ADH was then lyophilized and analyzed with ^{1}H-NMR. All of the HA-ADH was then reacted with 4.46 g N-acryloxysuccinimide (NHS-Ac) in 10mM HEPES, 150mM NaCl, 10mM EDTA at pH 7.4 overnight at room temperature before purification via dialysis against a NaCl gradient for 1 day and in DI water for 4 days. The purified product HA-Ac was then lyophilized and analyzed with ^{1}H-NMR (D_2O). 1H-NMR indicated a 54.67% modification of the carboxyl groups on the HA backbone to ADH groups by taking the ratio of peaks δ = 1.6 and 23, which correspond to the eight H of the methylene groups on the ADH to the singlet peak of the acetyl methyl protins in HA (δ = 1.88). After the second step in which HA-ADH was reacted with N-acryloxysuccinimide (NHS-Ac), ^{1}H-NMR (D_2O) spectroscopy confirmed 11.42% acrylate modification (HA-Ac) by taking the ratio of the multiplet peak at δ = 6.2 corresponding to the acrylate H to the singlet peak of the acetyl methyl protons in HA (δ = 1.88).

4.2.11 Polyplex lyophilization by caged nanoparticle encapsulation (CnE)

For CnE, plasmid DNA (8.3 μg) and either sPEG-PEG or LPEI (13.4 μg or 9.1 μg, respectively) were mixed in 3.5 mL water in the presence of 3.5mg (0.01 mmol) of sucrose (Ultrapure, MP Biomedicals, Santa Ana, CA) and incubated at room temperature for 15 min. Low-melting point agarose (0.1 mg, Ultrapure Agarose, T – 34.5-37.5°C, Invitrogen, Grand Islands, NY) in 150 mL water was added before lyophilization. Each aliquot was intended for a 10 μL hydrogel.

4.2.12 Porous hydrogel design template using PMMA microspheres

Chemically sintered microsphere templates were prepared as previously described[26]. Briefly, polymethyl methacrylate (PMMA) microspheres (53-63 μm, Cospheric, Santa Barbara, CA) were suspended in sintering solution (70% ethanol, 1% acetone) at a concentration of 0.4444mg μL^{-1}, and 75 μL of this bead solution was then added to each well of 6-mm diameter flexiPERM molds (Sigma-Aldrich, St. Louis, MO) adhered to glass slides treated with Sigmacote (Sigma-Aldrich, St. Louis, MO). The molds were sintered at 37°C for 2 hours before use.

4.2.13 Porous and nonporous hydrogel formation and characterization

Porous and nonporous HA hydrogels were prepared as previously described[25]. Hydrogels were formed by Michael-addition of acrylate functionalized HA (HA-Ac) with bis-cysteine containing MMP peptide crosslinkers at pH 7.6-7.8. Prior to the reaction, a hydrogel precursor solution was made by mixing HA-Ac with a lyophilized aliquot of the cell adhesion peptide RGD for 30 min at 37°C. After incubation, HA-RGD was mixed with the remaining HA-Ac and 0.3M triethanolamine (TEOA, pH 8.8), for a final hydrogel concentration of 3.5% weight/volume% HA and 100uM RGD. Finally, lyophilized aliquots of the crosslinker (0.8mg HS-MMP-SH) were

diluted in 16 μL of TEOA buffer, pH 8.2, immediately before addition to the hydrogel precursor solution. This hydrogel precursor solution was then mixed with either lyophilized (CnE) or fresh (direct encaspulation) DNA/polymer polyplexes for hydrogels containing polyplexes. For direct encapsulation, DNA and sPEG-PEI or LPEI were mixed according to the aforementioned protocol. For nonporous hydrogels, 20uL of the hydrogel solution was added between 2 slides with a 1mm spacer to separate the two slides. Hydrogels were incubated at 37°C for 30 min, then hydrated in phosphate-buffered saline (PBS) and left in PBS until used. For the porous hydrogels, 20 μL of the hydrogel solution was then added directly on top of a PMMA microsphere template and perfused into the template by centrifugation at 500 g for 15min at 4°C. The template was then incubated at 37°C for an additional 20 min to induce complete crosslinking. Once complete, the hydrogels were removed from the flexiPERM molds and placed directly into 100% acetone for 48 h to dissolve the PMMA microsphere template. The acetone solution was replaced 3 times a day for the 48 h wash. The hydrogels were then serially hydrated in PBS, and stored in PBS until used.

The storage and loss modulus of nonporous and microporous hydrogels were measured with a plate-to-plate rheometer (Physica MCR, Anton Paar, Ashland, VA) using a 8 mm plate under a constant strain of 0.1% and frequency ranging from 0.1 to 10 rad/s. Nonporous and porous hydrogels were synthesized according the aforementioned protocol and cut to 8 mm using an 8 mm biopsy punch. To prevent the hydrogel from drying, a humidity hood was utilized and the stage was set to 37°C.

4.2.14 Statistical analysis

Statistical analyses were performed using Prism (GraphPad, San Diego, CA). Data were analyzed using a one-way analysis of variance (ANOVA) test followed by a Tukey post-hoc test. The results are presented as mean ± SD. Polyplex size data was analyzed using a t-test, and the

results are presented as mean ± SD. Single, double, and triple asterisks represent $p < 0.05$, $p < 0.01$, $p < 0.001$, respectively. A p value of < 0.05 was considered statistically significant.

4.3 Results and Discussion

4.3.1 sPEG-PEI synthesis

sPEG-PEI was synthesized using the reaction between the activated carboxylic acid in 8-arm PEG-Succinimidyl carboxyl methyl ester (PEG-SCM) and the amines in PEI. Due to insoluble nature of PEI at basic pH, LMW-PEI was first dissolved in acidic conditions and once fully dissolved the pH of this solution was slowly increased to 7.4 in order to prevent precipitation. The extent of conjugation was calculated through NMR by comparing the integration of the observed peaks of LMW-PEI and PEG-SCM at δ=2.85 and δ=3.6, respectively, which indicated that 94.9% of the PEG arms were conjugated with PEI (Figure 4.1C).

4.3.2 Polyplex Characterization

Polyplexes of either sPEG-PEI or LPEI with plasmid DNA were formed at an N/P ratio of 7 and 12 to study the influence of polymer composition on particle size and stability. After the addition of salt to physiological salt conditions, sPEG-PEI polyplexes doubled in size but showed no significant increase in size thereafter until day 5. Conversely, LPEI polyplexes experienced a significant seven-fold increase after the addition of salt, and showed a 130-fold increase from the initial size just after day 1[136]. To assess polyplex zeta potential, sPEG-PEI and LPEI polyplexes were synthesized in either 150 mmol NaCl or PBS solutions. The average charge of sPEG-PEI polyplexes N/P 7 in 150 mmol NaCl and PBS was 10.47 mV and 2.16 mV, respectively, and for polyplexes N/P 12 in 150 mmol NaCl and PBS was 22.17 mV and 5.68 mV, respectively[136]. The average charge of LPEI polyplexes N/P 7 in 150 mmol NaCl and PBS was 25.00 mV and 11.03

mV, respectively, and for polyplexes N/P 12 in 150 mmol NaCl and PBS was 30.43 mV and 12.83 mV, respectively[136].

The efficiency of the polymer/DNA interactions was evaluated by determining the amount of conjugate required to retard the migration of DNA through an agarose gel over a range of N/P ratios 0-7. Complete retardation of sPEG-PEI polyplexes was observed at an N/P ratio of 6 while complete retardation of LPEI polyplexes was observed at an N/P ratio of 4. In addition, the complete shielding of DNA by sPEG-PEI occurs at a higher N/P ratio than by LPEI[136].

These results indicate sPEG-PEI forms a smaller, more stable polyplex when complexed to pDNA compared to LPEI. The charges of the LPEI polyplexes were higher than their relative sPEG-PEI counterparts, which can be attributed to the higher number of nitrogen groups on the LPEI backbone compared to the sPEG-PEI backbone (25.25 nmol N/1 μg LPEI, 15.63 nmol N/1 μg sPEG-PEI). The less charged nature of sPEG-PEI polyplexes may be the reason for smaller particle size upon addition of salt when compared to LPEI polyplexes, which aggregate with a much higher tendency in a highly charged environment. This is an important property difference that we hypothesize may be the underlying reason for differences seen in characterizing polyplex loading in hydrogels as well as in transgene expression profile differences upon transfection. Furthermore, the ability of LPEI to more tightly complex DNA may be due to the higher number of nitrogen groups on the LPEI backbone that can interact with the phosphate groups on the DNA backbone. This is supported by the complete shielding of DNA by LPEI occurring at a lower N/P ratio than by sPEG-PEI. The presence of PEG groups on sPEG-PEI may also interfere with complexation due to steric hindrance.

4.3.3 Cell-polyplex interactions

An MTT assay was performed to compare the toxicity of sPEG-PEI to LPEI polyplexes (Figure 4.2A). Since the concentrations used in this study were high for *in vitro* culture systems, some toxicity was expected. Cells exposed to sPEG-PEI polyplexes of N/P 7 show no decrease in metabolic activity up to 200 ng/μL, while cells exposed to LPEI at N/P 7 had a significant decrease starting at 100ng/mL ($p < 0.001$). Similarly, cell exposed to sPEG-PEI polyplexes at N/P 12 show no decrease in metabolic activity up to 100 ng/μL, while cells exposed to LPEI N/P 12 had a significant decrease starting at 50ng/mL ($p < 0.001$). In addition, cell viability was overall higher with exposure to sPEG-PEI polyplexes than with LPEI polyplexes with equal dosing of DNA, indicating that the administration of sPEG-PEI as a complexing agent may be less cytotoxic than LPEI. Electrostatic interactions between sPEG-PEI and DNA are relatively weak compared to between LPEI and DNA, which may result in more free sPEG-PEI being present in the cellular microenvironment due to more random decomplexation, posing concerns of cytotoxicity. However, sPEG-PEI complexes were less cytotoxic than LPEI complexes.

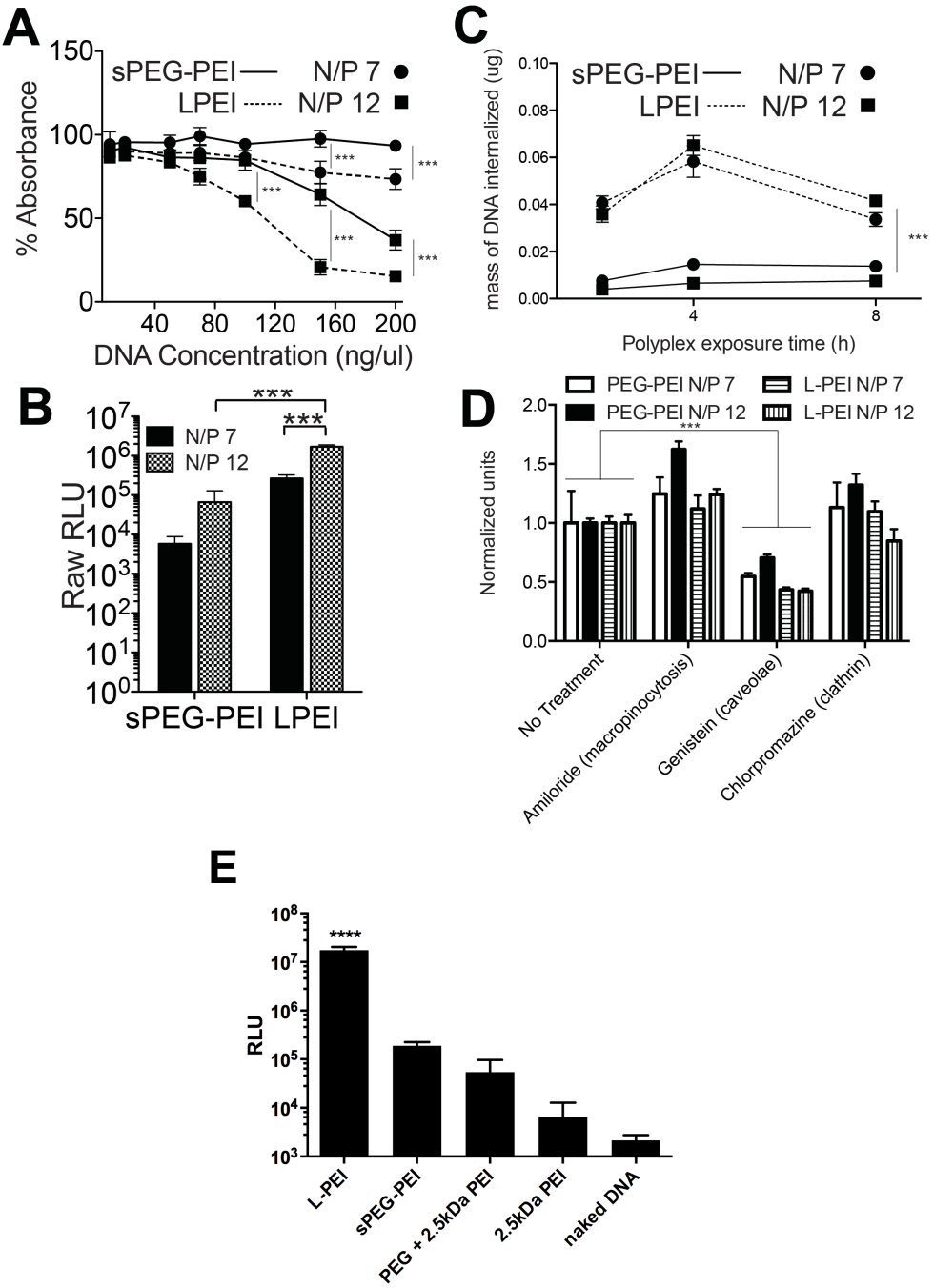

Figure 4.2: Characterization of sPEG-PEI polyplex-cell interactions.
MTT assay assessing cytotoxicity of polyplexes formed with sPEG-PEI and L-PEI (A). Relative GLuc expression after 48 h of a 2-D bolus transfection with polyplexes formed with sPEG-PEI and L-PEI (B). Internalized radiolabelled DNA over different polyplex exposure times (C). Internalized radiolabelled DNA after 4 h exposure to polyplexes with the inhibition of different endocytosis pathways (D). A 2-D bolus transfection was performed on 40,000 D1 cells per well, with GLuc expression assayed at 48 h after initial exposure to conditions. DNA was complexed with LPEI, sPEG-PEI, a simple mixture of nonfunctionalized 8-arm PEG and 2.5kDa PEI, 2.5 kDa PEI, and no carrier (E).

A bolus transfection using the Gaussia luciferase vector was performed to compare the transfection abilities of sPEG-PEI and LPEI polyplexes to D1 cells in 2D. Transgene expression at both N/P 7 and N/P 12 for sPEG-PEI were significantly lower than those for LPEI at the same N/P ratios ($p < 0.001$) (Figure 4.2B). In addition, a control bolus transfection experiment was performed to evaluate the transfection efficiency of a simple mixture of the components of sPEG-PEI (non-functionalized 8-arm PEG and 2.5kDa PEI) compared to the reacted product sPEG-PEI (Figure 4.2E). While not significant, there was an increase in transgene expression with sPEG-PEI compared to the simple mixture, to using 2.5kDa PEI only, and to the use of no gene carrier polymer (naked DNA).

To understand whether the difference in transgene expression between using sPEG-PEI and LPEI polyplexes was due to a difference in the extent of internalization of those polyplexes, D1 cells were plated and transfected over different exposure times using the four different polyplex compositions with radiolabelled DNA to determine how much DNA is being internalized at each time point (Figure 4.2C). It was observed that the mass of DNA internalized when transfecting with LPEI polyplexes was significantly higher over all exposure times than when transfecting with sPEG-PEI. A surprising observation in Figure 4.2C was the drop in internalized DNA at the 8-h time point compared to the 4-h time point when using LPEI as the cationic polymer for complexing. This decrease may suggest substantial amounts of DNA polyplexes that are unable to escape the endosome into the cytoplasm. Instead, this subset of total internalized polyplexes during the first 4 hours was eventually exocytosed.

In addition, to examine whether there is a difference in the dependence of the uptake of the different polyplexes on different internalization pathways, macropinocytosis, caveolae-mediated

endocytosis, or clathrin-mediated endocytosis was pharmacologically inhibited (Figure 4.2D). Dhaliwal et al reported no effects on cell viability after four hours of exposure to each of the inhibitors used in this study, permitting the use of these inhibitors to study internalization after four hours of exposure[148]. When caveolae-mediated endocytosis was inhibited with genistein, the amount of DNA internalized was significantly lower than a no-treatment transfection for both sPEG-PEI and LPEI polyplexes. There was no decrease in amount of internalized DNA observed when macropinocytosis was inhibited using amiloride or when clathrin-mediated endocytosis was inhibited with chlorpromazine with either sPEG-PEI or LPEI-mediated transfection. Within treatments, there was no difference in the relative amounts of DNA internalized among the different polyplex compositions.

These results show that while the use of LPEI as the complexing polymer led to more DNA internalized, there was no difference in the dependence on specific endocytotic pathways for internalization between the two polymers. This suggests that the differences in both the chemical structure of the gene carrier polymers and the physical properties of the DNA polyplexes resulting from those polymers do not affect the dominant internalization pathway involved in polyplex uptake. Instead, this difference in extent of uptake may be due to the difference in surface charge densities of the two types of polyplexes, with the more highly charged LPEI polyplexes electrostatically binding more strongly to the cell membrane to result in higher uptake rates.

4.3.4 Visualization of polyplex aggregation

sPEG-PEI and LPEI polyplexes were incorporated into nonporous and porous hyaluronic acid hydrogels either by surface-association with the pore surfaces or by encapsulation within the gel phase. The storage (*G'*) and loss (*G"*) moduli of the hydrogels were analyzed using a plate-to-plate rheometer. Results showed that the *G'* and *G"* did not cross at any measured frequency (0.1

– 10 Hz) and were frequency-independent for both porous and nonporous hydrogels, both of which are consistent with typical hydrogel characteristics. We reported *G'* of 523 ± 32 Pa and 222 ± 23 Pa for our porous and nonporous hydrogels, respectively. This difference in mechanical stiffness was statistically significant between the two gel types.

To assess aggregation, porous and nonporous hydrogels containing either sPEG-PEI or LPEI polyplexes were stained and imaged (Figure 4.3). Complexing DNA with sPEG-PEI resulted in noticeably less aggregation than with LPEI after encapsulating these DNA polyplexes in both nonporous and porous hydrogels. This observation is consistent with and without the use of the caged nanoparticle encapsulation (CnE) technique. This difference in aggregation behavior may be attributed to the decrease in surface charge density when using sPEG-PEI polyplexes, which may result in a lower tendency for the occurrence of particle-particle charge-based interactions. By using sPEG-PEI polyplexes, it is possible to load DNA into hydrogels via encapsulation at higher DNA loading concentrations when compared to LPEI polyplexes. By surface coating porous hydrogels with either sPEG-PEI or LPEI polyplexes, a more homogenous surface distribution of DNA polyplexes was observed throughout the hydrogel when compared to the aggregation seen in porous hydrogels with encapsulated LPEI polyplexes.

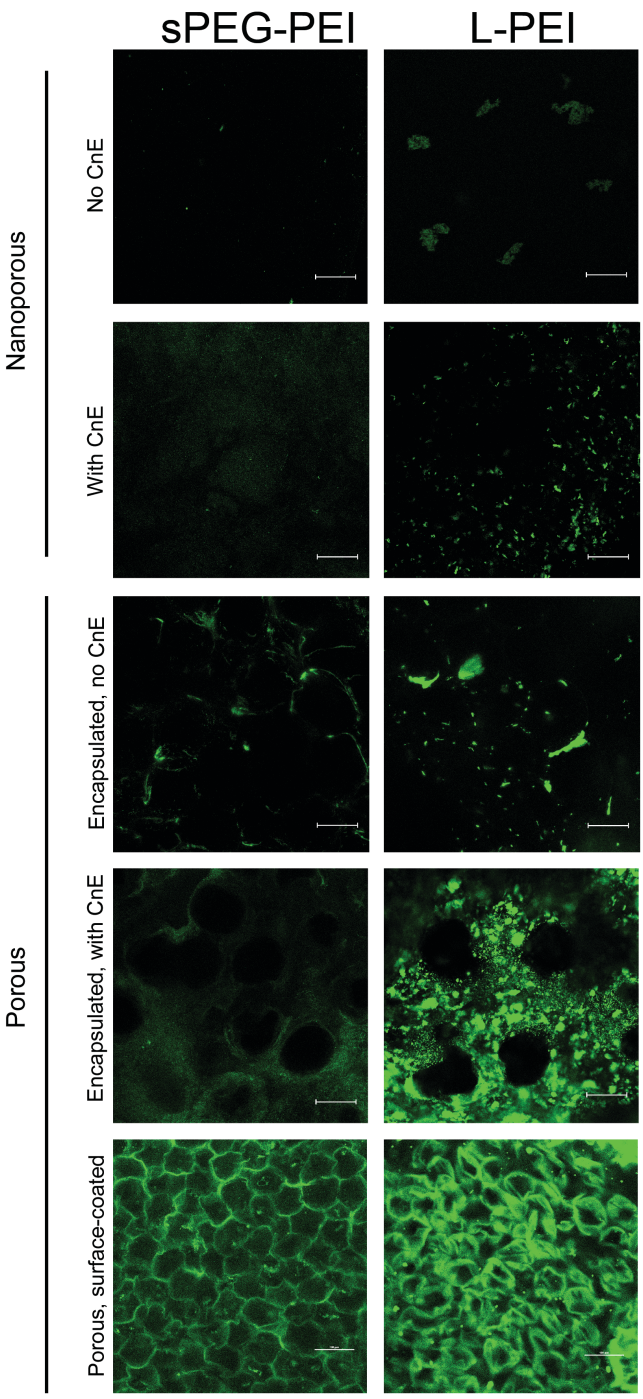

Figure 4.3: Visualization of polyplex aggregation in polyplex-loaded HA hydrogels. Fluorescently labelled DNA polyplexes were incorporated into porous and nonporous hydrogels and imaged.

With results indicating that DNA polyplexes complexed with sPEG-PEI at both N/P ratios of 7 and 12 were less toxic to cells at higher levels of DNA exposure, sPEG-PEI polyplexes can serve as a less toxic alternative to LPEI polyplexes in systems where polyplex toxicity presents issues. In two-dimensional cell culture, it was also seen that while sPEG-PEI polyplexes were less toxic, their usage also resulted in lower levels of transgene expression when compared to LPEI polyplexes at both N/P ratios of 7 and 12. These findings suggest that in order to obtain comparable levels of transgene expression when using sPEG-PEI polyplexes as LPEI polyplexes, it will be necessary to increase DNA polyplex loading concentrations.

4.4 Conclusion

In this study, using PEGylated PEI and surface-coating DNA along pores of porous hydrogels were explored as alternatives to LPEI-polyplex loading in hydrogels via caged nanoparticle encapsulation as means to decrease polyplex aggregation when loading DNA at higher concentrations. Using PEGylated PEI resulted in lower toxicity to cells upon exposure and less aggregation when encapsulating in HA hydrogels, but also led to decreased transgene expression levels, which was attributed to lower amounts of DNA being internalized by cells when complexed with sPEG-PEI. sPEG-PEI and LPEI polyplexes were both internalized via the same endocytosis pathway, suggesting that the difference in levels of internalization cannot be attributed to a difference in endocytosis pathway dependence. The options explored in this study can be used to further inform future development of gene delivery systems and tune individual transgene expression profiles for a wide range of therapeutic applications.

4.5 Acknowledgements

This work was done in collaboration with Shayne Siegman. We thank Dr. Donald Griffin for his help with the sPEG-PEI chemistry.

V Sustained transfection from polyplex-coated porous hyaluronic acid scaffolds

5.1 Introduction

As discussed earlier, porous HA hydrogels can serve as depots for the local delivery of polyplexes to infiltrating cells. Porosity, which facilitates cell proliferation and infiltration, can be introduced into HA hydrogels through techniques such as sphere templating[10] and salt-leaching[11]. By developing a hydrogel with a porous architecture, DNA can be introduced in two phases – via encapsulation into the hydrogel itself and via surface association on the pore surfaces. We believe that these methods of DNA loading into hydrogel scaffolds are promising in achieving sustained transgene expression by enabling long-term DNA availability to cells.

Encapsulation of DNA polyplexes within hydrogels has been previously reported for gene delivery[12,71,117,118]. DNA polyplexes are nanoparticles comprised of DNA, which is negatively charged, complexed with a cationic polymer, such as polyethyleneimine (PEI), which functions as a delivery vehicle and facilitates cellular uptake of DNA. One challenge of polyplex incorporation into hydrogels is the tendency of these charged particles to aggregate when incorporated into a

hydrogel precursor solution, resulting in inefficient and inconsistent gene transfer; our lab has addressed this problem by developing a method called caged nanoparticle encapsulation (CnE) for the incorporation of DNA polyplexes into HA scaffolds in the presence of agarose and sucrose to mitigate electrostatic interactions to decrease the extent of aggregation[12,71]. This technique has been extended to incorporate polyplexes into porous hydrogels formed via the sphere templating method for *in vitro* culture; however, relatively low levels of transgene expression were observed[72]. We speculate that the reason for this is the slow cell-mediated degradation of the hydrogel by the cells to release and access the encapsulated polyplexes.

An alternative method for loading porous hydrogels with polyplexes is to associate the polyplexes on the cell culturing substrate surface, also referred to as a reverse transfection[172]. We hypothesize that coating the pores of porous HA scaffolds with polyplexes can be achieved by harnessing electrostatic interactions between the positively charged polyplexes and the negatively charged HA that makes up the scaffold, and that the resulting surface coating presentation of polyplexes enables greater access and facilitates availability of polyplexes to cells over time to enable long-term sustained transgene expression. While surface coating of DNA polyplexes to porous fibrin scaffolds was previously reported by Saul et al[135], we herein report a thorough characterization of a surface-coated DNA presentation in HA porous scaffolds to this basic presentation method to enhance and further modulate transgene expression from loaded DNA polyplexes. Significant levels of transgene expression were observed for up to a month. Subsequently, we study mechanistic reasons for the sustained expression.

5.2 Materials and Methods

5.2.1 Materials

Peptides Ac-GCRDGPQGIWGQDRCG-NH_2 (HS-MMP-SH) and Ac-GCGYGRGDSPG-NH_2 (RGD) were purchased from Genscript (Piscataway, NJ). Sodium hyaluronan (HA) was a gift from Genzyme Corporation (60 kDa, Cambridge, MA). Poly(methyl methacrylate) microspheres were purchased from Cospheric (Santa Barbara, CA). High molecular weight linear poly(ethylene imine) (LPEI, 25kDa) was purchased from Polysciences (Warrington, PA). The vector for the mammalian expression of Gaussia luciferase (pGluc) was purchased from New England Biolabs (Ipswich, MA). Both vectors were expanded using a Giga Prep kit from Qiagen (Valencia, CA) per manufacturer's protocol. Human plasma fibronectin was purchased from EMD Millipore (Billerica, MA). All other chemicals were purchased from Fisher Scientific (Pittsburgh, PA) unless otherwise noted. YOYO-1 was purchased from Life Technologies (Carlsbad, CA).

5.2.2 HA modification

Sodium hyaluronan was modified to contain acrylate function groups via a two-step reaction as previously described[117]. HA (2.0 g, 60 kDa) was reacted with 36.77 g (211.07 mmol) adipic acid dihydrazide (ADH) at pH 4.75 with 4 g 1-ethyl-3-[3-dimethylaminopropyl] carbodiimide hydrochloride (EDC) overnight. The product was purified through dialysis (8000 MWCO) against a NaCl gradient for 1 day. Further dialysis was done in DI water for 4 days. The purified product HA-ADH was then lyophilized and analyzed with ^{1}H-NMR. All of the HA-ADH was then reacted with 4.46 g N-acryloxysuccinimide (NHS-Ac) in 10mM HEPES, 150mM NaCl, 10mM EDTA at pH 7.4 overnight at room temperature before purification via dialysis against a NaCl gradient for 1 day and in DI water for 4 days. The purified product HA-Ac was then lyophilized and analyzed with ^{1}H-NMR (D_2O). 1H-NMR indicated a 65.94% modification of the

carboxyl groups on the HA backbone to ADH groups by taking the ratio of peaks δ = 1.6 and 23, which correspond to the eight H of the methylene groups on the ADH to the singlet peak of the acetyl methyl protons in HA (δ = 1.88). After the second step in which HA-ADH was reacted with N-acryloxysuccinimide (NHS-Ac), ^{1}H-NMR (D_2O) spectroscopy confirmed 11.03% acrylate modification (HA-Ac) by taking the ratio of the multiplet peak at δ = 6.2 corresponding to the acrylate H to the singlet peak of the acetyl methyl protons in HA (δ = 1.88).

5.2.3 Porous hydrogel formation

Chemically sintered microsphere templates were prepared as previously described[173]. Briefly, polymethyl methacrylate (PMMA) microspheres (53-63 μm, Cospheric, Santa Barbara, CA) were suspended in sintering solution (70% ethanol, 1% acetone) at a concentration of 0.4444mg μL^{-1}, and 75 μL of this bead solution was then added to every well of flexiPERM molds (Sigma-Aldrich, St. Louis, MO) adhered to Sigmacote (Sigma-Aldrich, St. Louis, MO) glass slides. The molds were sintered at 37°C for 2 hours before use.

Porous HA hydrogels were prepared as previously described[117]. Hydrogels were formed by Michael addition of acrylate functionalized HA (HA-Ac) with HS-MMP-SH peptide crosslinkers at pH 7.6-7.8. 20 μL of the hydrogel solution was then added directly on top of a PMMA microsphere template and perfused into the template by centrifugation at 500 g for 15min at 4°C. The template was then incubated at 37°C for an additional 20 min to induce complete crosslinking. Once complete, the hydrogels were removed from the flexiPERM molds and placed directly into 100% acetone for 48 h to dissolve the PMMA microsphere template. The acetone solution was replaced 3 times a day for the 48 h wash. The hydrogels were then serially hydrated, cut with a 4-mm-diameter biopsy punch, and stored in PBS until used. The storage modulus of the hydrogels was measured using a plate-to-plate rheometer (Physica MCR, Anton Paar, Ashland,

VA) with an 8-mm diameter plate under a constant strain of 0.8% and angular frequency ranging from 0.5 to 10 s^{-1}.

5.2.4 Polyplex formation and surface coating

To form polyplexes, 3 μg of plasmid DNA was diluted in 150 μl of nuclease-free water, and the desired amount of PEI to achieve an N/P ratio (ratio of the number of nitrogen groups on the polymer to the number of phosphate groups on the DNA backbone) of 7 (2.73 μg) was diluted into a separate 150-μl volume of nuclease-free water. The PEI solution was slowly added to the DNA while vortexing, and the resulting mixture was incubated at room temperature for 15 min. 1.5M NaCl solution was then added to the polyplex solution to achieve a final salt concentration of 150 mM.

To coat hydrated hydrogels with polyplexes, hydrogels were incubated in 50μL/gel solutions of polyplexes at desired concentrations for 2 h with agitation every 20 min to allow for the polyplexes to electrostatically attach to the hydrogel pore surfaces. The hydrogels were then washed three times in PBS.

5.2.5 Polyplex visualization

The coated gels were stained with YOYO-1, a DNA stain, for 1 h before repeated washing with PBS and imaging using a Nikon confocal microscope.

5.2.6 DNA release from hydrogels

In order to determine the overall the extent of release of surface coated polyplexes, gels were formed and surface coated using the aforementioned protocols with 0.25% radiolabelled DNA polyplexes. 1.25 μg plasmid DNA was radiolabelled with ^{32}P-dCTP (250μCi, PerkinElmer, Waltham, MA) using a Nick translation kit (Roche, Indianapolis, IN) according to the manufacturer's protocol. The reaction mixture was purified using the DNA Clean and

Concentrator kit from Zymo Research (Irvine, CA) and mixed with 498.75 μg non-radiolabelled DNA to result in a 0.25% "hot" plasmid DNA solution. Polyplexes were then formed with the radiolabelled DNA and PEI at an N/P ratio of 7. After coating gels with radiolabelled polyplexes at different concentrations, the gels were then incubated in 500μL PBS at 37°C. At each timepoint, the PBS medium was harvested, added to 2 mL BioSafe II scintillation cocktail (Research Products International Corp., Mt. Prospect, IL) and measured using a scintillation counter at the UCLA chemistry facility. The readout was analyzed using a standard curve. The medium was replenished at each timepoint. At the last timepoint, the gels themselves were harvested and added to scintillation cocktail to be read.

5.2.7 Cell culture

Mouse-bone-marrow-derived mesenchymal stem cells (D1, CRL12424) were purchased from ATCC (Manassas, VA) and cultured in Dulbecco's modified Eagle medium (DMEM) (Life Technologies) supplemented with 10% bovine growth serum (BGS, Hyclone, Logan, UT) and 1% penicillin/streptomycin (Life Technologies) at 37°C and 5% CO_2. The cells were passaged using trypsin or replenished with fresh media following standard cell culture protocols every 2-3 days.

5.2.8 3-D transfection from surface-coated hydrogels

Gels were surface-coated with DNA polyplexes containing a vector for the expression of Gaussia luciferase driven by the cytomegalovirus (CMV) promoter (pCMV-GLuc) and washed according to the above protocol. Gels were then seeded with D1 cells by incubating gels in 250 μL/gel of media with suspended cells at 1000000 cells/mL for 3 hr at 37°C with gentle flicking every 20 min, and washed to remove any unbound cells. Seeded gels were then transferred into fresh media and incubated at 37°C and 5% CO_2. At various timepoints, conditioned medium was collected from all samples and frozen at -20°C, and Gaussia luciferase expression was determined

with the BioLux Gaussia Luciferase assay kit (New England Biolabs, Ipswich, MA) per manufacturer's protocol. Briefly, 20 μL of each thawed sample were mixed with 50 μL of substrate solution, pipetted for 2 to 3 seconds to mix, and read for luminescence with a 5 s integration time using a Modulus Fluorometer (Turner BioSystems, South San Francisco, CA).

To determine how many cells were seeded in the gels, porous hydrogels without polyplexes were seeded with D1 cells via the aforementioned method and allowed to incubate in media for 12 h to allow for cell attachment. The CyQUANT assay (Life Technologies, Grand Island, NY) was used to quantify the number of cells seeded in the gel per manufacturer's protocol. The same number of cells (43000 cells) that were seeded in the porous scaffolds were also seeded in 2D on tissue culture plastic as bolus transfection controls. These cells were then transfected via bolus administration of polyplexes 16 hours after seeding.

5.2.9 Assessment of toxicity of polyplex administration

To assess toxicity of repeated bolus transfections in 2-D culture, 20000 cells/well were seeded in tissue culture-treated 48-well plates. The cells were then administered bolus doses of 0.5 ug DNA polyplexes encoding for GLuc once, twice, or three times every other day. The AQueous One solution cell proliferation assay (MTS) (Promega, Madison, WI) was then used at each time point to determine cell numbers in each condition in addition to a no-treatment condition by use of a standard curve to relate MTS absorbance values to cell count. In addition, Gaussia luciferase assay was performed at each of these time points to assess relative levels of transgene expression at each time point with each dosing program.

To assess toxicity of surface-coated porous hydrogel scaffolds relative to non-coated porous hydrogels, porous hydrogels were surface coated with DNA polyplexes and seeded with cells as described above. At designated time points, the alamarBlue non-terminal cell viability

assay (Thermo Fisher) was used to assess live cell count by use of a standard curve to relate alamarBlue fluorescence values to cell count.

5.2.10 Assessment of effect of space availability on transfection and transgene expression

To test cell density's effects on transfection, 20000 D1 cells were seeded in wells in 6-, 12-, 24-, and 48-well plates and transfected with 0.5 μg DNA polyplexes 16 hours after seeding. Media was harvested and assayed for relative transfection levels with the Gaussia luciferase assay at specified time points. To test cell density's effects on transgene expression after transfection, a bulk population of 1000000 cells were transfected with 50 μg DNA polyplexes 16 hours after seeding. The next day, cells were trypsinized and re-plated at different densities by seeding 20000 cells/well in 6-, 12-, 24-, and 48-well plates. Cells were then cultured over time to assess transgene expression with the Gaussia luciferase assay at specified time points.

5.2.11 Assessment of cell re-transfection in porous hydrogels

D1 cells cultured on tissue culture plastic were transfected with DNA polyplexes. The next day, transfected and non-transfected cells were trypsinized, seeded in porous hydrogels (with or without loaded DNA by surface coating) as noted above, and cultured over 6 days to assess transfection efficiency.

To determine whether there are indeed sustained higher levels of internalized DNA in cells cultured in surface-coated hydrogels, porous hydrogels were surface coated with 2.71 ug radiolabelled DNA polyplexes, then seeded with D1 cells. At various time points, gels were degraded in 5000 U/mL hyaluronidase for 1 h at 37C, (Sigma-Aldrich) and centrifuged to pellet the cells. The cells were then washed once with PBS, once with CellScrub buffer (Thermo Fisher) to remove membrane-bound polyplexes, and twice again with PBS before being transferred into BioSafe II scintillation cocktail for analysis of internalized DNA content by scintillation counting.

In addition, a control of non-surface-coated porous hydrogels seeded with D1 cells was administered one bolus transfection of 2.71 ug radiolabelled DNA polyplexes. Internalized DNA content at various timepoints was normalized to internalized DNA content at day 2.

5.2.12 Statistical analysis

Statistical analyses were performed using Prism (GraphPad, San Diego, CA). Data were analyzed using a one-way analysis of variance (ANOVA) test followed by a Tukey post-hoc test. The results are presented as mean ± SD. Polyplex size data was analyzed using a t-test, and the results are presented as mean ± SD. Single, double, and triple asterisks represent $p < 0.05$, $p < 0.01$, $p < 0.001$, respectively. A p value of < 0.05 was considered statistically significant.

5.3 Results and Discussion

In this study, a surface coating presentation of porous HA hydrogels as a method to load DNA into hydrogel scaffolds for long-term local non-viral gene delivery was studied and characterized, and a mechanistic analysis of possible causes of long-term gene delivery was explored. A comparison of transfection efficiency between encapsulation of polyplexes within a porous hydrogel scaffold and a surface presentation in a scaffold has already been presented, with a consistent conclusion drawn that a surface presentation of DNA results in significantly higher transgene expression levels than encapsulation allows in culture, primarily because a surface presentation allows for immediate exposure of cells to polyplexes as cells infiltrate the scaffold; rate of transfection is independent of cell-mediated gel degradation to result in cell-polyplex contact[135,136].

5.3.1 Characterization of surface-coated hydrogels

After generation of the porous HA hydrogel, the physical properties of the hydrogel were characterized. The storage modulus of porous HA hydrogels was 245 ± 26 Pa as measured using oscillation rheometry. The average pore diameter in the hydrogel was measured to be 83.7 ± 15.2 μm, which is consistent with the size of the porogen used after accounting for swelling.

Incubation of hydrogel scaffolds in a polyplex-rich solution was evaluated as a method for efficient DNA loading into hydrogels. Hydrogels incubated in this polyplex solution were stained with YOYO-1 and imaged to visualize the immobilized polyplexes on the hydrogels (Figure 5.1A). This method resulted in a relatively homogenous and spatially consistent distribution of polyplexes across the pore surfaces. In addition, no large polyplex aggregates were observed. Seeding of porous hydrogels with D1 cells by incubation in cell-dense media resulted in even distribution and spreading of cells throughout the hydrogel, as indicated by fluorescence microscopy at day 5 (Figure 5.1B). Cells seeded 2-D or on polyplex-coated gels exhibited DNA polyplex internalization (Figure 5.1C, 1D).

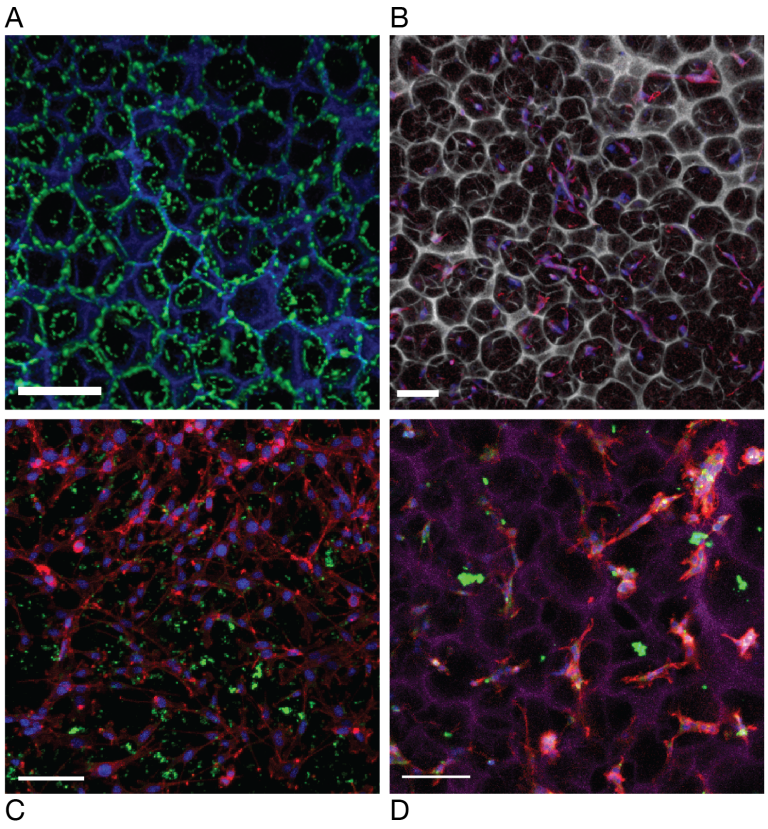

Figure 5.1: Confocal microscopy characterization of surface coating and cell seeding.
(A) Confocal microscopy image of a porous HA hydrogel (blue) surface-coated with DNA polyplexes (green). (B) Porous HA hydrogel (white) seeded with D1 mouse mesenchymal stem cells stained with DAPI (blue) and phalloidin (red) after 6 d of culture, imaged with confocal microscopy via a 3-D render of a 252-μm z-stack. (C) D1 cells cultured 2-D 48 h after transfection stained with DAPI (blue), phalloidin (red), and YOYO-1 for polyplexes (green). (D) D1 cells cultured in surface-coated porous gel 48 h after transfection with stained gel (magenta), DAPI (blue), phalloidin (red), and polyplexes (green). Arrowheads denote instances of internalization of polyplexes. Scale bars represent 100 μm.

Varying the concentration of the DNA polyplex coating solution resulted in the modulation of DNA loaded into each hydrogel scaffold. The masses of DNA loaded into the 20-μL hydrogels using DNA polyplex coating concentrations of 0.05, 0.1 and 0.2 μg/μL are 1.03 ± 0.20, 1.66 ± 0.26, and 2.71 ± 0.6 μg per hydrogel (Figure 5.2A).

The release profile of polyplexes from the hydrogel in PBS was then quantified in order to understand the robustness of the polyplex-hydrogel interactions that govern the surface coating.

The amount of DNA released was quantified as a percent of the total DNA initially loaded into each gel, which varies depending on the coating condition. It was observed that less than 5% of loaded DNA was released over 7 days for hydrogels of the two highest loading amounts (Figure 5.2B). In terms of absolute quantities of DNA release, hydrogels with the lowest DNA load exhibited the least release, while hydrogels with the highest DNA load exhibited the most. One driving force for the cause of this polyplex release from the hydrogel may be agitation from the induced of flow of medium around and to an extent through the porous hydrogel due to pipetting during the medium harvest step of this assay. To test this, porous hydrogels were formed, loaded with identical amounts of DNA polyplexes by surface coating, and incubated in PBS over time, with solution harvests either every day or every three days (Figure 5.2C). Daily harvesting resulted in more DNA released than with a less frequent harvest, with 0.3191 +/- 0.0321 µg DNA cumulatively released by day 15 with a daily harvest and 0.1335 µg +/- 0.0033 µg DNA released with harvests every three days. Daily harvests resulted in significantly more DNA polyplexes being released from the hydrogels, suggesting that actual release may be lower than reported in Figure 5.2B due to experimental design limitations.

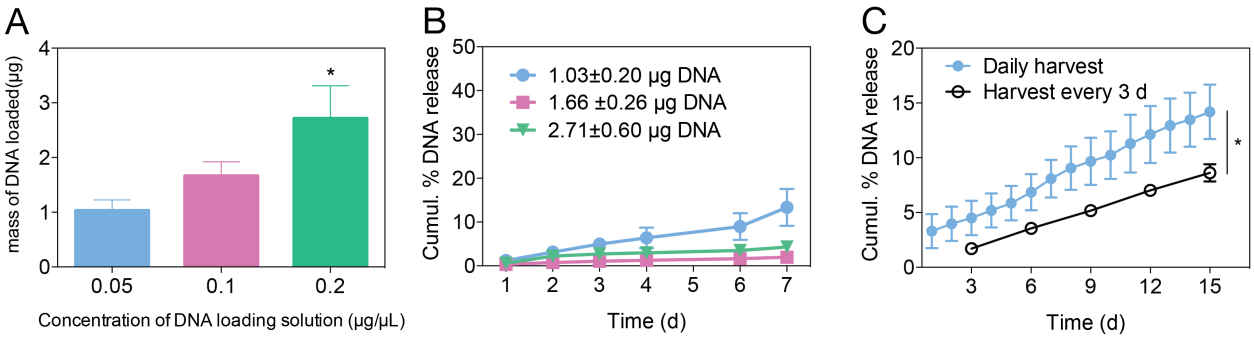

Figure 5.2: Characterization of DNA loading and release by surface coating.
(A) Amount of DNA coated in porous HA hydrogels as a function of the concentration of DNA polyplex coating solution. (B) Cumulative DNA release from surface-coated hydrogels with different amounts of loaded DNA polyplexes. (C) DNA release from surface-coated gels, daily harvest versus harvest every 3 d.

5.3.2 Long-term transfection

After characterization of the system, we then proceeded to implement the system for *in vitro* transfection. Porous hydrogels surface coated with DNA polyplexes encoding for Gaussia luciferase were seeded with D1 cells and cultured for 30 days. The CyQUANT assay confirmed that about 43000 cells were seeded in each scaffold. Transfection efficiency was monitored by quantifying transgene expression levels over time (Figure 5.3A). Seeded hydrogels loaded with more DNA resulted in increased transgene expression, expressed both in cumulative (Figure 5.3A) and per-day (Figure 5.3B) expression profiles. Significant transgene expression was observed over the course of the 30 days, with transgene expression on day 30 being only an order of magnitude below the first time point (Figure 5.3B). The 2D bolus condition was halted at day 8 due to the culture being overconfluent and presence of cell detachment. Overall, transgene expression from surface-coated hydrogels resulted in higher and more sustained expression levels than the analogous 2-D and porous gel bolus transfection models in which the same amount of DNA loaded into the hydrogel was administered as a bolus dose.

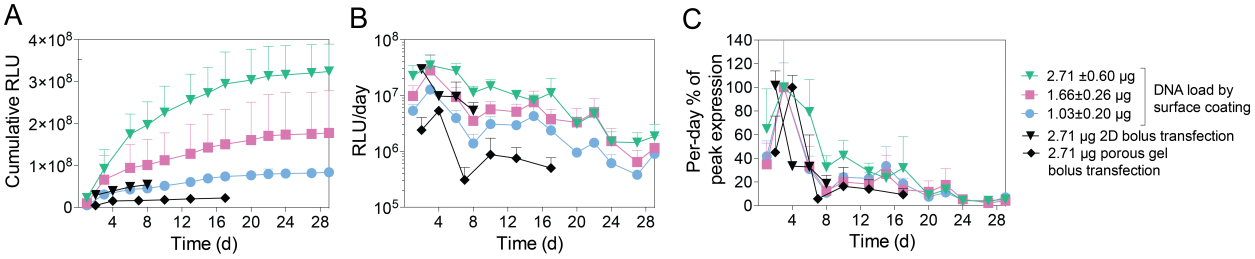

Figure 5.3: Transgene expression in surface-coated porous scaffolds.
(A) Cumulative and (B) per-day transgene expression of D1 cell culture in surface-coated porous HA hydrogels over time as a function of DNA concentration of gel coating solution, as compared to the per-day expression profile of bolus transfections 2D and in non-coated porous hydrogels. (C) Percent of peak expression at each timepoint.

Toxicity of the surface coated scaffolds was then assessed in comparison to repeated bolus transfections of 2D cell culture and porous scaffolds not containing DNA. D1 cells cultured in 2D

that were repeatedly administered bolus polyplex transfections exhibited progressively decreasing cell numbers with each subsequent transfection, revealing the cumulative toxic effect of repeated bolus polyplex transfections (Figure 5.4A). In addition, the repeated bolus transfection did not lead to a sustained transgene expression profile, suggesting that toxicity effects of repeated bolus transfections significantly impact transgene expression (Figure 5.4B). In surface-coated porous hydrogel scaffolds, cell count was also impacted in comparison to noncoated scaffolds, with a decrease in viability similar to that of one- and two-dose 2D bolus transfections but not as significant as that of a three-dose 2D bolus transfection (Figure 5.4C). In addition, the effect of cell viability impact on transgene expression in surface-coated hydrogels was not as impacted (Figure 5.3B).

In this study, PEI was used as a model polymer to study surface association of polyplexes in scaffolds as a method for long-term expression, and it is known to exhibit significant levels of cytotoxicity (Figure 5.4). This aspect can be improved on by using less toxic polymers to prepare polyplexes for surface coating; this will result in better overall viability but may still demonstrate long-term expression for at least 30 days.

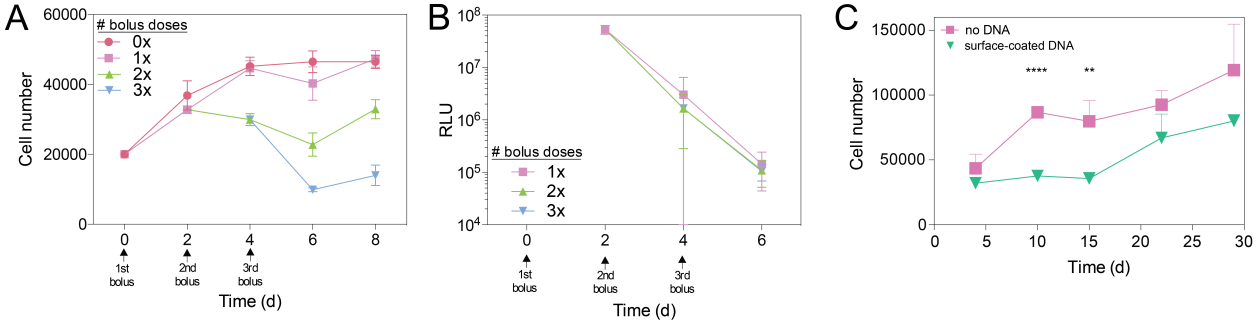

Figure 5.4: Toxicity in 2-D culture and culture in porous-coated scaffolds.
(A) Live cell count (toxicity) and (B) relative GLuc expression following transfection of D1 2-D cell culture on TCP with bolus administration of 0.5 μg DNA polyplexes once, twice, or thrice at two-day intervals. (C) Live cell count of cell culture in surface-coated porous hydrogels.

5.3.3 Assessment of mechanisms for long-term expression

To understand more clearly which mechanism is responsible for sustained transgene expression, we hypothesized that the sustained expression observed could be attributed to increased availability of space in this 3D culture system when compared to 2D cell culture, or the re-transfection of cells already being cultured in the hydrogel, both of which may affect transgene expression. We studied the effects of space availability on both transfection and on transgene expression resulting from transfection; if space availability is responsible for the observed sustained expression, lower seeding density should result in higher transgene expression. First, bolus transfections of 2D D1 cultures of equal number of cells plated at different plating densities resulted in decreased transfection with lower seeding density (Figure 5.5A). We believe that this decrease in transfection may be attributed to lower density of polyplex exposure due to settling of polyplexes over the increased surface area. Next, to test if space availability has any effect on transgene expression by cells after transfection, pre-transfected cells were trypsinized and seeded at different seeding densities. No significant difference in transgene expression levels between different plating densities of transfected cells was observed (Figure 5.5B). These findings suggest that the increased availability of space within the porous hydrogel cannot explain the increased and sustained transgene expression levels observed.

Next, the hypothesis that the occurrence of re-transfection events within the hydrogel scaffold as cells proliferate and migrate through the scaffold was the main reason for the sustained expression profile was tested. Cells that were or were not transfected with GLuc on TCP were then trypsinized and used to seed a porous hydrogel that was or was not surface coated with DNA polyplexes. Previously transfected cells which were seeded in a surface coated hydrogel scaffold exhibited significantly higher transgene expression than cells which were not previously

transfected before seeding in a surface-coated hydrogel scaffold (Figure 5.5C). This finding suggests that cells are able to undergo re-transfection events from surface-coated polyplexes within the surface-coated hydrogel. To determine if there were higher levels of internalized DNA in cells cultured in surface-coated hydrogels, internalized DNA content was tracked using radiolabelled DNA in cells cultured in surface-coated hydrogels compared to cells cultured in non-coated hydrogels which were transfected through a conventional bolus transfection technique. Cells cultured in surface-coated hydrogels exhibited sustained levels of internalized DNA over the 19-day culturing period, whereas cells that were cultured in non-coated hydrogels and administered a bolus transfection saw a statistically significant decline in internalized DNA (Figure 5.5D). This result strongly suggests that surface coating hydrogels with polyplexes allows for extended availability and internalization of polyplexes through the proliferation and migration of cells throughout the scaffold, which in turn suggests re-transfection as a mechanism for sustained expression. It is in agreement with the sustained transgene expression observed in surface-coated hydrogel culture in comparison to bolus administration of polyplexes (Figure 5.3A).

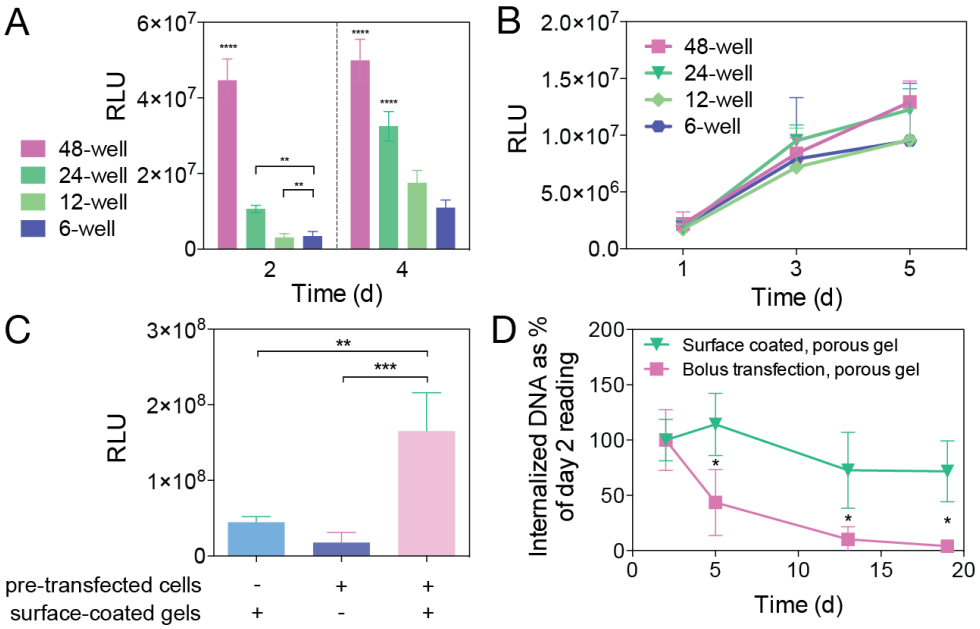

Figure 5.5: Investigation of mechanisms for sustained expression.
(A) Cell density effects on transfection. 20,000 cells/well were seeded in a 6-, 12-, 24-, or 48-well plate and transfected with identical amounts of DNA to test effects on transfection of culture in differing levels of space availability. (B) Cell density effects on transgene expression. 20,000 pre-transfected cells/well were seeded in a 6-, 12-, 24-, or 48-well plate to test effects on transgene expression in differing levels of space availability. (C) To assay ability of cell populations to be re-transfected, cells that were pre-transfected (+) or not pre-transfected (-) with GLuc were seeded in porous hydrogels that were surface-coated with DNA (+) or not surface-coated with DNA (-) and cultured over 5 d. Cumulative RLUs, representative of relative cumulative levels of GLuc expression in each of the conditions, are plotted. (D) Internalized radiolabeled DNA over time in cells cultured in surface-coated porous gels versus cells cultured in non-coated gels administered a bolus transfection.

5.3.4 Further Discussion

Surface association of polyplexes to cell-adhesive substrates was previously demonstrated in 2-D culture as a method to enhance the level and duration of transgene expression over the more conventional bolus transfection method[172]. Hydrogel surfaces have also been used as substrates for polyplex coating using both non-specific adsorption and biotin/avidin interactions[174]. Three-dimensional implementations of surface adsorption of polyplexes was enabled with the development of porous scaffolds, allowing for the coating of pore surfaces of scaffolds as

previously reported by Jang et al[134] and Saul et al[135]. The former study demonstrated surface association of DNA/PEI polyplexes to the surfaces of poly(lactide-*co*-glycolide) (PLG) disks as well as throughout a porous PLG scaffold and demonstrated higher levels of transgene expression than bolus transfections after 48 hours of polyplex exposure and cell culture[134]. However, this study did not continue to assess longer-term transgene expression outcomes in comparison to bolus transfection. Furthermore, surface association of DNA/PEI polyplexes to HA porous scaffolds in this study demonstrated less release over time than association to PLG scaffolds. In the latter study, porous fibrin scaffolds produced with the sphere templating method were coated with DNA/PEI polyplexes using a similar dip-coating method. The authors also observed significant levels of transgene expression over 27 days and reported comparable levels of DNA release from the scaffolds over time. This current study builds upon the work reported in these studies by demonstrating long-term transgene expression from a hydrogel and suggests that the long-term expression observed is due to re-transfection events occurring over time from surface-immobilized polyplexes.

The mechanistic studies described above strongly suggest that the sustained long-term expression observed is at least in part due to re-transfection events taking place in the culture. We believe that this re-transfection takes place via a few methods. First, cells are able to be re-transfected after some refractory period after the occurrence of the first transfection, which may be related to the average duration of internalization of polyplex DNA. Future studies may be done to elaborate on the length of this refractory period and on what factors affect the length of this period. Second, cells within the culture population that may not have been initially transfected may be transfected at a later period of time from migrating to areas within the gel with greater polyplex availability. Third, daughter cells of transfected dividing cells may exhibit transfection at later time

points. Further studies involving single-cell analysis and isolation of transfected cells by flow cytometry may be performed to confirm hypotheses regarding re-transfection mechanisms.

This platform for transgene expression is especially useful for applications in which long-term transgene expression is useful *in vitro* and *in vivo*, but where it is beneficial to employ nonviral methods of gene delivery to allow researchers to bypass the immunogenic risks associated with viral delivery methods. One notable example is the elucidation of transdifferentiation pathways for cell therapies, in which the fate of a subset of patient's cells of a particular type can potentially be transitioned to a different cell type in need through induction of various factors[175,176].

5.5 Conclusion

The need for a method of long-term sustained gene delivery by non-viral means is evident in developing therapies for treating disease. In this study, we have designed and characterized a system for sustained non-viral delivery through the surface-coating of HA porous hydrogels. Cells seeded in these hydrogels exhibited a transgene expression profile of 30 days. It is suggested that this is due to the occurrence of multiple re-transfection events. This platform can in the future be used for a wide range of *in vitro* and *in vivo* applications.

5.6 Acknowledgements

We thank Adrian Siew, Ben Krahenbuhl, and Nairi Tahmizyan for their laboratory assistance.

VI Physical and cell adhesion properties of microporous annealed particle (MAP) hydrogels control fibroblast spreading, proliferation, and gene transfer

6.1 Introduction

Non-viral gene delivery has been an invaluable tool used not only to study biological processes such as differentiation, but also as a therapy for regenerative medicine applications. However, the broader applicability of non-viral gene delivery is limited by overall low transfection efficiency. Thus, strategies to increase the efficiency of non-viral gene delivery are critical to improving biological studies both *in vitro* and *in vivo*. While there has been considerable research done on improving gene carriers[129,177] and vector DNA constructs[125], many studies have also explored the role the cellular microenvironment on key cellular processes which influence gene transfer. Such features of the microenvironment include substrate chemistry and charge[146], extracellular matrix protein composition[148,149], cell adhesion ligand presentation and concentration[18,53], substrate stiffness[18,145], and surface topography[147]. Importantly, these key

features triggered different responses when cells were seeded in two dimensions compared to in three dimensions. Culturing cells in three dimensions (3-D) in hydrogel scaffolds is crucial for biomedical applications, as it more accurately mimics the native tissue environment, serving as a more accurate *in vitro* model to study biological processes or to test new therapies[8]. The locally observed cellular microenvionment is especially relevant to the development of new hydrogel biomaterials used to locally deliver therapeutic genes to infiltrating cells for regenerative medicine applications such as in wound healing, stroke recovery, or cartilage and bone regeneration.

One class of biomaterials recently developed by our laboratory for such tissue regeneration applications is the microporous annealed particle (MAP) hydrogel, which consists of microscale modular hydrogel-based building blocks that anneal to one another *in situ* upon injection to form a porous scaffold[13,14]. The microscale pores allow for homogeneous distribution of incorporated cells for culture *in vitro*. The MAP scaffold also promotes cell proliferation and infiltration throughout the scaffold differently from culture in nonporous hydrogels *in vivo*, as rates of cell spreading and infiltration are no longer dependent on the local cell-mediated degradation of the hydrogel. In addition, the MAP scaffold shows significant promise in promoting tissue regeneration in large part due to its inherent porous structure and the ability to seamlessly fill the wound cavity due to its injectability. In a murine cutaneous wound healing model, MAP scaffold injections accelerated tissue formation and vascularization[13]. Similarly, in a murine stroke model, the MAP scaffold reduced inflammation, increased peri-infarct vascularization, and induced migration of neuroprogenitor cells into the stroke site[15]. Coupling such a material with the therapeutic potential of non-viral gene delivery may yield positive outcomes for therapy development.

Here we investigated the effects of several different physical and cell adhesion properties of MAP hydrogels on non-viral gene delivery. Specifically, we explored how MAP scaffold properties such as modular block size, stiffness, cell adhesion ligand concentration and presentation, and integrin specificity can modulate both cell spreading and non-viral gene transfer to cells cultured within the scaffold. Since our laboratory has previously demonstrated that dimensionality affects the mechanisms by which cationic polymer-mediated gene transfer occurs[156], we sought to understand if and how gene transfer in MAP cell culture would be different from that in 2-D cell culture on tissue culture plastic. In addition, the roles of endocytic pathways, cytoskeletal dynamics, and RhoGTPase-mediated signaling in transfection from cells cultured in MAP were investigated in comparison to 2-D culture. Ultimately, this enhancement of knowledge of these mechanisms will enable the development of strategies to enhance gene transfer from therapeutically relevant MAP hydrogels.

6.2 Methods

6.2.1 Preparation of hyaluronic acid-norbornene (HA-Norb)

To modify hyaluronic acid (HA) to contain norbornene functional groups, 1 g of 60 kDa sodium hyaluronan (Genzyme, Cambridge, MA) and 3.111 g 4-(4,6-dimethoxy-1,3,5-triazin-2-yl)-4-methyl-morpholinium chloride (DMTMM) (Thermo Fisher Scientific, Waltham, MA) were each dissolved in 40 mL 200 mM MES buffer pH 5.5. The two solutions were combined and stirred for 10 min to allow for activation of the carboxylic acid. 0.677 mL 5-norbornene-2-methylamine (TCI America, Portland, OR) was added dropwise to the reaction mixture, which was then allowed to react overnight at 25°C with constant stirring. The reaction product was then precipitated in ethanol, filtered to collect the solid, dissolved in 2 M NaCl in water, and dialyzed under running

deionized water for 24 hours. The final product was then filtered, flash-frozen, and lyophilized. The extent of modification was confirmed via ^{1}H-NMR spectrometry. 1H NMR shifts of attached norbornene groups in the product in D2O are δ = 6.33 and 6.02 (vinyl protons, endo), and 6.26 and 6.23 ppm (vinyl protons, exo). The integrations of these peaks were normalized to the peak corresponding to the methyl group on the HA monomer at δ = 2.0 ppm to determine percent of HA monomers modified to contain norbornene groups.

6.2.2 Synthesis of polyethylene glycol-tetrazine (PEG-tet)

PEG-tet was synthesized by combining 100 mg 4-arm 20kDa PEG-thiol (NOF America, White Plains, NY) and 15 mg methyltetrazine-PEG_4-maleimide (Kerafast, Boston, MA), each dissolved in 0.5 mL dichloromethane (DCM). 1 μL of trimethylamine was added and the mixture was allowed to stir at 25°C for 4 hours while protected from light. The reaction product was precipitated in 50 mL of cold diethyl ether and allowed to dry under vacuum overnight.

6.2.3 HA microgel formation and purification

HA-Norb microgels were prepared using a batch water-in-hexane emulsion technique. 1 mL of gel precursor solution was prepared in HEPES buffer pH 8.3 with HA-Norb at a final concentration of 3.5 wt%, lithium phenyl(2,4,6-trimethylbenzoyl)phosphinate photo-initiator (LAP; TCI America) at 2.2 mM, thiolated RGD peptide (RGDSPGERCG; Genscript, Piscataway, NJ) at 100, 250, 500, or 1000 μM, and tris(2-carboxyethyl)phosphine (TCEP) at 25% of the total thiol molarity (i.e. mmol TCEP:mmol thiols = 1:4). Once all the components were mixed, a 50 mM stock of dithiothreitol (DTT) (Thermo Fisher Scientific) was added as the crosslinker to achieve a crosslinking ratio (mmol SH/mmol HA) of 14, 28, or 56. For RGD clustering, a portion of the HA-Norb was combined with the total amount of RGD peptide and pre-reacted by exposing the solution to UV light for 1 minute at 10 mW/cm^2 in the presence of the appropriate amount of

LAP and TCEP, after which the remaining HA-Norb, LAP, and TCEP were added, along with DTT. To generate microgels containing different fibronectin fragments without clustering, the recombinant fragments, provided to us by Dr. Thomas Barker of the University of Virginia, were combined in lieu of RGD along with the other gel components as described above to a final concentration of 5μM. This final gel precursor solution was then pipetted into a round-bottom flask containing 10 mL 3% span-80 in hexane continuously stirring at 800 rpm, then mixed by pipetting up and down 9 times to generate a stable emulsion. The flask's contents were then purged with argon and exposed to UV light at 15 mW/cm^2 for 10 minutes to trigger the norbornene-thiol crosslinking reaction to form microgels.

Next, the crosslinked microgels in hexane was transferred into a conical tube and centrifuged at 1000 x g and washed with hexane three times. The microgels were then transferred to 1% Pluronic F107 in PBS for 30 min to allow for swelling before sieving using 200μm, 100μm, 60μm, and 20μm (PluriSelect, Leipzig, Germany) pore size strainers. During sieving, microgels were washed with 10mL 1% Pluronic in PBS and 50mL PBS. The collected microgels were then autoclaved and pelleted by centrifugation at 14000 x g for 5 minutes, after which the supernatant was removed and microgels were stored at 4°C until further use.

6.2.4 Alexa Fluor 647 tetrazine synthesis and labelling of microgels

To synthesize Alexa Fluor 647 tetrazine, 2.8 mg PEG dithiol (MW 3500 Da) (JenKem Technology USA, Plano, TX) and 0.41 mg methyltetrazine-PEG4-maleimide (Kerafast) were each dissolved in 1 mL dichloromethane and combined in a glass vial. 0.11 μL triethylamine (Sigma-Aldrich) and 1 mg Alexa Fluor-647 maleimide (Thermo Fisher Scientific) were then added and the reaction was allowed to proceed overnight at 25°C protected from light. The reaction was then precipitated in 10 mL cold diethyl ether, centrifuged at 14000 x g for 5 minutes to pellet the

precipitate, and the diethyl ether was decanted. The residual diethyl ether was removed under vacuum overnight. The resulting product was dissolved at 1 mg/mL in dimethylformamide and stored at -20ºC.

To fluorescently tag 200 μL microgels, Alexa Fluor 647 tetrazine was diluted in 100 μL PBS to a concentration of 0.015 mM and combined with the microgels. The mixture was then incubated at 37°C for 1 hour with agitation. Microgels were washed three times by filling tube with PBS, centrifuging at 14000 x g for 5 min to pellet beads, and aspirating liquid.

6.2.5 Microgel size distribution

After sieving and tagging with fluorophore, free microgels in PBS were imaged as z-stacks using confocal microscopy using a 10x objective to obtain a maximum intensity projection. These images were then analyzed using the particle analysis toolkit in ImageJ to obtain diameter measurements of 400 to 1700 microgels for each condition, which were subsequently plotted using the Seaborn visualization package in Python.

6.2.6 Microgel annealing to generate MAP scaffolds

A 5.32 mM solution of PEG-Tet in PBS was mixed with microgels at a 1:6 volumetric ratio of PEG-Tet to microgels and immediately centrifuged at 14000 x g for 3 min. Excess liquid was removed, and 15 μL of gel was pipetted into each well and allowed to anneal for 1 hour at 37°C.

6.2.7 Preparation of cell culturing devices

A custom negative mold was printed using a 3D, Form 2 stereolithography printer (Formlabs, Inc.). Cell culture devices were cast using soft lithography to produce a PDMS reservoir for cell culture. The culture wells were composed of a cylindrical culture section (3 mm in diameter and 5 mm tall), enabling a maximum of 35 μL of volume. Additionally. a conical media reservoir above the cylindrical culturing section was able to contain up to 150 μL of media.

Specific dimensions of the mold, and subsequently the PDMS wells, can be found in Supplementary Figure 6.1. To fabricate PDMS culturing devices, 70 g of Sylgard 184 PDMS (Dow Corning) was preparing according to the manufacturer's instructions and poured into a 10 cm x 10 cm square dish. The mold was placed in the PDMS, and the PDMS was degassed by applying a vacuum for 1 hour. Subsequently, the PDMS was allowed to cure at 60°C for 4 hours in a convection oven. The PDMS slab was then cut into three-well pieces and plasma-bonded to cover glass slides using a corona plasma gun. PDMS triplicate well-slides were then autoclaved prior to use for cell culture and experimental evaluation.

6.2.8 Cell culture and seeding HDFs in MAP scaffolds

Human dermal fibroblasts (HDF; Cell Applications, Inc., San Diego, CA) were maintained in culture in Dulbecco's modified Eagle's medium (Thermo Fisher Scientific) containing 10% fetal bovine serum (Thermo Fisher Scientific) at 37°C and 5% CO_2. Media was changed every 2-3 days.

To seed cells in MAP scaffolds, 100 μL microgels were first equilibrated in supplemented media for 30 minutes before pelleting and removing supernatant. HDFs were trypsinized and 1.2 x 10^5 cells were pelleted by centrifugation at 250 x g for 5 minutes. Media supernatant was aspirated and equilibrated microgels in PEG-Tet solution (as described in section 2.6) were then added to the cell pellet and mixed thoroughly by pipetting. Importantly, prior to gel/cell seeding, 6 μL of sterile 1% agarose in PBS was added to the wells to coat the glass surface and allowed to cool to 25°C to prevent cell attachment to glass. 15 μL of gel plus cells was then pipetted into each well in the PDMS culturing device. The MAP gel was allowed to anneal for 1 hour at 37°C. After annealing, the wells were filled with 150 μL supplemented media containing 50 μg/mL primocin (InvivoGen, San Diego, CA).

6.2.9 Void space analysis

Annealed MAP scaffolds of various microgel bead sizes were incubated with PBS containing 1 μg/mL 500 kDa tetramethylrhodamine isothiocyanate-dextran (TRITC-dextran) (Sigma-Aldrich, St. Louis, MO) to fill the void space in between microgels, as it is too large to penetrate the microgel's polymer network. The labelled void space was imaged using confocal microscopy to obtain 200-μm z-stacks. The z-stacks were imported into IMARIS to generate surface renders, and void space volumes were quantified as a fraction of the total volume represented by the z-stack. A minimum of 4 measurements were made for each MAP scaffold.

6.2.10 Oscillation rheometry

Stiffness of both nonporous HA-Norb hydrogels and of annealed MAP gels were measured as the storage modulus (G') using a plate-to-plate rheometer (Physica MCR, Anton Paar, Ashland, VA). To create a nonporous HA-Norb gel, 45 μL of the gel precursor solution was prepared as described in section 2.3 and pipetted onto a Sigmacote-treated (Sigma-Aldrich) glass slide. 1mm-thick spacers were placed on either side of the slide and a second Sigmacote-treated slide was placed on top to sandwich the gel precursor solution and fastened into place using binder clips. The gel was exposed to UV light at 15 mW/cm^2 for 1 minute, then flipped and exposed for another minute for uniform crosslinking. The crosslinked gel was transferred into PBS and allowed to swell overnight. A frequency sweep was performed on the hydrogels using a strain of 0.2% with an angular frequency range of 0.5 to 10 rad/s. To measure the storage modulus of an annealed MAP gel, 50 μL microgels with PEG-Tet were pipetted directly onto the rheometer stage. The measuring position was set to 1mm and the gel was allowed to incubate with humidity for 1 hour

to allow for annealing. Once the gel was annealed, a frequency sweep was performed on the hydrogels using a strain of 1% with an angular frequency range of 0.5 to 10 rad/s.

6.2.11 Cell staining and imaging

MAP gels with cells cultured for 2 days were fixed in 1% paraformaldehyde for 15 minutes at 25°C. The cultures were permeabilized in 0.1% Triton X-100 in PBS and stained using DAPI (Sigma-Aldrich) for cell nuclei and rhodamine phalloidin (Thermo Fisher) for cell actin per manufacturer's guidelines for 1 hour. Gels were washed with PBS before z-stack imaging with a Nikon confocal.

6.2.12 Transfection of MAP gel culture and assay for transgene expression

Transfection was performed two days after seeding cells in MAP gels to allow for adequate spreading. DNA polyplexes were prepared by complexing plasmid DNA encoding for Gaussia luciferase (GLuc) with jetPEI (Polyplus-Transfection, Illkirch, France) according to manufacturer's instructions. Briefly, 0.25 μg DNA was diluted in 10 μL of 150 mM NaCl and 0.5 μL jetPEI was diluted in a separate tube in 10 μL of 150 mM NaCl. The jetPEI solution was then added to the DNA solution, immediately vortexed, and allowed to incubate for 15 min at 25°C to allow for complexation. Amounts were scaled up depending on DNA dose and number of wells, but the polyplex volume administered to each well remained constant (20 μL of polyplexes were added to each well as a bolus administration). After 4 hours of polyplex exposure, the polyplex-containing media was removed and replenished with fresh media.

To verify that cells throughout the scaffold were uniformly transfected in the z-direction, plasmid DNA was mixed with the fluorescent dye, YOYO-1 (Thermo Fisher Scientific), at a ratio of 1:50 YOYO-1:base-pair DNA and was allowed to incubate for 30 min at 25°C. YOYO-1-labeled DNA was then used to prepare polyplexes as mentioned above. MAP gels containing cells

and YOYO-1 polyplexes were then imaged using confocal microscopy to obtain z-stacks, and percent co-localization of YOYO-1 polyplexes with cell actin was quantified for each image in the z-stack to confirm consistent transfection in the z-direction.

Transfection was quantified by measuring expression of GLuc using the BioLux Gaussia Luciferase assay kit (New England Biolabs, Ipswich, MA) per manufacturer's protocol. Conditioned media was collected from each well at each time point. Briefly, 20 μL of each sample was mixed with 50 μL of substrate solution, pipetted for 2 to 3 seconds to mix, and read for luminescence with a 5 second integration time using a Modulus Fluorometer (Turner BioSystems, South San Francisco, CA).

6.2.13 Cell viability

Cell viability was quantified using the PrestoBlue assay (Thermo Fisher Scientific) per manufacturer's instructions. At specified times, the media in each well was replaced with a solution of 10 μL of the PrestoBlue reagent mixed with 90 μL of media. After 3 hours, 90 μL from each well were transferred into a 96-well plate and fluorescence was read using a BioTek plate reader at an excitation wavelength of 560 nm and an emission wavelength of 590 nm.

6.2.14 Endocytic pathway inhibition

Analysis of endocytic pathways was performed using various small molecule inhibitors as described in another study[156]. All inhibitors were purchased from Sigma-Aldrich. Macropinocytosis was inhibited using 100 μM amiloride, caveolae-mediated endocytosis was inhibited using 200 μM genistein and 0.1 mM methyl-β-cyclodextrin, and clathrin-mediated endocytosis was inhibited using 10 μg/mL chlorpromazine and indirectly inhibited using 50 μM dynasore. Inhibitor pretreatment of cells was administered 2 days after seeding cells in MAP gels. For comparison to 2-D cell culture, 1.8×10^4 HDFs, which is the same number of cells seeded per

15-μL MAP gel, were seeded per well in a 48-well tissue-culture plate for 16 hours before pretreatment with inhibitors. For genistein, chlorpromazine, and amiloride, the pretreatment was administered for 0.5 and 1.5 hours for cells cultured in 2-D and MAP gels, respectively. For methyl-β-cyclodextrin and dynasore, cells were pretreated for 1 hour in both 2-D and MAP gels. After the initial pretreatment with pathway inhibitors, 0.25 μg polyplexes were added to each well for a 4-hour transfection in the presence of the inhibitors. The media was then replaced with fresh media. Transgene expression was analyzed on samples of media collected from the wells 2 days after transfection for all culture samples.

6.2.15 Cytoskeletal inhibition and activation

All cytoskeletal inhibitors and activators were purchased from Sigma-Aldrich. 20 μM cytochalasin D was used to inhibit actin polymerization, 10 μM nocodozole was used to depolymerize microtubules, and 10 mM butanedione monoxime was used to inhibit myosin ATPase. 20 nM endothelin I, 500 nM jasplakinolide, and 10μM paclitaxel were administered to activate actin/myosin, actin, and microtubule dynamics, respectively. 2-D cell cultures were prepared as described above. Pretreatment was administered for 1.5 hours for all inhibitors, 2.5 minutes for endothelin I, and 2 hours for the other activators. After the pretreatment, 0.25 μg polyplexes were added to each well for a 4-hour transfection in the presence of the inhibitors/activators. The media was then replaced with fresh media. Transgene expression was analyzed on samples of media collected from the wells 2 days after transfection.

6.2.16 RhoGTPase and YAP/TAZ inhibition and activation

All inhibitors and activators were purchased from Cytoskeleton, Inc. (Denver, CO) unless otherwise stated. RhoA, B, and C were inhibited using 1 μg/mL C3 transferase with a 4-hour pretreatment, ROCK was inhibited using 10 μM Y27632 (Selleck Chemicals, Houston, TX)

for a 30-minute pretreatment, and PAK1 was inhibited using 10 μM IPA-3 (Sigma-Aldrich) for a 30-minute pretreatment. To test RhoGTPase activation, 2-D and MAP gel cultures were serum starved for 8 hours prior to 4-hour pretreatment with 1 μg/mL Rho/Rac/Cdc42 activator or 1 μg/mL Rho activator II. YAP was inhibited using 3 μM verteporfin (Sigma-Aldrich) for a 12-hour pretreatment. After the pretreatment, 0.25 μg polyplexes were added to each well for a 4-hour transfection in the presence of the inhibitors. The media was then replaced with fresh media. Transgene expression was analyzed on samples of media collected from the wells 2 days after transfection.

6.2.17 Statistical analysis

Statistical analysis and plotting were performed using Prism 6. Experiments were repeated two times with three independent gel samples in each experiment. Statistics assumed that gel samples, which were cast independently, were statistically independent from each other. Statistical significance was assessed using a 95% confidence interval using a one-way ANOVA with Tukey post-hoc test, unless otherwise noted. All error is reported as the standard deviation of error (SD).

6.3 Results and discussion

6.3.1 Analysis of gel physical properties

To synthesize microgels, HA-Norb was first prepared using amine-carboxylic acid chemistry utilizing the carboxylic acid in the backbone of HA (one per monomer) and a free amine-containing norbornene molecule. NMR analysis of the modified polymer revealed that 41.85% of the HA monomers were reacted to contain the norbornene functional group. HA microgels were produced using a water-in-hexane emulsion and UV light to trigger a thiolene reaction between the norbornene groups on the HA backbone and the thiols of the DTT crosslinker. The resulting

microgels were polydisperse with diameters ranging from 10 to greater than 200 µm, but are all spherical in shape. To narrow down the size range, microgels were purified to remove hexane and surfactant and swelled in PBS before sieving through pore size ranges of 20-60µm, 60-100 µm, and 100-200 µm to generate microgel populations of different sizes and of reduced polydispersity. A size distribution of each size range was obtained via analysis of confocal microscopy images (Figure 6.1A-B). The average diameters and standard deviations of these populations were 54.25 ± 29.11 µm, 86.04 ± 20.25 µm, and 150.76 ± 44.14 µm, respectively. Microgels with diameters outside the nominal sieving boundaries were also binned, which may be due to the ability of the viscoelastic microgels to squeeze through sieve pores.

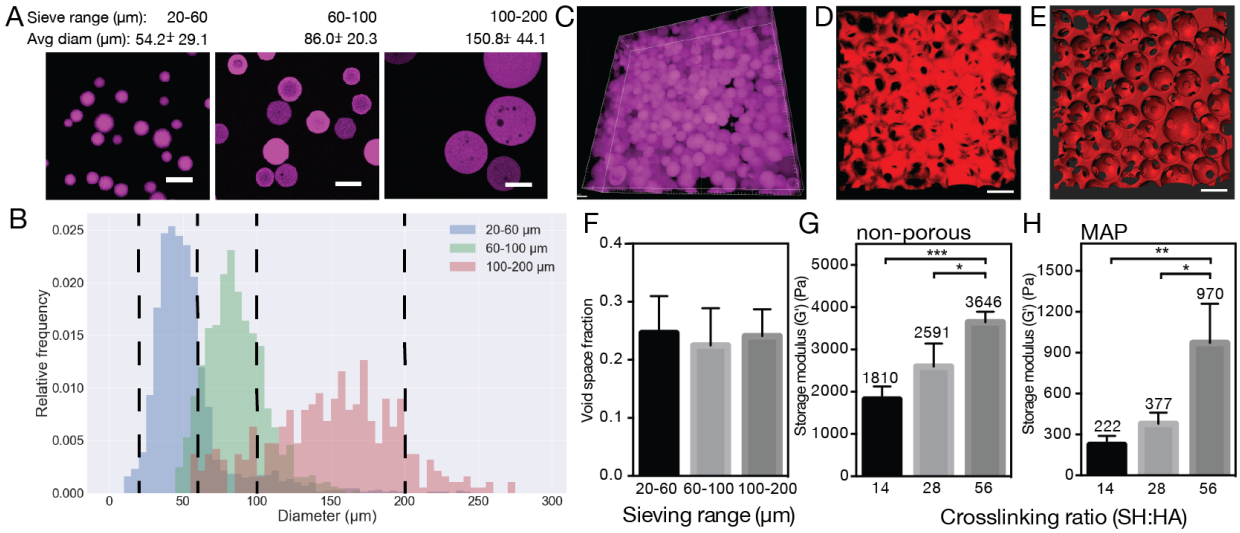

Figure 6.1: Characterization of MAP gel properties.
A) Confocal microscopy images of Alexa Fluor 647-tagged HA microgels after swelling and sieving to collect gel between the 20-µm and 60-µm filters, between the 60-µm and 100-µm filters, and between the 100-µm and 200µm filters. B) Size distributions of gel collected between the different sieving ranges. Dashed lines indicate filter pore size. C) Z-stack of annealed MAP gel using gel collected between the 60- and 100-µm filters. D) Visualization of void space within the MAP scaffold by using high-molecular-weight TRITC-dextran to fill pores of MAP gel. E) IMARIS rendering of void space volume from z-stack in Figure 6.1D. F) Void space fraction of annealed MAP gel consisting of the different sieving ranges as calculated from IMARIS rendering of void space volume. Storage moduli of G) nonporous HA-Norb gel crosslinked at different

crosslinking ratios and H) annealed MAP gel with microgels crosslinked at different crosslinking ratios as measured by oscillation rheometry with average storage moduli noted above each condition. Statistical analysis was conducted using one-way ANOVA with correction for multiple comparisons using Tukey's post-hoc test (* $p < 0.05$, ** $p < 0.01$, and *** $p < 0.001$). Error bars indicate standard deviation (SD).

MAP scaffolds were generated by annealing microgels within a culture well using a click reaction of the norbornene groups at the surfaces of the beads and a separate 4-arm PEG-tetrazine (PEG-Tet) crosslinker. Concentrated fluorescently tagged microgels were mixed with PEG-Tet crosslinker and allowed to anneal to generate MAP scaffolds within custom PDMS culture devices (Figure 6.1C). To enable visualization and quantification of the void space between each scaffold, a high-molecular-weight fluorescent TRITC-dextran solution which does not penetrate the microgels was added to to fill the void space within the annealed gel. Z-stack images were taken to obtain images of the void space between the microspheres (Figure 6.1D). Use of IMARIS to detect and render surfaces of these void spaces in three dimensions subsequently allowed us to measure void space fractions of these scaffolds (Figure 6.1E-F). No significant differences in void fraction between gels of different microgel diameters were observed, with void fractions ranging from 0.22 to 0.25. While the close random packing void fraction of a stiff monodisperse bead population is reported to be ~0.36, this value has been demonstrated to decrease with increasing polydispersity of the bead population, such as the ones observed in this study (polydispersity index 0.537, 0.235, and 0.293 for the small, medium, and large microgel populations, respectively)[178]. Furthermore, the viscoelastic nature of the microgels may allow them to pack more densely than an identically distributed population of stiff beads. We speculate that packing density may increase with decreasing stiffness of microgels. In a previous study, Sideris et al. calculated the void fraction of MAP scaffolds formed with microfluidics-generated microgels as 11-15%[14]. This discrepancy with our results may be due to two factors. First, this earlier study computed void fraction by

analyzing two-dimensional images individually instead of performing analysis on a three-dimensional render. Second, the inherent mechanical properties of the microgels used in this study were different, due to the different crosslinking chemistry and ratio of crosslinker used to form the microgels.

We next characterized the rheological properties of the MAP scaffolds used in this study. Three crosslinking ratios of 14, 28, and 56 mmol SH:mmol HA were used to generate microgels to be used for annealing. Oscillation rheometry was performed on both the nonporous gel formulation as well as the annealed MAP scaffold. The storage modulus (G') measurement of the nonporous gel formulation is representative of the local microgel stiffness experienced by a cell which is adhered to a microgel, while the storage modulus of the annealed MAP scaffold provides an overall characterization of the bulk rheological properties of the scaffold as a whole. We believe that taken together, these two measurements provide a more comprehensive characterization which is relevant to cell mechanosensing of the microenvironment. As expected, gels were stiffer with higher concentrations of crosslinker (Figures 6.1G-H).

6.3.2 Cell culture and transfection in MAP gel

Before beginning to evaluate which factors govern transfection and spreading for cells cultured inside MAP scaffolds, we first wanted to ensure seeded cells could be uniformly transfected after cell spreading had occurred within MAP pores. HA microgels were mixed with human dermal fibroblasts (HDF) and subsequently annealed to form a cell-seeded scaffold (Figure 2A). To confirm cells throughout the scaffold were able to be transfected with a bolus polyplex administration, cells and polyplexes in the scaffold were simultaneously visualized by transfection with polyplexes labeled with YOYO-1, a nucleic acid dye, and subsequently fixing and staining

cell actin with phalloidin (Figure 6.2B). Percent co-localization of YOYO-1-tagged polyplexes with the labeled cytoskeletal actin was relatively consistent throughout the scaffold, confirming that cells throughout the scaffold, especially in the z-direction, were able to be uniformly transfected (Figure 6.2C-D).

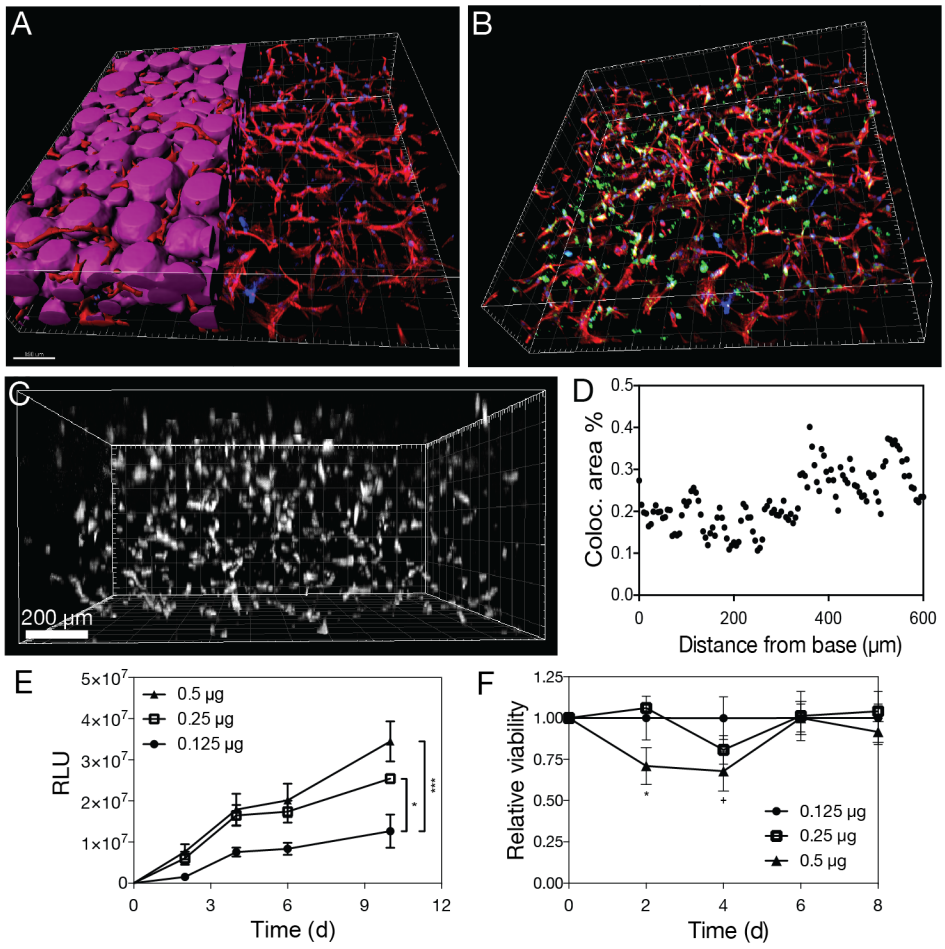

Figure 6.2: Characterization of HDF cell culture and transfection in MAP gel.
A) 3-D rendering of z-stack of HDFs cultured in MAP gel 2 d after seeding. IMARIS was used to generate a volume render of the MAP gel of the left half of the image. B) 3-D render of HDFs cultured in MAP gel (MAP gel not shown) with YOYO-1-labelled polyplexes after 4 h of polyplex exposure. C). 3-D render of co-localization of YOYO-1 polyplexes and cell actin after 4-h transfection in MAP gel. Vertical axis represents the z-axis. D) Quantification of area of polyplex and actin co-localization as a function of z. E) Transgene expression after 4-h transfection of HDF culture in MAP gel as a function of DNA polyplex dose. Cumulative expression at last timepoint was analyzed using one-way ANOVA with correction for multiple comparisons using Tukey's post-hoc test (* $p < 0.05$ and *** $p < 0.001$).. F) Relative cell viability as measured using the PrestoBlue assay as a function of DNA polyplex dose (* $p < 0.05$ between 0.5 μg and other two

conditions; + $p < 0.05$ between 0.5 μg and 0.125 μg). All error bars indicate standard deviation (SD).

To measure and compare levels of transfection between conditions, plasmid DNA encoding for the secreted marker protein Gaussia luciferase was complexed with jetPEI, an efficient commercially available polyethyleneimine-derived cationic polymer, to form polyplexes. Levels of GLuc expression were easily tunable by controlling the amount of DNA polyplexes used during transfection, with more DNA achieving higher transgene expression (Figure 6.2E). However, administering high doses of DNA polyplexes initially had an adverse effect on cell viability, although viability was largely restored by day 6 (Figure 6.2F). Cell viability can also be improved with the use of less toxic cationic polymers to complex with DNA.

6.3.3 Effects of MAP physical properties on transfection

We next sought to understand how the physical properties of MAP hydrogels, specifically microgel bead size and stiffness, can be controlled to modulate cell spreading, proliferation, and transgene expression. Multiple studies have previously investigated the role of scaffold microarchitecture, namely pore size, on cell morphology and proliferation, albeit with different conclusions on the nature of the relationship depending on cell type, void fraction, and pore shape[179–183]. For example, HDFs seeded in silk fibroin scaffolds 200-250 μm diameter pores exhibited more proliferation than those seeded in scaffolds of smaller pore sizes[182]. In addition, pore shape and topography may also affect cell spreading and migration, as converging or diverging orientations of paths ahead of migrating cells in a matrix have been demonstrated to result in different patterns of cell cytoskeleton polarization and migration[184]. Here we tested the effects of changing microgel size to control scaffold architecture, which would not only increase

or decrease pore size while maintaining a constant overall porosity (Figure 6.1F) but would also modify the topographical curvature of the pore surfaces. Other methods of modifying the architecture include changing the shape of the microgels, which would also affect tortuosity and substrate curvature, although this was not evaluated here.

To investigate microgel size, the three microgel distributions as described in Figures 1A-B were used, while the other gel formulation parameters were kept constant at a crosslinking ratio (SH/HA) of 14, RGD concentration of 500 μM, and RGD clustering ratio of 2:1 mmol RGD:mmol HA. Seeding HDFs in gels of the smallest bead size (20-60 μm sieving range) resulted in less spreading, lower levels of proliferation, and decreased transgene expression than in gels of either of the two larger bead size ranges (60-100 μm and 100-200 μm sieving range) (Figure 6.3). The relatively low spreading and proliferation in MAP scaffolds made using the smallest microgel size may be due to the smaller pore size of these scaffolds, which can limit the extent of cell spreading. This finding may be extended to the MAP scaffold architecture, in which changing substrate curvature as determined by microgel and diameter may potentially modulate cell morphology, migration, proliferation, and subsequently transfection.

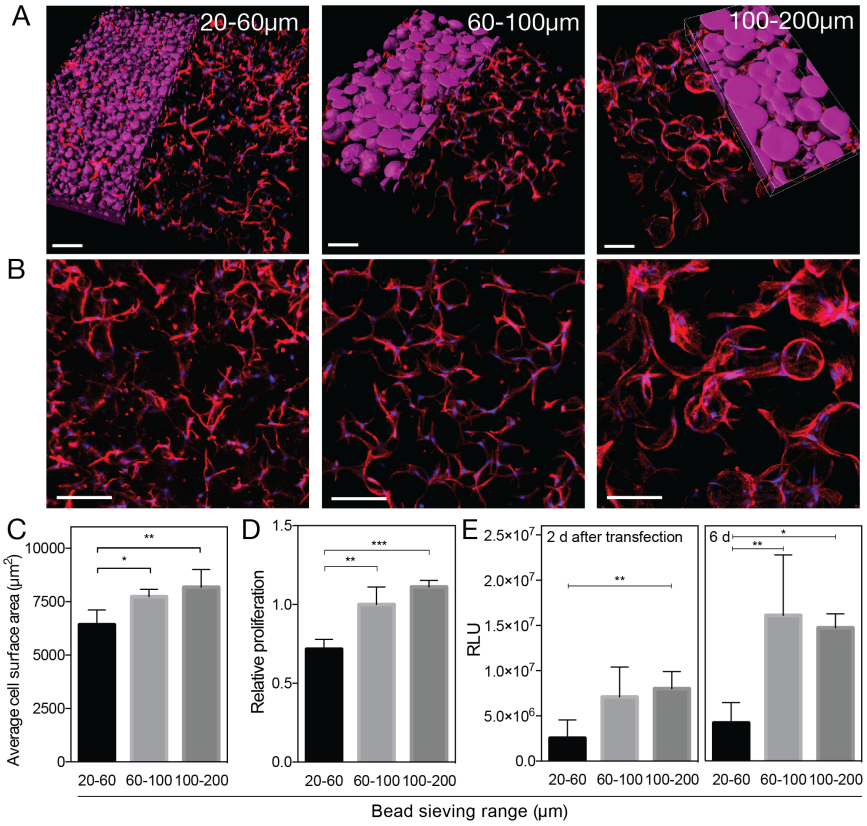

Figure 6.3: Effect of microgel diameter on HDF spreading and transfection in MAP gel.
A) 3-D renders and B) aerial views of HDF spreading in MAP gels of different microgel sizes after 2 d of culture. Scale bar = 150 μm. C) Quantification of average cell surface area in each size condition using IMARIS. D) Relative cell activity/proliferation 2 d after seeding using PrestoBlue assay. E) Cumulative transgene expression 2 d and 6 d after transfection. Statistical analysis was conducted using one-way ANOVA with correction for multiple comparisons using Tukey's post-hoc test (* $p < 0.05$, ** $p < 0.01$, and *** $p < 0.001$). Error bars indicate standard deviation (SD).

The effects of substrate stiffness on various cellular processes have been well-documented. In general, adhesion, spreading, and proliferation of fibroblasts and other adherent cell lines increase with increasing substrate stiffness for cells cultured in 2-D[185,186]. The range of microgel stiffnesses tested in this study (nonporous G' 1810 – 3646 Pa) corresponds with a subset of stiffnesses which was previously shown to result in a highly differential spreading response in mouse fibroblasts cultured in 2-D, with an approximate doubling in the cell circumference with an increase in substrate stiffness from 1600 to 3600 Pa[186]. However, cells encapsulated in a nonporous

hydrogel observe the inverse effect as a function of stiffness, likely due to higher resistance to cell-mediated degradation of the hydrogel at higher stiffnesses, which can be controlled by modifying polymer backbone concentration or crosslinking ratio[16,18]. A similar relationship has been observed for transfection as a function of stiffness and dimensionality, suggesting a correlation between cell spreading and transfection[18,145]. Given this, we next sought to evaluate the effect of tuning MAP scaffold stiffness on cell spreading, proliferation, and transfection by increasing the microgel crosslinking ratio. Gel formulations resulting in a nonporous G' range of 1810 to 3646 Pa—corresponding to overall MAP G' of 222 to 970 Pa (Figure 6.1G-H)—were tested. The other gel formulation parameters were kept constant at 100-200 μm microgel filter range, RGD concentration of 500 μM, and RGD clustering ratio of 2:1 mmol RGD:mmol HA. Increasing MAP stiffness by increasing the crosslinking ratio enhanced cell spreading and cell proliferation (Figures 6.4A-D). Furthermore, transgene expression increased by 2.28-fold and 2.25-fold by 2 and 6 days after transfection, respectively, when the scaffold stiffness was increased 4.4-fold from 222 to 970 Pa (Figure 6.4E). Overall, spreading, proliferation, and transfection appear to increase with increasing MAP scaffold stiffness, in agreement with results from studies of 2-D culture. This suggests that cell spreading and transfection in MAP scaffolds may be characterized as more similar to that in 2-D than in 3-D.

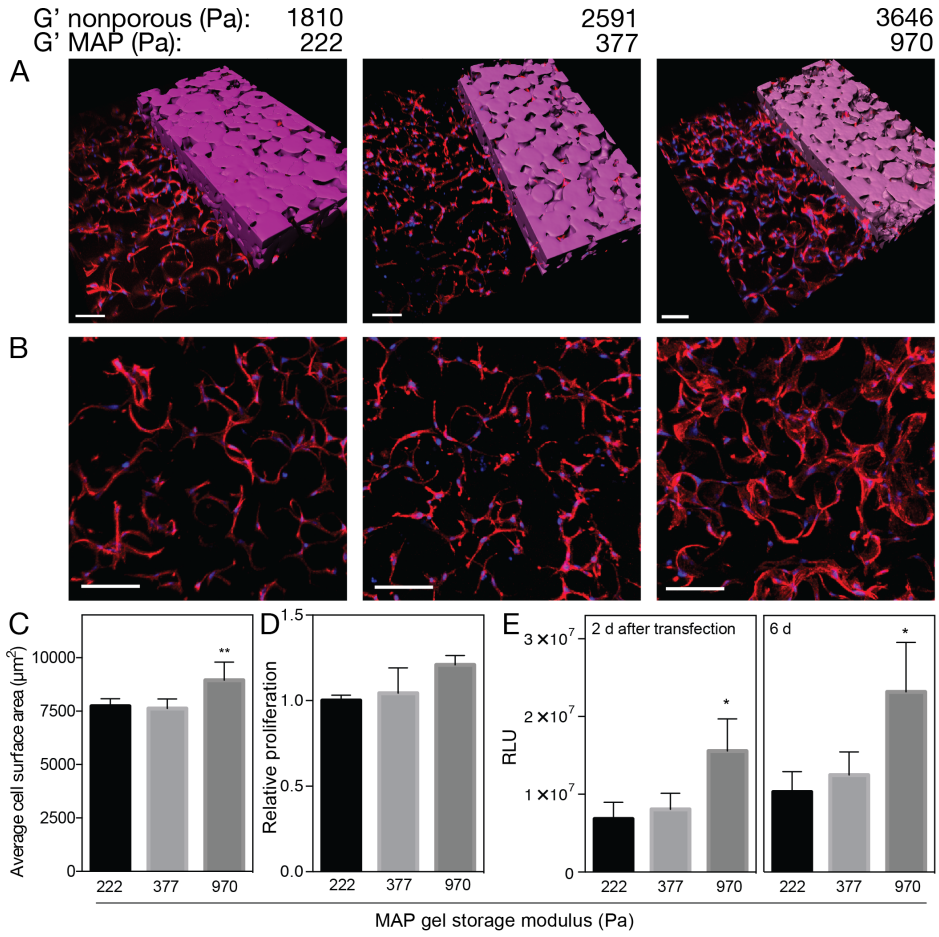

Figure 6.4: Effect of MAP gel stiffness on HDF spreading and transfection in MAP gel.
A) 3-D renders and B) aerial views of HDF spreading in MAP gels of different storage moduli after 2 d of culture. C) Quantification of average cell surface area in each stiffness condition using IMARIS. D) Relative cell activity/proliferation 2 d after seeding using PrestoBlue assay. E) Cumulative transgene expression 2 d and 6 d after transfection. Statistical analysis was conducted using one-way ANOVA with correction for multiple comparisons using Tukey's post-hoc test (* $p < 0.05$, ** $p < 0.01$, and *** $p < 0.001$). Error bars indicate standard deviation (SD).

6.3.4 Effects of MAP cell adhesion properties on transfection

A popular strategy to promote cell attachment to biomaterials is to incorporate integrin-binding peptides such as RGD into the biomaterial formulation. It has previously been demonstrated that the concentration and presentation of cell adhesion motifs on a substrate can affect both cell spreading and subsequent gene transfer[16,18,53,56]. To understand how tuning cell adhesion characteristics of the MAP hydrogel can affect cell spreading and gene transfer, we

manipulated either the concentration or clustering presentation of RGD peptides throughout the gel. Kong et al. found that while increasing RGD concentration increased cell surface area, proliferation, and gene transfer in 2-D, maintaining a constant RGD concentration but with increased peptide clustering resulted in a decrease in proliferation rate and gene transfer without any effect on cell spreading[53]. To first test the effects of overall RGD concentration in MAP scaffolds, the gel was formulated to contain RGD peptides at an overall concentration of 100, 250, 500, or 1000 μM. In all four of these conditions, the formulations were such that there were two RGD peptides conjugated to one HA molecule for the subset of HA molecules containing RGD (Figure 6.5A). Regardless of RGD concentration, all physical properties were kept constant, including the stiffness and size of microgels at a MAP G' of 222 Pa and sieving range 100-200 μm, respectively. HDFs cultured in MAP gels containing an RGD concentration lower than 500 μM resulted in overall significantly less spreading, lower proliferation, and lower transgene expression than in gel with RGD concentrations of 500 or 1000 μM (Figure 6.5B-F). These results are consistent with what has previously been reported for the effects of RGD concentration on gene transfer in 2-D[53]. In contrast, it was found that an intermediate concentration of 100 μM RGD resulted in the highest transfection as compared to 10 and 400 μM for D1 mouse mesenchymal stem cells encapsulated within a 3-D nonporous hydrogel[18], a difference which may be due to the use of a different cell line or the difference in cellular microenvironment between the MAP gel and a nonporous gel.

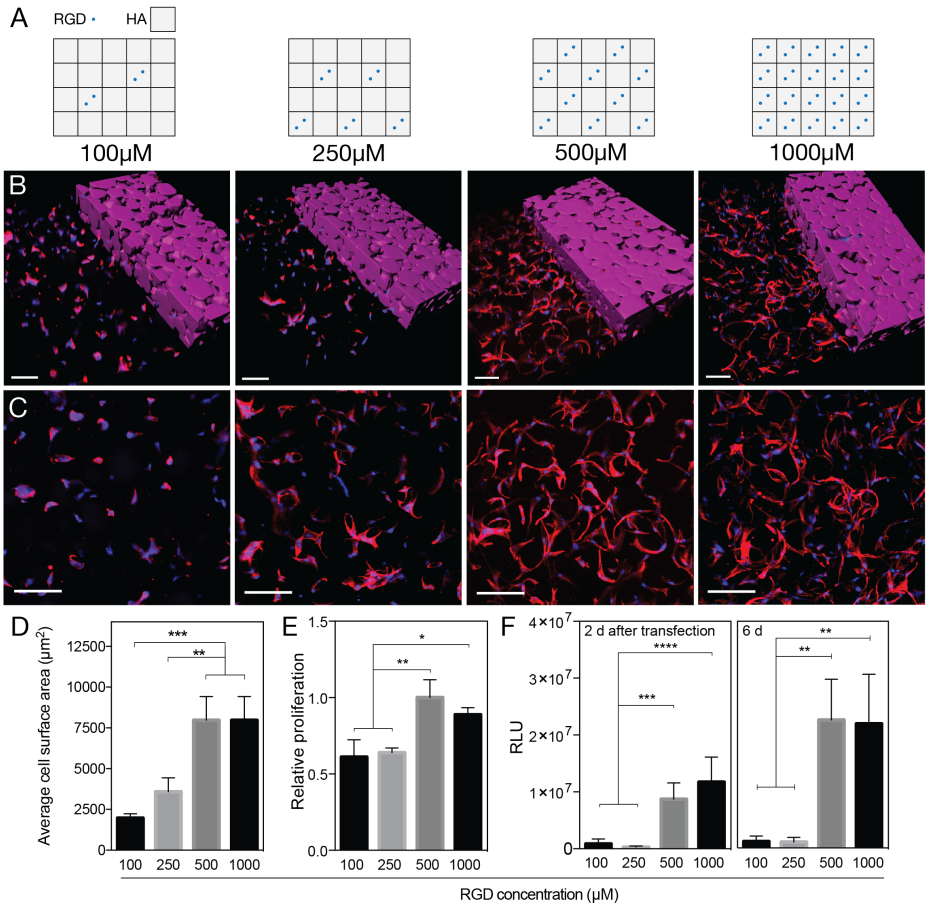

Figure 6.5: Effect of RGD concentration on HDF spreading and transfection in MAP gel.
A) Schematic of RGD presentation in conditions of varying RGD concentrations, in which each square represents an HA molecule and each dot represents an RGD peptide. B) 3-D renders and C) aerial views of HDF spreading in MAP gels of different RGD concentrations after 2 d of culture. D) Quantification of average cell surface area in each RGD concentration condition using IMARIS. E) Relative cell activity/proliferation 2 d after seeding using PrestoBlue assay. F) Cumulative transgene expression 2 d and 6 d after transfection. Statistical analysis was conducted using one-way ANOVA with correction for multiple comparisons using Tukey's post-hoc test (* $p < 0.05$, ** $p < 0.01$, and *** $p < 0.001$). Error bars indicate standard deviation (SD).

To test the effects of RGD clustering, 1, 2, 4, or 12 RGD peptides were conjugated to one HA molecule for the subset of HA molecules containing RGD, while the overall RGD concentration of all four conditions was kept constant at 500 μM (Figure 6.6A). Again, all other physical properties were kept constant. Interestingly, there was no significant effect on cell spreading and overall viability as a function of RGD clustering, though 2 and 4 mmol RGD:mmol

HA did result in higher average cell surface areas (Figure 6.6B-E). However, transgene expression in the highest clustering ratio of 12 mmol RGD:mmol HA did exhibit the lowest cumulative transgene expression especially by 6 days (Figure 6.6F). Kong et al. did also report lower transgene expression at the highest clustering ratio tested and suggested that this may be due to the relatively large spacing between RGD ligand clusters adversely affecting integrin signaling and therefore overall growth rate[53].

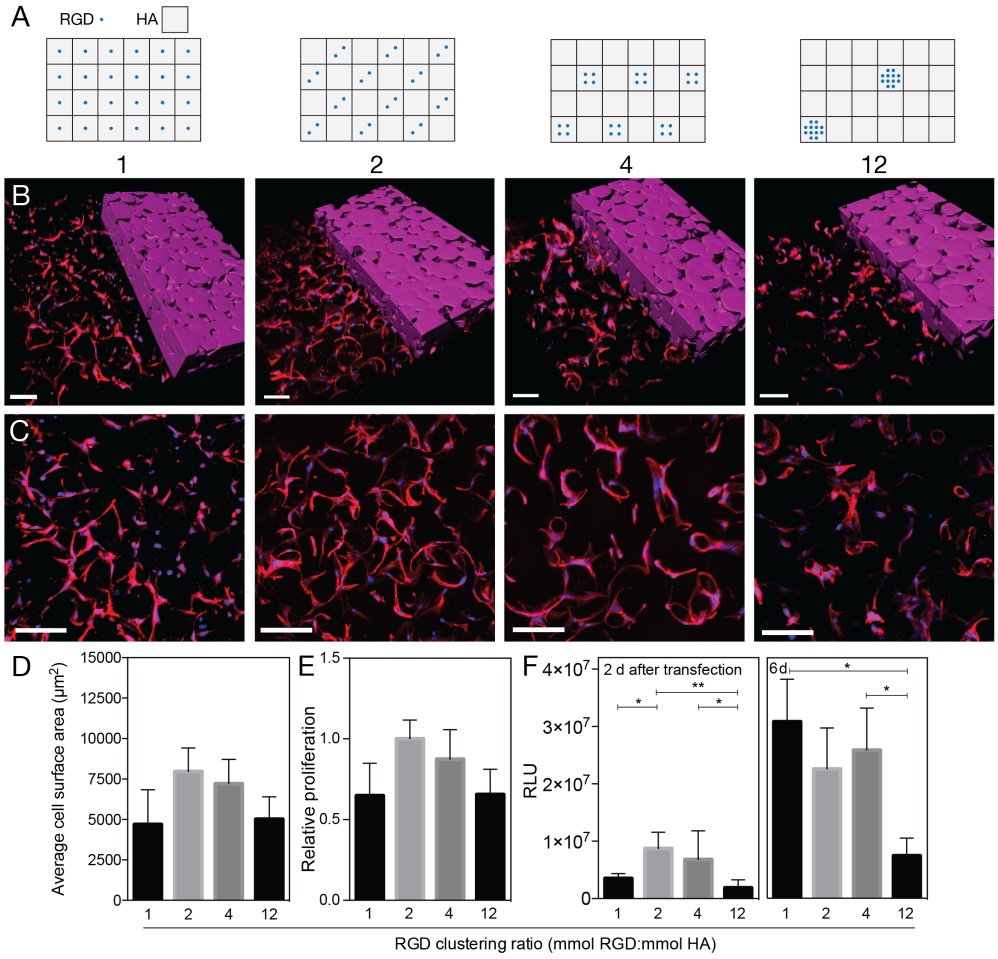

Figure 6.6: Effect of RGD clustering ratio (mmol RGD/mmol HA) on HDF spreading and transfection in MAP gel.
A) Schematic of RGD presentation in conditions of varying RGD clustering ratios, in which each square represents an HA molecule and each dot represents an RGD peptide. B) 3-D renders and C) aerial views of HDF spreading in MAP gels of different RGD clustering ratios after 2 d of culture. D) Quantification of average cell surface area in each RGD clustering condition using IMARIS. E) Relative cell activity/proliferation 2 d after seeding using PrestoBlue assay. F) Cumulative transgene expression 2 d and 6 d after transfection. Statistical analysis was conducted using one-

way ANOVA with correction for multiple comparisons using Tukey's post-hoc test (* $p < 0.05$, ** $p < 0.01$, and *** $p < 0.001$). Error bars indicate standard deviation (SD).

6.3.5 Effect of integrin specificity on transfection

We next studied the role of integrin binding in guiding gene transfer. Previous studies have demonstrated that specific or preferential integrin activation has differential effects on stem cell differentiation[187], epithelial cell phenotype[58], and vessel regeneration[188], demonstrating the importance of integrin specificity in cellular processes. This suggests that the current near-ubiquitous strategy of incorporating RGD ligands into biomaterials may not be optimal for promoting specific cellular processes, given the primary ability of RGD to bind to αv integrins[58]. Furthermore, presenting short integrin-binding peptides in biomaterials result in significantly reduced cell adhesion affinity when compared to identical molar concentrations of the same peptide included in its endogenous three-dimensional full-length protein structure[188]. Here, we sought to study the effects of integrin specificity on HDF spreading, proliferation, and gene transfer. To our knowledge, this is the first investigation of the role of specificity of integrin activation in modulating gene transfer.

One method of determining integrin specificity is to control the conformational stability of the RGD-containing ninth and tenth domains of fibronectin (Fn III9-10) by introducing either a Leu-Pro point mutation at position 1408 (9*10) or a labile 4 x Gly linker (9(4G)10) between the two domains; these variants have been demonstrated to preferentially bind to α3/α5β1 or αvβ3 integrins, respectively[187,188]. In place of RGD, these recombinant fibronectin fragments were covalently tethered to the HA-Norb backbone at a final concentration of 5 μM and used to form microgels. This concentration was chosen in light of previous studies which demonstrated spreading with fibronectin fragment concentrations of that magnitude, levels comparable to

spreading observed in environments with RGD concentrations on the order of 10^2 μM[9,58]. The stiffness and size of microgels were also kept constant at a MAP G' of 222 Pa and sieving range 100-200 μm, respectively. HDFs cultured in MAP gels which preferentially activate α3/α5β1 integrins exhibited lower average cell surface area than in MAP gels which preferentially activate αvβ3 integrins (Figure 6.7A-C). However, α3/α5β1-activating gels interestingly resulted in higher overall proliferation and, notably, higher transgene expression after transfection despite less spreading (Figures 6.7D-E).

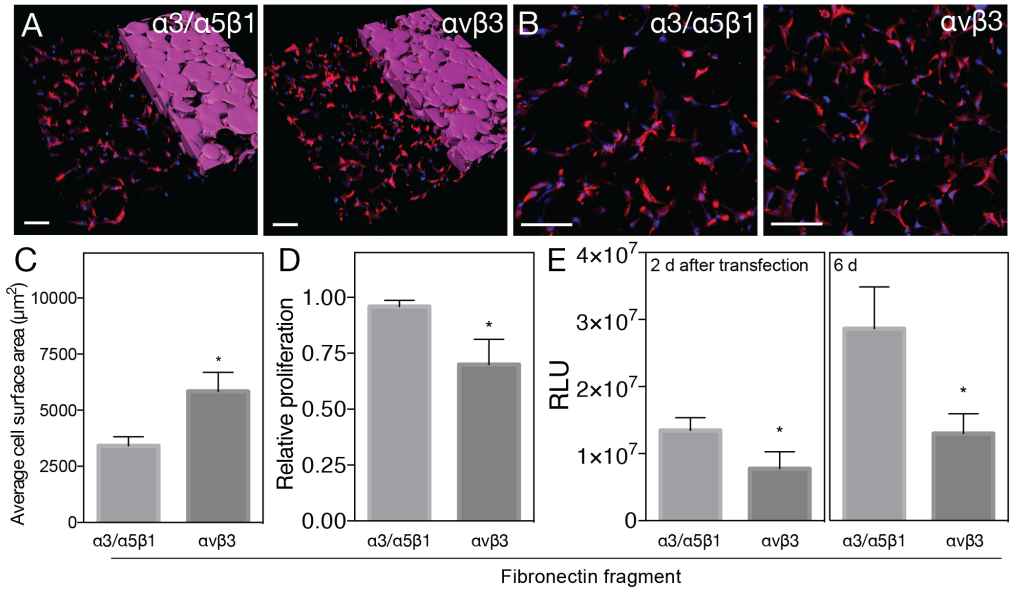

Figure 6.7: Effect of integrin specificity as controlled by cell adhesion ligand on HDF spreading and transfection in MAP gel.
A) 3-D renders and B) aerial views of HDF spreading in MAP gels of different cell adhesion ligand (fibronectin fragment 9*10 or fibronectin fragment 9(4G)10 after 2 d of culture. C) Quantification of average cell surface area in each integrin ligand condition using IMARIS. D) Relative cell activity/proliferation 2 d after seeding using PrestoBlue assay. E) Cumulative transgene expression 2 d and 6 d after transfection. Statistical analysis was conducted using one-way ANOVA with correction for multiple comparisons using Tukey's post-hoc test (* $p < 0.05$, ** $p < 0.01$, and *** $p < 0.001$). Error bars indicate standard deviation (SD).

In investigating effects of both physical and cell-adhesive properties of MAP scaffolds on cell behavior, we noticed that the extent of cell spreading appeared to correlate with cell proliferation and that both properties appeared to correlate with transgene expression in studies of microgel size, stiffness, and RGD concentration. The trends were maintained even after normalizing expression to proliferation levels at time of transfection at day 2 (Supplementary Figure 6.2). This is consistent with previous 2-D studies of preosteoblasts and mesenchymal stem cells which found similar trends[53,145,189]. However, we speculate that proliferation more heavily influences gene transfer and transgene expression, given our finding that α3/α5β1-activating gels increased overall proliferation and transgene expression despite a decrease in spreading. This suggests that integrin-dependent differences in gene transfer may in fact be independent of the extent of cell spreading, with a stronger correlation to proliferation (Figure 6.7). The dependence of polyplex-mediated gene transfer on cell cycle has previously been reported in 2-D[190]. Transgene expression was 10x-50x higher when polyplex-mediated transfection occurred during S, G2, or M phases of cell division, perhaps due to nuclear membrane degradation during phases closer to the mitotic M phase. This suggests that if certain substrate characteristics can trigger increased cell proliferation, this can directly affect the ability of seeded cells to be effectively transfected and significantly increase downstream transgene expression.

6.3.6 Analyzing dependence of endocytic, cytoskeletal, RhoGTPase, and YAP/TAZ pathways on transfection

We finally wanted to study the role of various pathways and processes, specifically those contributing to endocytosis, cytoskeletal dynamics, and RhoGTPase- and YAP/TAZ-mediated pathways, in gene transfer in MAP gel culture in comparison to cells plated in 2-D on conventional

2-D tissue culture plastic. Previous studies have demonstrated in both 2-D and 3-D culture that transfection occurs preferentially through specific endocytic pathways and that the nature of the dependence differs as a function of dimensionality[148,156]. Micropinocytosis, caveolae-mediated endocytosis, and clathrin-mediated endocytosis were directly and indirectly inhibited using various chemical inhibitors which were administered before and during transfection. It was found that inhibition of micropinocytosis and caveolae-mediated endocytosis enhanced transgene expression in 2-D but decreased transgene expression in MAP gels (Figure 6.8A). Direct inhibition of clathrin-mediated endocytosis using chlorpromazine significantly decreased transgene expression in both 2-D and MAP culture conditions, while there was no significant effect with indirect inhibition of dynamin via dynasore treatment. Together these findings suggest that gene transfer in 2-D predominantly occurs through clathrin-mediated endocytosis, while the more consistent suppression of gene transfer in MAP culture across all endocytic pathways suggests that gene transfer in MAP is dependent not only on clathrin-mediated endocytosis, but also to some extent on micropinocytosis and caveolae-mediated endocytosis. A previous study investigating the effects of inhibition of endocytic pathways in D1 mouse mesenchymal stem cells observed a dependence of gene transfer on both caveolae- and clathrin-mediated endocytosis in both 2-D and nonporous 3-D hydrogels[156]; however, the dominant internalization route of polyplexes seems to be cell line dependent, suggesting that comparisons drawn between findings in different cell lines may not necessarily be true[191].

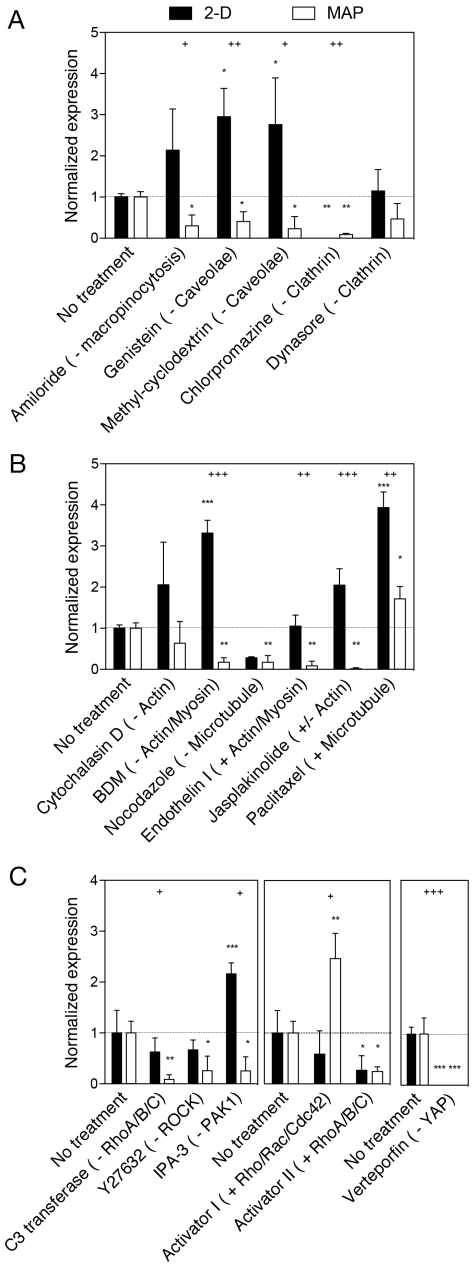

Figure 6.8: Analyzing dependence of endocytic, cytoskeletal, RhoGTPase, and YAP/TAZ pathways on transfection.
A) Effects of endocytic inhibitors on transgene expression two days after 4-h bolus transfection with polyplexes of HDFs cultured on tissue culture plastic (2-D) or in MAP gel. B) Effects of cytoskeletal inhibitors and activators on transgene expression 2 days after transfection. C) Effects of inhibitors and activators of RhoGTPases and inhibition of YAP on transgene expression 2 days after transfection. Statistical analysis was conducted using one-way ANOVA with correction for multiple comparisons using Dunnett's post-hoc test (* $p < 0.05$, ** $p < 0.01$, and *** $p < 0.001$) as compared to no-treatment control for 2-D or for MAP. For each treatment, 2-D and MAP were compared to each other using unpaired two-tailed t tests ($^{+}p < 0.05$, $^{++}p < 0.01$, and $^{+++}p < 0.001$). Error bars indicate standard deviation (SD).

The role of cytoskeletal dynamics in gene transfer in MAP gels and 2-D culture was studied by inhibiting actin, myosin, and microtubule dynamics (Figure 6.8B). Previous studies have illustrated the importance of cytoskeletal activity in gene transfer mechanisms, mostly in 2-D culture[151,192,193]. While there was no significant effect of inhibition of actin polymerization via cytochalasin D, expression significantly decreased with jasplakinolide administration. Jasplakinolide enhances the frequency of actin nucleation; however, it does so at the expense of actin polymeric organization, adversely affecting endosomal trafficking[194]. Therefore, jasplakinolide may not be a true promoter of actin polymerization in an organized fashion. Stabilization of microtubules with paclitaxel enhanced transgene expression both in 2D and in MAP gels, while inhibition of microtubule polymerization with nocodazole resulted in a decrease in expression, suggesting a strong dependence of polyplex trafficking on microtubule dynamics. Previous reports have also similarly identified the importance of microtubules in the trafficking of polyplexes towards the nucleus[192,193,195].

Next, the roles of the RhoGTPases Rho, Rac, and Cdc42 in the gene transfer process were investigated (Figure 6.8C). Rho proteins are GTPases which regulate a variety of cell processes but play an integral role in mediating integrin binding to the cell's ECM and actin cytoskeletal and microtubule dynamics in response to that[151,196]. The Rho, Rac, and Cdc42 GTPases have previously been shown to regulate cell polarity, lamellipodial protrusion, and cell adhesion during migration in 2-D[197]. Inhibition, activation, and overexpression of RhoGTPases have also been found to modulate the intracellular processing of polyplexes in 2-D[151]. Here, inhibition of RhoA/B/C using C3 transferase significantly decreased transgene expression in MAP gels, with a nonsignificant effect in 2-D. A similar pattern was seen in the inhibition of ROCK, a downstream

effector of RhoA. However, inhibition of PAK1, a downstream effector of Rac and Cdc42, with IPA-3 increased transgene expression in 2-D but decreased expression in MAP gels, suggesting a difference in gene transfer mechanism between 2-D and MAP gels. Activation of Rho, Rac, and Cdc42 resulted in a significant increase in transfection in MAP gels but no significant effect in 2-D. However, the activation of RhoA/B/C resulted in a decrease in transgene expression in both 2-D and MAP gels, suggesting that the activation of Rac and Cdc42 may be more integral to gene transfer in MAP gels.

Lastly, the role of YAP/TAZ (Yes-associated protein/Transcriptional coactivator with PDZ-binding motif), a key sensor and regulator of cell mechanotransduction[198,199], in gene transfer was studied. YAP/TAZ relays extracellular mechanical cues to the nucleus, thereby triggering downstream pathways[200]. It has been shown to play an integral role in the stiffness-dependent differentiation of mesenchymal stem cells and in fibroblast activation and fibrogenesis as a function of substrate stiffness[198,201], and YAP/TAZ nuclear localization has been shown to be correlated with the extent of cell spreading[200]. Given that multiple studies have reported a consistent correlation between cell spreading and gene transfer, we next investigated whether gene transfer is dependent on YAP/TAZ-mediated signaling, which has not been studied prior to this study. YAP was inhibited with the administration of verteporfin, which upregulates a chaperon protein that localizes YAP in the cytoplasm and targets it for degradation[202]. Inhibiting YAP resulted in a dramatic decrease in transgene expression in both 2-D and MAP gels to near-zero levels (Figure 6.8C), demonstrating that YAP/TAZ signaling is integral to gene transfer. The dependence of gene transfer on stiffness and cell adhesion ligand presentation may also be mediated by YAP/TAZ, but further studies will need to be conducted to verify this.

6.4 Conclusion

In this study, we performed *in vitro* studies to examine how MAP hydrogel properties can be tuned to enhance non-viral gene transfer from polyplexes. Microgel diameters of 60-200 μm, increased microgel stiffness, RGD concentrations of at least 500 μM, and an RGD clustering ratio of less than 12 mmol RGD:mmol HA resulted in the highest transgene expression. These modifications initially appeared to correlate both with cell spreading and cell proliferation. However, MAP gels which preferentially activated β_1 integrins resulted in enhanced proliferation and transgene expression but decreased average cell spreading, decoupling the trend of proliferation from spreading and suggesting that transgene expression may be independent of cell spreading. By analyzing the role of endocytic pathways, cytoskeletal dynamics, and RhoGTPases and YAP/TAZ, which are important downstream mediators of integrin signaling, we found that: (1) clathrin-mediated endocytosis is less dominant in driving gene transfer in MAP gels than in 2-D culture; (2) that as in 2-D culture, microtubule dynamics are integral to polyplex trafficking and efficiency of gene transfer; (3) Rac and Cdc42 may be important to the efficiency of polyplex-mediated gene transfer; and (4) just as in 2-D culture, YAP activity is crucial to enabling gene transfer. Overall these findings demonstrate that MAP scaffolds can serve as a highly tunable platform for studying polyplex-mediated gene transfer in a homogeneously seeded, uniformly transfected 3-D culture environment. These findings will also inform future design criteria when integrating non-viral gene delivery with therapeutically relevant MAP scaffolds for tissue repair *in vivo*.

6.5 Acknowledgements

We would like to thank Sasha Cai Lesher-Perez for assistance in designing cell culture devices, Nairi Tahmizyan and Mabel Chen for technical and troubleshooting assistance as well as input in designing cell culture devices, Nicole Darling and Weixian Xi for development of the click-based MAP crosslinking and annealing platform, Talar Tokatlian for proofreading the manuscript, and Shruti Sharma for technical assistance.

6.6 Supplementary Data

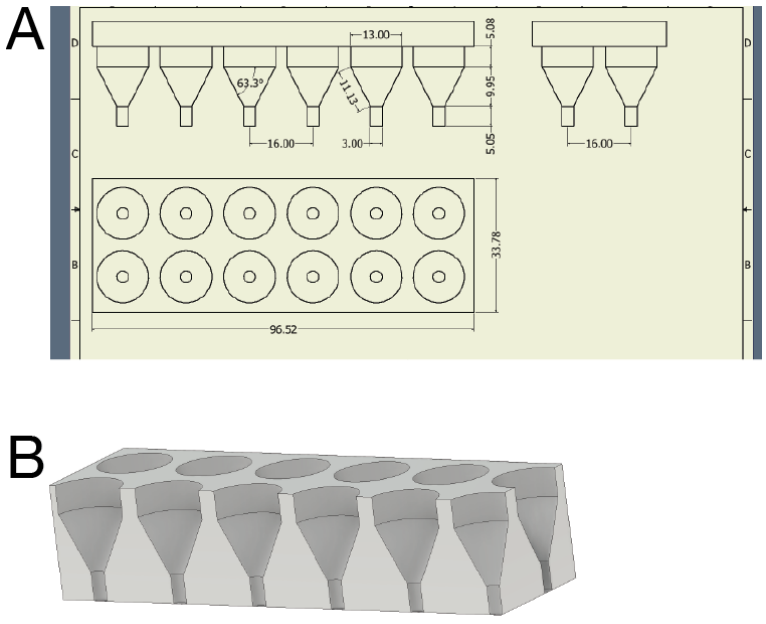

Supplementary Figure 6.1: Cell culture device mold.
A) PDMS cell culture device diagram containing dimentions in mm. B) 3-D render of device.

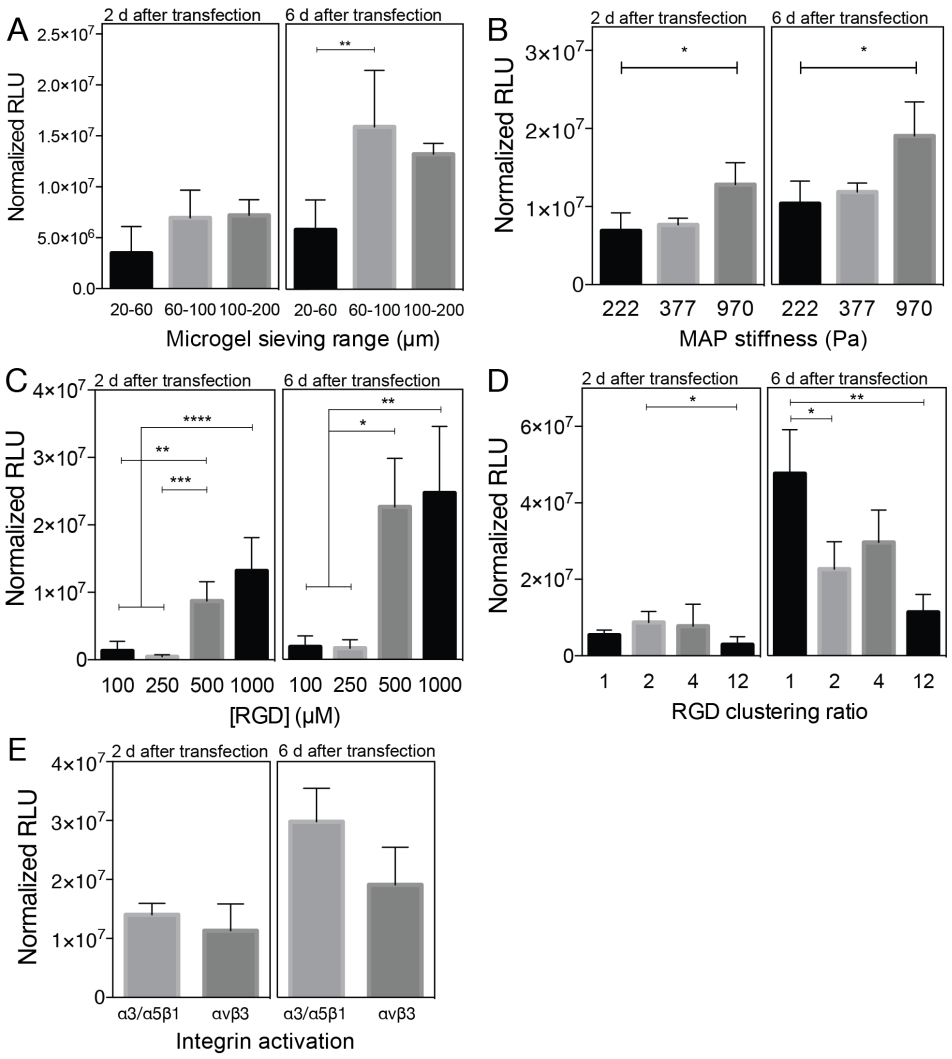

Supplementary Figure 6.2: Gaussia luciferase expression at days 2 and 6 normalized to proliferation level at time of transfection to remove effect of cell count differences at time of transfection.

As a function of A) microgel sieving range, B) MAP stiffness, C) RGD concentration, D) RGD clustering ratio, and E) integrin activation specificity. (* $p < 0.05$, ** $p < 0.01$, and *** $p < 0.001$)

VII Conclusions and future directions

7.1 Introduction

In the work presented in Chapters IV through VI of this dissertation, we pursued different strategies to enhance transgene expression through scaffold-mediated non-viral gene delivery and to study mechanisms governing the scaffold-mediated gene delivery methods used. In this chapter, we will revisit the objectives of the specific aims, discuss the aims' major conclusions and significance, and present future experimental directions.

7.2 Specific aim 1

In this aim, we hypothesized that PEGylating the cationic polymer PEI used to prepare polyplexes can decrease the overall polyplex surface charge and subsequently reduce aggregation upon encapsulation in HA hydrogels. We PEGylated PEI by conjugating the ends of the arms of 8-arm PEG with 2.5 kDa PEI to form sPEG-PEI. sPEG-PEI reduced polyplex surface charge and cell toxicity in comparison to linear 25 kDa PEI. sPEG-PEI subsequently reduced aggregation

upon complexation with DNA and encapsulation in HA hydrogels. However, transfecting sPEG-PEI polyplexes also resulted in significantly decreased levels of transgene expression due to decreased polyplex internalization by cells. This result was not entirely unexpected; while the internalization pathways taken by sPEG-PEI polyplexes remained the same, the decreased surface charge of the resulting sPEG-PEI/DNA polyplexes likely resulted in lower extents of association with the plasma membrane, contributing to decreased overall internalization.

Several strategies may be taken to improve this outcome. First, low-molecular-weight PEI was conjugated to multi-armed PEG, resulting in a PEGylated variant of branched PEI. Branched PEI has previously been demonstrated to have lower transfection efficiency than linear PEI[191]. Therefore, PEGylating linear PEI may result in increased transgene expression. Also, in this study we only tested one PEG:PEI ratio. Decreasing the overall ethylene glycol:ethylene imine molar ratio in the polymer by decreasing the molecular weight of PEG may result in a polymer with an intermediate chemical makeup which may sufficiently reduce aggregation but still lead to comparable levels of transfection.

Another future direction for this project may be to develop system to introduce a "sheddable" PEG shell around a PEI-DNA core. This strategy may be executed by synthesizing a diblock PEG-PEI copolymer with a degradable linker between the PEG and PEI blocks. This polymer may be complexed with DNA to form polyplexes with a PEI-DNA core with PEG facing outward to reduce surface charge and ultimately to reduce polyplex aggregation upon encapsulation in hydrogels. The degradation of the PEG-PEI linker may be triggered by a byproduct of the hydrogel crosslinking reaction. Ultimately, once this polymer has been optimized for this use, it can be tested in *in vivo* applications such as in a murine subcutaneous or cutaneous wound healing model.

7.4 Specific aim 2

In this aim, we hypothesized that surface coating porous HA hydrogel scaffolds would result in sustained transgene expression and that this sustained expression was due to the occurrence of multiple transfection events. We observed tunable, enhanced, and sustained transgene expression over 30 days of cell culture, a marked improvement over comparable bolus transfection techniques. Finally, we investigated mechanisms thought to be responsible for the sustained expression profile, finding, notably, that multiple transfection events are likely responsible for the observed sustained expression. However, we did observe nontrivial toxic effects on cell viability in the form of some initial cell death and slower cell growth over time. We believe that this aspect is where there may be significant room for improvement, as the linear PEI used here, though known for exhibiting high transfection efficiency, also is relatively toxic to cells. Future studies may be performed to test other gene carrier polymers and assess toxicity and transfection effects. We can then test different *in vitro* applications of this which require long-term transfection, such as for guiding cell differentiation. As surface coating of hydrogel pores grants more immediate access of infiltrating cells to polyplexes, an optimized formulation may be implanted in wound healing models to assess *in vivo* transfection via bioluminescence or immunostaining assays and ultimately to test for any therapeutic effects if delivering a therapeutic gene.

In studying the mechanisms by which sustained expression occurs, our conclusion that multiple transfection events are responsible for the sustained expression may be arrived at more confidently if experimental methods to assess individual cell transfection levels, e.g. flow

cytometry, were used in addition to overall culture transfection assays such as the one used in this study. Flow cytometry would allow us to determine whether the same cells exhibit repeated transfections or if a subset of cells that were not initially transfected are being transfected at a later time point due to the continuous polyplex availability.

7.5 Specific aim 3

The objectives of this aim were to understand how MAP scaffold material properties modulate transfection and how transfection mechanisms in culture in MAP scaffolds differ from culture on tissue culture plastic. While the effects of tuning substrate properties on gene transfer have been studied before in 2-D and nonporous 3-D encapsulated cell culture, cell behavior can vary dramatically as a function of dimensionality and the nature of the cellular microenvironment, and this relationship should be studied for each substrate modality. In the first objective, adjusting bead size, stiffness, RGD concentration, RGD clustering presentation, and induced integrin specificity affected transgene expression due to transfection. Extent of cell spreading and proliferation generally correlated with transgene expression levels; however, the preferential activation of $\alpha 3/\alpha 5\beta 1$ integrins resulted in less spreading than when $\alpha v\beta 3$ integrins were activated but increased proliferation and transgene expression, suggesting that integrin-dependent transfection may be more strongly correlated to proliferation than to spreading.

This is the first report elucidating the effects of integrin specificity on gene transfer. To more deeply understand this dependence of transfection on integrin specificity, flow cytometry studies can be performed using fluorescently-labelled polyplexes to understand the differences in the distribution of polyplex internalization per cell. Lastly, mitotic checkpoint inhibitors or other

proliferation inhibitors or suppressors can be used to halt proliferation to investigate whether transfection is dependent on proliferation or if these two processes are non-causally correlated.

It would also be interesting to test the effects of stress relaxation on transfection. It was previously demonstrated that mouse mesenchymal stem cells cultured in alginate-based hydrogels exhibiting quick stress relaxation resulted in increased spreading, proliferation, and osteogenic differentiation[203]. We speculate that quick stress relaxation may also improve transfection efficiency. A potential application of this would be to culture stem cells in MAP gel and transfect with genes encoding for known differentiation factors to observe induced rates of differentiation or transdifferentiation and if these rates can be modulated by tuning material parameters.

Furthermore, there are differences in the extents of dependence on particular endocytosis and cytoskeletal processes when compared to transfection of a 2-D culture: 1) clathrin-mediated endocytosis is less dominant in driving gene transfer than in 2-D culture; 2) that as in 2-D culture, microtubule dynamics are integral to polyplex trafficking and efficiency of gene transfer; 3) Rac and Cdc42 may be important to the efficiency of polyplex-mediated gene transfer; and 4) just as in 2-D culture, YAP activity is crucial to enabling gene transfer. This study provides insight on which pathways are crucial for gene transfer, and we can further devise strategies on how to upregulate such pathways through material engineering to enhance gene transfer. To our knowledge, this is the first study investigating the role of YAP/TAZ in gene transfer, and given its known key role in regulating cell mechanotransduction, we can next further understand mechanistically how changing MAP mechanical and bioactive properties affect YAP/TAZ activity to in turn influence transfection. In addition, it would be interesting to more deeply investigate the formation of actin stress fibers as a function of MAP properties and as a function of the inhibitor treatments to further elaborate on the mechanistic understanding of transfection.

Ultimately, we would like to develop methods for loading DNA into MAP scaffolds. The knowledge learned in this aim regarding how MAP material properties affect gene transfer will provide insight in the design of DNA-loaded MAP scaffolds for *in vivo* implantation studies for tissue repair.

VIII References

1. Sayed N, Wong WT, Ospino F, et al. Transdifferentiation of Human Fibroblasts to Endothelial Cells: Role of Innate Immunity. *Circulation*. 2015;131(3):300–309. doi:10.1161/CIRCULATIONAHA.113.007394.

2. Badorff C. Transdifferentiation of Blood-Derived Human Adult Endothelial Progenitor Cells Into Functionally Active Cardiomyocytes. *Circulation*. 2003;107(7):1024–1032. doi:10.1161/01.CIR.0000051460.85800.BB.

3. Takahashi K, Tanabe K, Ohnuki M, et al. Induction of pluripotent stem cells from adult human fibroblasts by defined factors. *Cell*. 2007;131(5):861–72. doi:10.1016/j.cell.2007.11.019.

4. Thomas CE, Ehrhardt A, Kay M a. Progress and problems with the use of viral vectors for gene therapy. *Nat. Rev. Genet.* 2003;4(5):346–58. doi:10.1038/nrg1066.

5. Bonadio J, Smiley E, Patil P, Goldstein S. Localized, direct plasmid gene delivery in vivo: prolonged therapy results in reproducible tissue regeneration. *Nat. Med.* 1999;5(7):753–759. doi:10.1038/10473.

6. Jang JH, Rives CB, Shea LD. Plasmid delivery in vivo from porous tissue-engineering

scaffolds: Transgene expression and cellular transfection. *Mol. Ther.* 2005;12(3):475–483. doi:10.1016/j.ymthe.2005.03.036.

7. Wieland J a, Houchin-Ray TL, Shea LD. Non-viral vector delivery from PEG-hyaluronic acid hydrogels. *J. Control. Release*. 2007;120(3):233–41. doi:10.1016/j.jconrel.2007.04.015.

8. Tibbitt MW, Anseth KS. Hydrogels as extracellular matrix mimics for 3D cell culture. *Biotechnol. Bioeng.* 2009;103(4):655–663. doi:10.1002/bit.22361.

9. Lam J, Truong NF, Segura T. Design of cell-matrix interactions in hyaluronic acid hydrogel scaffolds. *Acta Biomater.* 2014;10(4):1571–1580. doi:10.1016/j.actbio.2013.07.025.

10. Bryant SJ, Cuy JL, Hauch KD, Ratner BD. Photo-patterning of porous hydrogels for tissue engineering. *Biomaterials*. 2007;28(19):2978–2986. doi:10.1016/j.biomaterials.2006.11.033.

11. Collins MN, Birkinshaw C. Hyaluronic acid based scaffolds for tissue engineering—A review. *Carbohydr. Polym.* 2013;92(2):1262–1279. doi:10.1016/j.carbpol.2012.10.028.

12. Lei Y, Rahim M, Ng Q, Segura T. Hyaluronic acid and fibrin hydrogels with concentrated DNA/PEI polyplexes for local gene delivery. *J. Control. Release*. 2011;153(3):255–61. doi:10.1016/j.jconrel.2011.01.028.

13. Griffin DR, Weaver WM, Scumpia PO, Di Carlo D, Segura T. Accelerated wound healing by injectable microporous gel scaffolds assembled from annealed building blocks. *Nat. Mater.* 2015;14(7):737–744. doi:10.1038/nmat4294.

14. Sideris E, Griffin DR, Ding Y, et al. Particle Hydrogels Based on Hyaluronic Acid Building Blocks. *ACS Biomater. Sci. Eng.* 2016;2(11):2034–2041. doi:10.1021/acsbiomaterials.6b00444.

15. Nih LR, Sideris E, Carmichael ST, Segura T. Injection of Microporous Annealing Particle (MAP) Hydrogels in the Stroke Cavity Reduces Gliosis and Inflammation and Promotes NPC Migration to the Lesion. *Adv. Mater.* 2017;29(32):1606471. doi:10.1002/adma.201606471.

16. Lei Y, Gojgini S, Lam J, Segura T. The spreading, migration and proliferation of mouse mesenchymal stem cells cultured inside hyaluronic acid hydrogels. *Biomaterials*. 2011;32(1):39–47. doi:10.1016/j.biomaterials.2010.08.103.

17. Kurisawa M, Chung JE, Yang YY, Gao SJ, Uyama H. Injectable biodegradable hydrogels composed of hyaluronic acid-tyramine conjugates for drug delivery and tissue engineering. *Chem. Commun. (Camb).* 2005;(34):4312–4. doi:10.1039/b506989k.

18. Gojgini S, Tokatlian T, Segura T. Utilizing cell-matrix interactions to modulate gene transfer to stem cells inside hyaluronic acid hydrogels. *Mol. Pharm.* 2011;8(5):1582–91. doi:10.1021/mp200171d.

19. Prehm P. Hyaluronate is synthesized at plasma membranes. *Biochem. J.* 1984;220(2):597–600. Available at: http://www.ncbi.nlm.nih.gov/pubmed/6743290.

20. Girish KS, Kemparaju K. The magic glue hyaluronan and its eraser hyaluronidase: a biological overview. *Life Sci.* 2007;80(21):1921–43. doi:10.1016/j.lfs.2007.02.037.

21. West DC, Kumar S. Hyaluronan and angiogenesis. *Ciba Found. Symp.* 1989;143:187-201–7, 281–5. Available at: http://www.ncbi.nlm.nih.gov/pubmed/2478344.

22. Tempel C, Gilead A, Neeman M. Hyaluronic acid as an anti-angiogenic shield in the preovulatory rat follicle. *Biol. Reprod.* 2000;63(1):134–40. Available at: http://www.ncbi.nlm.nih.gov/pubmed/10859252.

23. Day AJ, de la Motte CA. Hyaluronan cross-linking: a protective mechanism in inflammation? *Trends Immunol.* 2005;26(12):637–43. doi:10.1016/j.it.2005.09.009.

24. Milner CM, Higman VA, Day AJ. TSG-6: a pluripotent inflammatory mediator? *Biochem. Soc. Trans.* 2006;34(Pt 3):446–50. doi:10.1042/BST0340446.

25. West DC, Hampson IN, Arnold F, Kumar S. Angiogenesis induced by degradation products

of hyaluronic acid. *Science*. 1985;228(4705):1324–1326. Available at: http://europepmc.org/abstract/MED/2408340.

26. Noble PW, Lake FR, Henson PM, Riches DW. Hyaluronate activation of CD44 induces insulin-like growth factor-1 expression by a tumor necrosis factor-alpha-dependent mechanism in murine macrophages. *J. Clin. Invest.* 1993;91(6):2368–77. doi:10.1172/JCI116469.

27. Lees VC, Fan TP, West DC. Angiogenesis in a delayed revascularization model is accelerated by angiogenic oligosaccharides of hyaluronan. *Lab. Invest.* 1995;73(2):259–66. Available at: http://www.ncbi.nlm.nih.gov/pubmed/7543630.

28. Knudson CB. Hyaluronan and CD44: strategic players for cell-matrix interactions during chondrogenesis and matrix assembly. *Birth Defects Res. C. Embryo Today*. 2003;69(2):174–96. doi:10.1002/bdrc.10013.

29. Toole BP. Hyaluronan: from extracellular glue to pericellular cue. *Nat. Rev. Cancer*. 2004;4(7):528–39. doi:10.1038/nrc1391.

30. Schmits R, Filmus J, Gerwin N, et al. CD44 regulates hematopoietic progenitor distribution, granuloma formation, and tumorigenicity. *Blood*. 1997;90(6):2217–33. Available at: http://www.ncbi.nlm.nih.gov/pubmed/9310473.

31. Hall CL, Lange LA, Prober DA, Zhang S, Turley EA. pp60(c-src) is required for cell locomotion regulated by the hyaluronanreceptor RHAMM. *Oncogene*. 1996;13(10):2213–24. Available at: http://www.ncbi.nlm.nih.gov/pubmed/8950989.

32. Fieber C, Plug R, Sleeman J, Dall P, Ponta H, Hofmann M. Characterisation of the murine gene encoding the intracellular hyaluronan receptor IHABP (RHAMM). *Gene*. 1999;226(1):41–50. Available at: http://www.ncbi.nlm.nih.gov/pubmed/9889313.

33. Savani RC, Cao G, Pooler PM, Zaman A, Zhou Z, DeLisser HM. Differential involvement of

the hyaluronan (HA) receptors CD44 and receptor for HA-mediated motility in endothelial cell function and angiogenesis. *J. Biol. Chem.* 2001;276(39):36770–8. doi:10.1074/jbc.M102273200.

34. Stern R. Hyaluronidases in cancer biology. *Semin. Cancer Biol.* 2008;18(4):275–80. doi:10.1016/j.semcancer.2008.03.017.

35. Lokeshwar VB, Rubinowicz D, Schroeder GL, et al. Stromal and epithelial expression of tumor markers hyaluronic acid and HYAL1 hyaluronidase in prostate cancer. *J. Biol. Chem.* 2001;276(15):11922–32. doi:10.1074/jbc.M008432200.

36. Bharadwaj AG, Kovar JL, Loughman E, Elowsky C, Oakley GG, Simpson MA. Spontaneous metastasis of prostate cancer is promoted by excess hyaluronan synthesis and processing. *Am. J. Pathol.* 2009;174(3):1027–36. doi:10.2353/ajpath.2009.080501.

37. Sugahara KN, Murai T, Nishinakamura H, Kawashima H, Saya H, Miyasaka M. Hyaluronan oligosaccharides induce CD44 cleavage and promote cell migration in CD44-expressing tumor cells. *J. Biol. Chem.* 2003;278(34):32259–65. doi:10.1074/jbc.M300347200.

38. Stern R. Hyaluronan metabolism: a major paradox in cancer biology. *Pathol. Biol. (Paris).* 2005;53(7):372–82. doi:10.1016/j.patbio.2004.12.021.

39. Drury JL, Mooney DJ. Hydrogels for tissue engineering: Scaffold design variables and applications. *Biomaterials*. 2003;24(24):4337–4351. doi:10.1016/S0142-9612(03)00340-5.

40. Kopeček J, Yang J. Hydrogels as smart biomaterials. *Polym. Int.* 2007;56(9):1078–1098. doi:10.1002/pi.2253.

41. Liu Y, Shu XZ, Prestwich GD. Osteochondral defect repair with autologous bone marrow-derived mesenchymal stem cells in an injectable, in situ, cross-linked synthetic extracellular matrix. *Tissue Eng.* 2006;12(12):3405–16. doi:10.1089/ten.2006.12.3405.

42. Giancotti FG, Ruoslahti E. Integrin signaling. *Science*. 1999;285(5430):1028–32. Available

at: http://www.ncbi.nlm.nih.gov/pubmed/10446041.

43. Cukierman E, Pankov R, Stevens DR, Yamada KM. Taking cell-matrix adhesions to the third dimension. *Science*. 2001;294(5547):1708–1712. doi:10.1126/science.1064829.

44. Jones JL, Walker RA. Integrins: a role as cell signalling molecules. *Mol. Pathol.* 1999;52(4):208–13. Available at: http://www.ncbi.nlm.nih.gov/pubmed/10694941.

45. Prowse ABJ, Chong F, Gray PP, Munro TP. Stem cell integrins: implications for ex-vivo culture and cellular therapies. *Stem Cell Res.* 2011;6(1):1–12. doi:10.1016/j.scr.2010.09.005.

46. Davis GE, Senger DR. Endothelial extracellular matrix: biosynthesis, remodeling, and functions during vascular morphogenesis and neovessel stabilization. *Circ. Res.* 2005;97(11):1093–107. doi:10.1161/01.RES.0000191547.64391.e3.

47. Hood JD, Cheresh DA. Role of integrins in cell invasion and migration. *Nat. Rev. Cancer*. 2002;2(2):91–100. doi:10.1038/nrc727.

48. Comisar WA, Kazmers NH, Mooney DJ, Linderman JJ. Engineering RGD nanopatterned hydrogels to control preosteoblast behavior: a combined computational and experimental approach. *Biomaterials*. 2007;28(30):4409–17. doi:10.1016/j.biomaterials.2007.06.018.

49. Comisar WA, Mooney DJ, Linderman JJ. Integrin organization: Linking adhesion ligand nanopatterns with altered cell responses. *J. Theor. Biol.* 2011;274(1):120–130. doi:10.1016/j.jtbi.2011.01.007.

50. Maheshwari G, Brown G, Lauffenburger DA, Wells A, Griffith LG. Cell adhesion and motility depend on nanoscale RGD clustering. *J. Cell Sci.* 2000;113 (Pt 1:1677–86. Available at: http://www.ncbi.nlm.nih.gov/pubmed/10769199.

51. Koo LY, Irvine DJ, Mayes AM, Lauffenburger DA, Griffith LG. Co-regulation of cell adhesion by nanoscale RGD organization and mechanical stimulus. *J. Cell Sci.* 2002;115(Pt

7):1423–33. Available at: http://www.ncbi.nlm.nih.gov/pubmed/11896190.

52. Lee KY, Alsberg E, Hsiong S, et al. Nanoscale Adhesion Ligand Organization Regulates Osteoblast Proliferation and Differentiation. *Nano Lett.* 2004;4(8):1501–1506. doi:10.1021/nl0493592.

53. Kong HJ, Hsiong S, Mooney DJ. Nanoscale cell adhesion ligand presentation regulates nonviral gene delivery and expression. *Nano Lett.* 2007;7(1):161–6. doi:10.1021/nl062485g.

54. Alsberg E, Anderson KW, Albeiruti A, Franceschi RT, Mooney DJ. Cell-interactive alginate hydrogels for bone tissue engineering. *J. Dent. Res.* 2001;80(11):2025–9. doi:10.1177/00220345010800111501.

55. Lutolf MP, Lauer-Fields JL, Schmoekel HG, et al. Synthetic matrix metalloproteinase-sensitive hydrogels for the conduction of tissue regeneration: engineering cell-invasion characteristics. *Proc. Natl. Acad. Sci. U. S. A.* 2003;100(9):5413–8. doi:10.1073/pnas.0737381100.

56. Lam J, Segura T. The modulation of MSC integrin expression by RGD presentation. *Biomaterials*. 2013;34(16):3938–3947. doi:10.1016/j.biomaterials.2013.01.091.

57. Wall ST, Saha K, Ashton RS, Kam KR, Schaffer D V, Healy KE. Multivalency of Sonic hedgehog conjugated to linear polymer chains modulates protein potency. *Bioconjug. Chem.* 2008;19(4):806–12. doi:10.1021/bc700265k.

58. Brown AC, Rowe JA, Barker TH. Guiding Epithelial Cell Phenotypes with Engineered Integrin-Specific Recombinant Fibronectin Fragments. *Tissue Eng. Part A*. 2011;17(1–2):139–150. doi:10.1089/ten.tea.2010.0199.

59. Kisiel M, Martino MM, Ventura M, Hubbell J a, Hilborn J, Ossipov D a. Improving the osteogenic potential of BMP-2 with hyaluronic acid hydrogel modified with integrin-specific

fibronectin fragment. *Biomaterials*. 2013;34(3):704–12. doi:10.1016/j.biomaterials.2012.10.015.

60. Markowski MC, Brown AC, Barker TH. Directing epithelial to mesenchymal transition through engineered microenvironments displaying orthogonal adhesive and mechanical cues. *J. Biomed. Mater. Res. A*. 2012;100(8):2119–27. doi:10.1002/jbm.a.34068.

61. Brown AC, Fiore VF, Sulchek TA, Barker TH. Physical and chemical microenvironmental cues orthogonally control the degree and duration of fibrosis-associated epithelial-to-mesenchymal transitions. *J. Pathol.* 2013;229(1):25–35. doi:10.1002/path.4114.

62. Martino MM, Tortelli F, Mochizuki M, et al. Engineering the growth factor microenvironment with fibronectin domains to promote wound and bone tissue healing. *Sci. Transl. Med.* 2011;3(100):100ra89. doi:10.1126/scitranslmed.3002614.

63. Martino MM, Briquez PS, Ranga A, Lutolf MP, Hubbell JA. Heparin-binding domain of fibrin(ogen) binds growth factors and promotes tissue repair when incorporated within a synthetic matrix. *Proc. Natl. Acad. Sci. U. S. A.* 2013;110(12):4563–8. doi:10.1073/pnas.1221602110.

64. Ibrahim S, Kang QK, Ramamurthi A. The impact of hyaluronic acid oligomer content on physical, mechanical, and biologic properties of divinyl sulfone-crosslinked hyaluronic acid hydrogels. *J. Biomed. Mater. Res. A*. 2010;94(2):355–70. doi:10.1002/jbm.a.32704.

65. Perng C-K, Wang Y-J, Tsi C-H, Ma H. In vivo angiogenesis effect of porous collagen scaffold with hyaluronic acid oligosaccharides. *J. Surg. Res.* 2011;168(1):9–15. doi:10.1016/j.jss.2009.09.052.

66. Camci-Unal G, Aubin H, Ahari AF, Bae H, Nichol JW, Khademhosseini A. Surface-modified hyaluronic acid hydrogels to capture endothelial progenitor cells. *Soft Matter*. 2010;6(20):5120–5126. doi:10.1039/c0sm00508h.

67. Kim HD, Valentini RF. Retention and activity of BMP-2 in hyaluronic acid-based scaffolds in vitro. *J. Biomed. Mater. Res.* 2002;59(3):573–84. Available at: http://www.ncbi.nlm.nih.gov/pubmed/11774316.

68. Cai S, Liu Y, Zheng Shu X, Prestwich GD. Injectable glycosaminoglycan hydrogels for controlled release of human basic fibroblast growth factor. *Biomaterials*. 2005;26(30):6054–67. doi:10.1016/j.biomaterials.2005.03.012.

69. Li S, Overman JJ, Katsman D, et al. An age-related sprouting transcriptome provides molecular control of axonal sprouting after stroke. *Nat. Neurosci.* 2010;13(12):1496–504. doi:10.1038/nn.2674.

70. Xu X, Jha AK, Duncan RL, Jia X. Heparin-decorated, hyaluronic acid-based hydrogel particles for the controlled release of bone morphogenetic protein 2. *Acta Biomater.* 2011;7(8):3050–9. doi:10.1016/j.actbio.2011.04.018.

71. Lei Y, Huang S, Sharif-Kashani P, Chen Y, Kavehpour P, Segura T. Incorporation of active DNA/cationic polymer polyplexes into hydrogel scaffolds. *Biomaterials*. 2010;31(34):9106–16. doi:10.1016/j.biomaterials.2010.08.016.

72. Tokatlian T, Cam C, Siegman SN, Lei Y, Segura T. Design and characterization of microporous hyaluronic acid hydrogels for in vitro gene transfer to mMSCs. *Acta Biomater.* 2012;8(11):3921–31. doi:10.1016/j.actbio.2012.07.014.

73. Teixeira AI, Abrams G a, Bertics PJ, Murphy CJ, Nealey PF. Epithelial contact guidance on well-defined micro- and nanostructured substrates. *J. Cell Sci.* 2003;116(Pt 10):1881–92. doi:10.1242/jcs.00383.

74. Jiang L-Y, Luo Y. Guided assembly of endothelial cells on hydrogel matrices patterned with microgrooves: a basic model for microvessel engineering. *Soft Matter*. 2013;9(4):1113.

doi:10.1039/c2sm27126e.

75. Goubko C a, Basak A, Majumdar S, Cao X. Dynamic cell patterning of photoresponsive hyaluronic acid hydrogels. *J. Biomed. Mater. Res. A*. 2013;Accepted a:1–28. doi:10.1002/jbm.a.34712.

76. Vogel V, Sheetz M. Local force and geometry sensing regulate cell functions. *Nat. Rev. Mol. Cell Biol.* 2006;7(4):265–75. doi:10.1038/nrm1890.

77. Marklein R a., Soranno DE, Burdick J a. Magnitude and presentation of mechanical signals influence adult stem cell behavior in 3-dimensional macroporous hydrogels. *Soft Matter*. 2012;8(31):8113. doi:10.1039/c2sm25501d.

78. Ananthanarayanan B, Kim Y, Kumar S. Elucidating the mechanobiology of malignant brain tumors using a brain matrix-mimetic hyaluronic acid hydrogel platform. *Biomaterials*. 2011;32(31):7913–23. doi:10.1016/j.biomaterials.2011.07.005.

79. Engler AJ, Sen S, Sweeney HL, Discher DE. Matrix elasticity directs stem cell lineage specification. *Cell*. 2006;126(4):677–89. doi:10.1016/j.cell.2006.06.044.

80. Seidlits SK, Khaing ZZ, Petersen RR, et al. The effects of hyaluronic acid hydrogels with tunable mechanical properties on neural progenitor cell differentiation. *Biomaterials*. 2010;31(14):3930–40. doi:10.1016/j.biomaterials.2010.01.125.

81. Young JL, Engler AJ. Hydrogels with time-dependent material properties enhance cardiomyocyte differentiation in vitro. *Biomaterials*. 2011;32(4):1002–9. doi:10.1016/j.biomaterials.2010.10.020.

82. Yee D, Hanjaya-putra D, Bose V, Luong E, Gerecht S, Ph D. Hyaluronic Acid Hydrogels Support Cord-Like Structures from Endothelial Colony-Forming Cells. *Tissue Eng. Part A*. 2011;17(9). doi:10.1089/ten.tea.2010.0481.

83. Xu X, Jha AK, Harrington DA, Farach-Carson MC, Jia X. Hyaluronic acid-based hydrogels: from a natural polysaccharide to complex networks. *Soft Matter*. 2012;8(12):3280. doi:10.1039/c2sm06463d.

84. Owen SC, Fisher SA, Tam RY, Nimmo CM, Shoichet MS. Hyaluronic acid click hydrogels emulate the extracellular matrix. *Langmuir*. 2013;29(24):7393–400. doi:10.1021/la305000w.

85. Hu X, Li D, Zhou F, Gao C. Biological hydrogel synthesized from hyaluronic acid, gelatin and chondroitin sulfate by click chemistry. *Acta Biomater.* 2011;7(4):1618–26. doi:10.1016/j.actbio.2010.12.005.

86. Grover GN, Lam J, Nguyen TH, Segura T, Maynard HD. Biocompatible hydrogels by oxime Click chemistry. *Biomacromolecules*. 2012;13(10):3013–7. doi:10.1021/bm301346e.

87. Grover GN, Braden RL, Christman KL. Oxime cross-linked injectable hydrogels for catheter delivery. *Adv. Mater.* 2013;25(21):2937–42. doi:10.1002/adma.201205234.

88. Chang CY, Chan AT, Armstrong PA, et al. Biomaterials Hyaluronic acid-human blood hydrogels for stem cell transplantation. 2012;33:8026–8033.

89. Park KM, Yang J, Jung H, et al. In Situ Supramolecular Assembly and Modular Modification of Hyaluronic Acid Hydrogels for 3D Cellular Engineering. 2012;(4):2960–2968.

90. Hanjaya-Putra D, Wong KT, Hirotsu K, Khetan S, Burdick J a, Gerecht S. Spatial control of cell-mediated degradation to regulate vasculogenesis and angiogenesis in hyaluronan hydrogels. *Biomaterials*. 2012;33(26):6123–31. doi:10.1016/j.biomaterials.2012.05.027.

91. Slaughter B V, Khurshid SS, Fisher OZ, Khademhosseini A, Peppas NA. Hydrogels in regenerative medicine. *Adv. Mater.* 2009;21(32–33):3307–29. doi:10.1002/adma.200802106.

92. Hoffman AS. Hydrogels for biomedical applications. *Adv. Drug Deliv. Rev.* 2012;64(null):18–23. doi:10.1016/j.addr.2012.09.010.

93. Hollister SJ. Porous scaffold design for tissue engineering. *Nat. Mater.* 2005;4(7):518–24. doi:10.1038/nmat1421.

94. Jhon MS, Andrade JD. Water and hydrogels. *J. Biomed. Mater. Res.* 1973;7(6):509–22. doi:10.1002/jbm.820070604.

95. Molinaro G, Leroux J-C, Damas J, Adam A. Biocompatibility of thermosensitive chitosan-based hydrogels: an in vivo experimental approach to injectable biomaterials. *Biomaterials*. 2002;23(13):2717–22. Available at: http://www.ncbi.nlm.nih.gov/pubmed/12059021.

96. Noguchi T, Yamamuro T, Oka M, et al. Poly(vinyl alcohol) hydrogel as an artificial articular cartilage: evaluation of biocompatibility. *J. Appl. Biomater. An Off. J. Soc. Biomater.* 1991;2(2):101–107. doi:10.1002/jab.770020205.

97. de Vos P, Lazarjani HA, Poncelet D, Faas MM. Polymers in cell encapsulation from an enveloped cell perspective. *Adv. Drug Deliv. Rev.* 2014;67–68(4):15–34. doi:10.1016/j.addr.2013.11.005.

98. Lee KY, Mooney DJ. Hydrogels for tissue engineering. *Chem. Rev.* 2001;101(7):1869–1879.

99. Ahearne M, Wilson SL, Liu K-K, Rauz S, El Haj AJ, Yang Y. Influence of cell and collagen concentration on the cell-matrix mechanical relationship in a corneal stroma wound healing model. *Exp. Eye Res.* 2010;91(5):584–591. doi:10.1016/j.exer.2010.07.013.

100. Bott K, Upton Z, Schrobback K, et al. The effect of matrix characteristics on fibroblast proliferation in 3D gels. *Biomaterials*. 2010;31(32):8454–8464. doi:10.1016/j.biomaterials.2010.07.046.

101. Nöth U, Schupp K, Heymer A, et al. Anterior cruciate ligament constructs fabricated from human mesenchymal stem cells in a collagen type I hydrogel. *Cytotherapy*. 2005;7(5):447–455. doi:10.1080/14653240500319093.

102. Ahearne M, Yang Y, El Haj AJ, Then KY, Liu K-K. Characterizing the viscoelastic properties of thin hydrogel-based constructs for tissue engineering applications. *J. R. Soc. Interface*. 2005;2(5):455–63. doi:10.1098/rsif.2005.0065.

103. Bader RA. Synthesis and viscoelastic characterization of novel hydrogels generated via photopolymerization of 1,2-epoxy-5-hexene modified poly(vinyl alcohol) for use in tissue replacement. *Acta Biomater.* 2008;4(4):967–975. doi:10.1016/j.actbio.2008.02.015.

104. Mohtaram NK, Montgomery A, Willerth SM. Biomaterial-based drug delivery systems for the controlled release of neurotrophic factors. *Biomed. Mater.* 2013;8(2):22001. doi:10.1088/1748-6041/8/2/022001.

105. Burdick JA, Mason MN, Hinman AD, Thorne K, Anseth KS. Delivery of osteoinductive growth factors from degradable PEG hydrogels influences osteoblast differentiation and mineralization. *J. Control. Release*. 2002;83(1):53–63. doi:10.1016/S0168-3659(02)00181-5.

106. Anchordoquy TJ, Simberg D. Watching the gorilla and questioning delivery dogma. *J. Control. Release*. 2017;262(Supplement C):87–90. doi:10.1016/j.jconrel.2017.07.021.

107. Jang J-H, Schaffer D V, Shea LD. Engineering biomaterial systems to enhance viral vector gene delivery. *Mol. Ther.* 2011;19(8):1407–15. doi:10.1038/mt.2011.111.

108. Krebsbach PH, Hollister SJ, Hu W-W, Wang Z. Localized viral vector delivery to enhance in situ regenerative gene therapy. *Gene Ther.* 2007;14(11):891. doi:10.1038/sj.gt.3302940.

109. Hackett PB, Largaespada D a., Switzer KC, Cooper LJN. Evaluating risks of insertional mutagenesis by DNA transposons in gene therapy. *Transl. Res.* 2013;161(4):265–283. doi:10.1016/j.trsl.2012.12.005.

110. Meilander-lin NJ, Cheung PJ, Wilson DL, Bellamkonda R V. Sustained in Vivo Gene Delivery from Agarose Hydrogel Prolongs Nonviral Gene Expression in Skin. *Tissue Eng.*

2005;11(3):546–555.

111. Trentin D, Hall H, Wechsler S, Hubbell JA. Peptide-matrix-mediated gene transfer of an oxygen-insensitive hypoxia-inducible factor-1a variant for local induction of angiogenesis. 2006;103(8):1–6.

112. Fang J, Zhu YY, Smiley E, et al. Stimulation of new bone formation by direct transfer of osteogenic plasmid genes. *Proc. Natl. Acad. Sci. U. S. A.* 1996;93(12):5753–5758. doi:10.1073/pnas.93.12.5753.

113. Mao Z, Shi H, Guo R, et al. Enhanced angiogenesis of porous collagen scaffolds by incorporation of TMC/DNA complexes encoding vascular endothelial growth factor. *Acta Biomater.* 2009;5(8):2983–2994. doi:10.1016/j.actbio.2009.04.004.

114. Guo R, Xu S, Ma L, Huang A, Gao C. Enhanced angiogenesis of gene-activated dermal equivalent for treatment of full thickness incisional wounds in a porcine model. *Biomaterials*. 2010;31(28):7308–7320. doi:10.1016/j.biomaterials.2010.06.013.

115. Rose LC, Kucharski C, Uludağ H. Protein expression following non-viral delivery of plasmid DNA coding for basic FGF and BMP-2 in a rat ectopic model. *Biomaterials*. 2012;33(11):3363–74. doi:10.1016/j.biomaterials.2012.01.031.

116. Elangovan S, D'Mello SR, Hong L, et al. The enhancement of bone regeneration by gene activated matrix encoding for platelet derived growth factor. *Biomaterials*. 2014;35(2):737–747. doi:10.1016/j.biomaterials.2013.10.021.

117. Tokatlian T, Cam C, Segura T. Non-viral DNA delivery from porous hyaluronic acid hydrogels in mice. *Biomaterials*. 2014;35(2):825–35. doi:10.1016/j.biomaterials.2013.10.014.

118. Tokatlian T, Cam C, Segura T. Porous Hyaluronic Acid Hydrogels for Localized Nonviral DNA Delivery in a Diabetic Wound Healing Model. *Adv. Healthc. Mater.* 2015;4(7):1084–1091.

doi:10.1002/adhm.201400783.

119. Qin JY, Zhang L, Clift KL, et al. Systematic comparison of constitutive promoters and the doxycycline-inducible promoter. *PLoS One*. 2010;5(5):e10611. doi:10.1371/journal.pone.0010611.

120. Avilés MO, Lin C-H, Zelivyanskaya M, et al. The contribution of plasmid design and release to in vivo gene expression following delivery from cationic polymer modified scaffolds. *Biomaterials*. 2010;31(6):1140–7. doi:10.1016/j.biomaterials.2009.10.035.

121. Brooks AR, Harkins RN, Wang P, Qian HS, Liu P, Rubanyi GM. Transcriptional silencing is associated with extensive methylation of the CMV promoter following adenoviral gene delivery to muscle. *J. Gene Med.* 2004;6(4):395–404. doi:10.1002/jgm.516.

122. Ede C, Chen X, Lin M-Y, Chen YY. Quantitative Analyses of Core Promoters Enable Precise Engineering of Regulated Gene Expression in Mammalian Cells. doi:10.1021/acssynbio.5b00266.

123. Klein R, Ruttkowski B, Knapp E, Salmons B, Günzburg WH, Hohenadl C. WPRE-mediated enhancement of gene expression is promoter and cell line specific. *Gene*. 2006;372(1–2):153–161. doi:10.1016/j.gene.2005.12.018.

124. Chen Z-Y, He C-Y, Ehrhardt A, Kay MA. Minicircle DNA vectors devoid of bacterial DNA result in persistent and high-level transgene expression in vivo. *Mol. Ther.* 2003;8(3):495–500. doi:10.1016/S1525-0016(03)00168-0.

125. Hardee CL, Arévalo-Soliz LM, Hornstein BD, Zechiedrich L. Advances in Non-Viral DNA Vectors for Gene Therapy. *Genes (Basel)*. 2017;8(2):65. doi:10.3390/genes8020065.

126. Chen ZY, He CY, Meuse L, Kay M a. Silencing of episomal transgene expression by plasmid bacterial DNA elements in vivo. *Gene Ther.* 2004;11(10):856–64.

doi:10.1038/sj.gt.3302231.

127. Huang M, Chen Z, Hu S, et al. Novel minicircle vector for gene therapy in murine myocardial infarction. *Circulation*. 2009;120(11 Suppl):S230-7. doi:10.1161/CIRCULATIONAHA.108.841155.

128. Keeney M, Chung MT, Zielins ER, et al. Scaffold-mediated BMP-2 minicircle DNA delivery accelerated bone repair in a mouse critical-size calvarial defect model. *J. Biomed. Mater. Res. - Part A*. 2016;104(8):2099–2107. doi:10.1002/jbm.a.35735.

129. Yin H, Kanasty RL, Eltoukhy A a., Vegas AJ, Dorkin JR, Anderson DG. Non-viral vectors for gene-based therapy. *Nat. Rev. Genet.* 2014;15(8):541–55. doi:10.1038/nrg3763.

130. Shepard JA, Huang A, Shikanov A, Shea LD. Balancing cell migration with matrix degradation enhances gene delivery to cells cultured three-dimensionally within hydrogels. *J. Control. Release*. 2010;146(1):128–35. doi:10.1016/j.jconrel.2010.04.032.

131. Bauer S, Kirschning CJ, Hä Cker H, et al. Human TLR9 confers responsiveness to bacterial DNA via species-specific CpG motif recognition. Available at: http://www.pnas.org/content/98/16/9237.full.pdf. Accessed January 3, 2018.

132. Akira S, Hemmi H, Takeuchi O, et al. A Toll-like receptor recognizes bacterial DNA. *Nature*. 2000;408(6813):740–745. doi:10.1038/35047123.

133. Chiou HC, Tangco M V., Kormis K, et al. Enhanced resistance to nuclease degradation of nucleic acids complexed to asialoglycoprotein-polylysine carriers. *Nucleic Acids Res.* 1994;22(24):5439–5446. doi:10.1093/nar/22.24.5439.

134. Jang J-H, Bengali Z, Houchin TL, Shea LD. Surface adsorption of DNA to tissue engineering scaffolds for efficient gene delivery. *J. Biomed. Mater. Res. A*. 2006;77(1):50–8. doi:10.1002/jbm.a.30643.

135. Saul JM, Linnes MP, Ratner BD, Giachelli CM, Pun SH. Delivery of non-viral gene carriers from sphere-templated fibrin scaffolds for sustained transgene expression. *Biomaterials*. 2007;28(31):4705–16. doi:10.1016/j.biomaterials.2007.07.026.

136. Siegman S, Truong NF, Segura T. Encapsulation of PEGylated low-molecular-weight PEI polyplexes in hyaluronic acid hydrogels reduces aggregation. *Acta Biomater.* 2015;28:45–54. doi:10.1016/j.actbio.2015.09.020.

137. Rose LC, Kucharski C, Uludağ H. Protein expression following non-viral delivery of plasmid DNA coding for basic FGF and BMP-2 in a rat ectopic model. *Biomaterials*. 2012;33(11):3363–3374. doi:10.1016/j.biomaterials.2012.01.031.

138. Des Rieux A, Shikanov A, Shea LD. Fibrin hydrogels for non-viral vector delivery in vitro. *J. Control. Release*. 2009;136:148–154. doi:10.1016/j.jconrel.2009.02.004.

139. De Laporte L, Lei Yan A, Shea LD. Local gene delivery from ECM-coated poly(lactide-co-glycolide) multiple channel bridges after spinal cord injury. *Biomaterials*. 2009;30(12):2361–2368. doi:10.1016/j.biomaterials.2008.12.051.

140. Grijalvo S, Alagia A, Puras G, et al. Cationic Nioplexes-in-Polysaccharide-Based Hydrogels as Versatile Biodegradable Hybrid Materials to Deliver Nucleic Acids. *J. Mater. Chem. B*. 2017. doi:10.1039/C7TB01691C.

141. Paul A, Hasan A, Kindi H Al, et al. Injectable graphene oxide/hydrogel-based angiogenic gene delivery system for vasculogenesis and cardiac repair. *ACS Nano*. 2014;8(8):8050–8062. doi:10.1021/nn5020787.

142. Lei Y, Segura T. DNA delivery from matrix metalloproteinase degradable poly(ethylene glycol) hydrogels to mouse cloned mesenchymal stem cells. *Biomaterials*. 2009;30(2):254–265. doi:10.1016/j.biomaterials.2008.09.027.

143. Trentin D, Hubbell J, Hall H. Non-viral gene delivery for local and controlled DNA release. 2004. doi:10.1016/j.jconrel.2004.09.029.

144. Adolph EJ, Nelson CE, Werfel T a, et al. Enhanced Performance of Plasmid DNA Polyplexes Stabilized by a Combination of Core Hydrophobicity and Surface PEGylation. *J. Mater. Chem. B*. 2014:8154–8164. doi:10.1039/C4TB00352G.

145. Kong HJ, Liu J, Riddle K, Matsumoto T, Leach K, Mooney DJ. Non-viral gene delivery regulated by stiffness of cell adhesion substrates. *Nat. Mater.* 2005;4(6):460–4. doi:10.1038/nmat1392.

146. Kasputis T, Pannier AK. The role of surface chemistry-induced cell characteristics on nonviral gene delivery to mouse fibroblasts. *J. Biol. Eng.* 2012;6(1):17. doi:10.1186/1754-1611-6-17.

147. Teo BKK, Goh SH, Kustandi TS, Loh WW, Low HY, Yim EKF. The effect of micro and nanotopography on endocytosis in drug and gene delivery systems. *Biomaterials*. 2011;32(36):9866–9875. doi:10.1016/j.biomaterials.2011.08.088.

148. Dhaliwal A, Maldonado M, Han Z, Segura T. Differential uptake of DNA-poly(ethylenimine) polyplexes in cells cultured on collagen and fibronectin surfaces. *Acta Biomater.* 2010;6(9):3436–47. doi:10.1016/j.actbio.2010.03.038.

149. Bengali Z, Rea JC, Shea LD. Gene expression and internalization following vector adsorption to immobilized proteins: Dependence on protein identity and density. *J. Gene Med.* 2007;9(8):668–678. doi:10.1002/jgm.1058.

150. Rea JC, Gibly RF, Davis NE, Barron AE, Shea LD. Engineering Surfaces for Substrate-Mediated Gene Delivery Using Recombinant Proteins. *Biomacromolecules*. 2009;10(10):2779–2786. doi:10.1021/bm900628e.

151. Dhaliwal A, Maldonado M, Lin C, Segura T. Cellular cytoskeleton dynamics modulates non-viral gene delivery through RhoGTPases. *PLoS One*. 2012;7(4):e35046. doi:10.1371/journal.pone.0035046.

152. Christensen MD, Elmer JJ, Eaton S, Gonzalez-Malerva L, Labaer J, Rege K. Kinome-level screening identifies inhibition of polo-like kinase-1 (PLK1) as a target for enhancing non-viral transgene expression. *J. Control. Release*. 2015;204:20–29. doi:10.1016/j.jconrel.2015.01.036.

153. Plautz SA, Boanca G, Riethoven J-JM, Pannier AK. Microarray analysis of gene expression profiles in cells transfected with nonviral vectors. *Mol. Ther.* 2011;19(12):2144–51. doi:10.1038/mt.2011.161.

154. Martin TM, Plautz SA, Pannier AK. Network analysis of endogenous gene expression profiles after polyethyleneimine-mediated DNA delivery. *J. Gene Med.* 2013;15(3–4):142–54. doi:10.1002/jgm.2704.

155. Martin TM, Plautz SA, Pannier AK. Temporal endogenous gene expression profiles in response to lipid-mediated transfection. *J. Gene Med.* 2015;17(1–2):14–32. doi:10.1002/jgm.2821.

156. Dhaliwal A, Oshita V, Segura T. Transfection in the third dimension. *Integr. Biol.* 2013;5(10):1206–16. doi:10.1039/c3ib40086g.

157. Lavik E, Langer R. Tissue engineering: current state and perspectives. *Appl. Microbiol. Biotechnol.* 2004;65(1):1–8. doi:10.1007/s00253-004-1580-z.

158. Nerem RM, Sambanis a. Tissue engineering: from biology to biological substitutes. *Tissue Eng.* 1995;1(1):3–13. doi:10.1089/ten.1995.1.3.

159. Lutolf MP, Hubbell J a. Synthetic biomaterials as instructive extracellular microenvironments for morphogenesis in tissue engineering. *Nat. Biotechnol.* 2005;23(1):47–55.

doi:10.1038/nbt1055.

160. Cam C, Segura T. Matrix-based gene delivery for tissue repair. *Curr. Opin. Biotechnol.* 2013:1–9. doi:10.1016/j.copbio.2013.04.007.

161. Godbey WT, Wu KK, Mikos AG. Poly(ethylenimine) and its role in gene delivery. *J. Control. Release*. 1999;60:149–160.

162. Peattie R a, Nayate a P, Firpo M a, Shelby J, Fisher RJ, Prestwich GD. Stimulation of in vivo angiogenesis by cytokine-loaded hyaluronic acid hydrogel implants. *Biomaterials*. 2004;25(14):2789–98. doi:10.1016/j.biomaterials.2003.09.054.

163. Ahrens T, Assmann V, Fieber C, et al. CD44 is the principal mediator of hyaluronic-acid-induced melanoma cell proliferation. *J. Invest. Dermatol.* 2001;116(1):93–101. doi:10.1046/j.1523-1747.2001.00236.x.

164. Sherman L, Sleeman J, Herrlich P, Ponta H. Hyaluronate receptors: key players in growth, differentiation, migration and tumor progression. *Curr. Opin. Cell Biol.* 1994;6(5):726–733. doi:10.1016/0955-0674(94)90100-7.

165. Rooney P, Wang M, Kumar P, Kumar S. Angiogenic oligosaccharides of hyaluronan enhance the production of collagens by endothelial cells. *J. Cell Sci.* 1993;105 (Pt 1:213–218.

166. Gao F, Liu Y, He Y, et al. Hyaluronan oligosaccharides promote excisional wound healing through enhanced angiogenesis. *Matrix Biol.* 2010;29(2):107–16. doi:10.1016/j.matbio.2009.11.002.

167. Pardue EL, Ibrahim S, Ramamurthi A. Role of hyaluronan in angiogenesis and its utility to angiogenic tissue engineering. *Organogenesis*. 2008;4(4):203–214. doi:10.4161/org.4.4.6926.

168. Page-McCaw A, Ewald AJ, Werb Z. Matrix metalloproteinases and the regulation of tissue. *Nat Rev Mol Cell Biol.* 2007;8(3):221–233. doi:10.1038/nrm2125.Matrix.

169. Parks WC. Matrix metalloproteinases in repair. *Wound Repair Regen.* 1999;7(6):423–432. doi:10.1046/j.1524-475X.1999.00423.x.

170. Kim JKJ, Kim ISKIS, Hwang SJHSJ, Kim HCKHC, Park YPY, Sun KSK. Bone regeneration using MMP sensitive-hyaluronic acid based hydrogels. *2009 IEEE 35th Annu. Northeast Bioeng. Conf.* 2009. doi:10.1109/NEBC.2009.4967789.

171. Kim J, Park Y, Tae G, et al. Synthesis and characterization of matrix metalloprotease sensitive-low molecular weight hyaluronic acid based hydrogels. *J. Mater. Sci. Mater. Med.* 2008;19(11):3311–3318. doi:10.1007/s10856-008-3469-3.

172. Okazaki A, Jo J-I, Tabata Y. A reverse transfection technology to genetically engineer adult stem cells. *Tissue Eng.* 2007;13(2):245–51. doi:10.1089/ten.2006.0185.

173. Cam C, Segura T. Chemical sintering generates uniform porous hyaluronic acid hydrogels. *Acta Biomater.* 2014;10(1):205–213. doi:10.1016/j.actbio.2013.10.002.

174. Segura T, Chung PH, Shea LD. DNA delivery from hyaluronic acid-collagen hydrogels via a substrate-mediated approach. *Biomaterials*. 2005;26(13):1575–84. doi:10.1016/j.biomaterials.2004.05.007.

175. Cim A, Sawyer GJ, Zhang X, et al. In vivo studies on non-viral transdifferentiation of liver cells towards pancreatic β cells. *J. Endocrinol.* 2012;214(3):277–88. doi:10.1530/JOE-12-0033.

176. Kim J, Efe JA, Zhu S, et al. Direct reprogramming of mouse fibroblasts to neural progenitors. *Proc. Natl. Acad. Sci. U. S. A.* 2011;108(19):7838–43. doi:10.1073/pnas.1103113108.

177. Jafari M, Soltani M, Naahidi S, N. Karunaratne D, Chen P. Nonviral Approach for Targeted Nucleic Acid Delivery. *Curr. Med. Chem.* 2012;19(2):197–208. doi:10.2174/092986712803414141.

178. Desmond KW, Weeks ER. Influence of particle size distribution on random close packing of spheres. *Phys. Rev. E - Stat. Nonlinear, Soft Matter Phys.* 2014;90(2):1–6. doi:10.1103/PhysRevE.90.022204.

179. Zeltinger J, Sherwood JK, Graham DA, Müeller R, Griffith LG. Effect of Pore Size and Void Fraction on Cellular Adhesion, Proliferation, and Matrix Deposition. *Tissue Eng.* 2001;7(5):557–572. doi:10.1089/107632701753213183.

180. Loh QL, Choong C. Three-Dimensional Scaffolds for Tissue Engineering Applications: Role of Porosity and Pore Size. *Tissue Eng. Part B Rev.* 2013;19(6):485–502. doi:10.1089/ten.teb.2012.0437.

181. Murphy CM, Haugh MG, O'Brien FJ. The effect of mean pore size on cell attachment, proliferation and migration in collagen-glycosaminoglycan scaffolds for bone tissue engineering. *Biomaterials*. 2010;31(3):461–466. doi:10.1016/j.biomaterials.2009.09.063.

182. Mandal BB, Kundu SC. Cell proliferation and migration in silk fibroin 3D scaffolds. *Biomaterials*. 2009;30(15):2956–2965. doi:10.1016/j.biomaterials.2009.02.006.

183. Matsiko A, Gleeson JP, O'Brien FJ. Scaffold Mean Pore Size Influences Mesenchymal Stem Cell Chondrogenic Differentiation and Matrix Deposition. *Tissue Eng. Part A*. 2015;21(3–4):486–497. doi:10.1089/ten.tea.2013.0545.

184. Hu B, Leow WR, Amini S, et al. Orientational Coupling Locally Orchestrates a Cell Migration Pattern for Re-Epithelialization. *Adv. Mater.* 2017;29(29):1700145. doi:10.1002/adma.201700145.

185. Hopp I, Michelmore A, Smith LE, et al. The influence of substrate stiffness gradients on primary human dermal fibroblasts. *Biomaterials*. 2013;34(21):5070–5077. doi:10.1016/j.biomaterials.2013.03.075.

186. Yeung T, Georges PC, Flanagan LA, et al. Effects of substrate stiffness on cell morphology, cytoskeletal structure, and adhesion. *Cell Motil. Cytoskeleton*. 2005;60(1):24–34. doi:10.1002/cm.20041.

187. Martino MM, Mochizuki M, Rothenfluh DA, Rempel SA, Hubbell JA, Barker TH. Controlling integrin specificity and stem cell differentiation in 2D and 3D environments through regulation of fibronectin domain stability. *Biomaterials*. 2009;30(6):1089–1097. doi:10.1016/j.biomaterials.2008.10.047.

188. Li S, Nih LR, Bachman H, et al. Hydrogels with precisely controlled integrin activation dictate vascular patterning and permeability. *Nat. Mater.* 2017;16(September). doi:10.1038/nmat4954.

189. Dhaliwal A, Lam J, Maldonado M, Lin C, Segura T. Extracellular matrix modulates non-viral gene transfer to mouse mesenchymal stem cells. *Soft Matter*. 2012;8(5):1451–1459. doi:10.1039/C1SM06591B.

190. Brunner S, Sauer T, Carotta S, Cotten M, Saltik M, Wagner E. Cell cycle dependence of gene transfer by lipoplex, polyplex and recombinant adenovirus. *Gene Ther.* 2000;7(5):401–7. doi:10.1038/sj.gt.3301102.

191. von Gersdorff K, Sanders NN, Vandenbroucke R, De Smedt SC, Wagner E, Ogris M. The Internalization Route Resulting in Successful Gene Expression Depends on both Cell Line and Polyethylenimine Polyplex Type. *Mol. Ther.* 2006;14(5):745–753. doi:10.1016/j.ymthe.2006.07.006.

192. Suh J, Wirtz D, Hanes J. Efficient active transport of gene nanocarriers to the cell nucleus. *Proc. Natl. Acad. Sci.* 2003;100(7):3878–3882. doi:10.1073/pnas.0636277100.

193. Grosse S, Aron Y, Thévenot G, Monsigny M, Fajac I. Cytoskeletal involvement in the

cellular trafficking of plasmid/PEI derivative complexes. *J. Control. Release*. 2007;122(1):111–117. doi:10.1016/j.jconrel.2007.06.015.

194. Bubb M, Spector I, Beyer B, Fosen K. Effect of Jasplakinolide on the kinetics of actin polymerization. *J. Biol. Chem.* 1999;23(12):2613–2621. doi:10.1074/jbc.275.7.5163.

195. Ho YK, Zhou LH, Tam KC, Too HP. Enhanced non-viral gene delivery by coordinated endosomal release and inhibition of β-tubulin deactylase. *Nucleic Acids Res.* 2016;45(6). doi:10.1093/nar/gkw1143.

196. Etienne-Manneville S, Hall A. Rho GTPases in cell biology. *Nature*. 2002;420(6916):629–35. doi:10.1038/nature01148.

197. Nobes CD, Hall A. Rho GTPases control polarity, protrusion, and adhesion during cell movement. *J. Cell Biol.* 1999;144(6):1235–1244. doi:10.1083/jcb.144.6.1235.

198. Dupont S, Morsut L, Aragona M, et al. Role of YAP/TAZ in mechanotransduction. *Nature*. 2011;474(7350):179–184. doi:10.1038/nature10137.

199. Szeto SG, Narimatsu M, Lu M, et al. YAP/TAZ Are Mechanoregulators of TGF-β-Smad Signaling and Renal Fibrogenesis. *J. Am. Soc. Nephrol.* 2016;27(10):3117–3128. doi:10.1681/ASN.2015050499.

200. Caliari SR, Vega SL, Kwon M, Soulas EM, Burdick JA. Dimensionality and spreading influence MSC YAP/TAZ signaling in hydrogel environments. *Biomaterials*. 2016;103:314–323. doi:10.1016/J.BIOMATERIALS.2016.06.061.

201. Liu F, Lagares D, Choi KM, et al. Mechanosignaling through YAP and TAZ drives fibroblast activation and fibrosis. *Am. J. Physiol. - Lung Cell. Mol. Physiol.* 2015;308(4):L344–L357. doi:10.1152/ajplung.00300.2014.

202. Wang C, Zhu X, Feng W, et al. Verteporfin inhibits YAP function through up-regulating

14-3-3σ sequestering YAP in the cytoplasm. *Am J Cancer Res*. 2016;6(1):27–37. Available at: www.ajcr.us. Accessed December 18, 2017.

203. Chaudhuri O, Gu L, Klumpers D, et al. Hydrogels with tunable stress relaxation regulate stem cell fate and activity. *Nat. Mater.* 2015;15(3):326–334. doi:10.1038/nmat4489.